NASA CR-54013
ER-5088

TRW

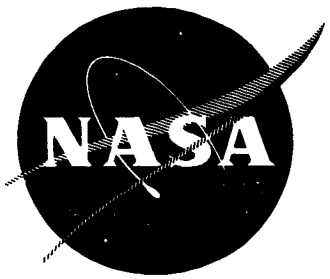

SUNFLOWER I
CONDENSER — SUBCOOLER

Prepared for

NATIONAL AERONAUTICS AND SPACE ADMINISTRATION

CONTRACT NAS 5-462

TRW ELECTROMECHANICAL DIVISION
THOMPSON RAMO WOOLDRIDGE INC.
23555 EUCLID AVENUE ■ CLEVELAND, OHIO 44117

NOTICE

This report was prepared as an account of Government sponsored work. Neither the United States, nor the National Aeronautics and Space Administration (NASA), nor any person acting on behalf of NASA:

A.) Makes any warranty or representation, expressed or implied, with respect to the accuracy, completeness, or usefulness of the information contained in this report, or that the use of any information, apparatus, method, or process disclosed in this report may not infringe privately owned rights; or

B.) Assumes any liabilities with respect to the use of, or for damages resulting from the use of any information, apparatus, method or process disclosed in this report.

As used above, "person acting on behalf of NASA" includes any employee or contractor of NASA, or employee of such contractor, to the extent that such employee or contractor of NASA, or employee or such contractor prepares, disseminates, or provides access to, any information pursuant to his employment or contract with NASA, or his employment with such contractor.

Request for copies of this report should be referred to

National Aeronautics and Space Administration
Office of Scientific and Technical Information
Attention: AFSS-A
Washington, D. C. 20546

NASA CR-54013
ER-5088

TOPICAL REPORT

SUNFLOWER I
CONDENSER — SUBCOOLER

Prepared for

NATIONAL AERONAUTICS AND SPACE ADMINISTRATION

JUNE 1, 1964

CONTRACT NAS 5-462

Technical Management
NASA-Lewis Research Center
Cleveland, Ohio
Space Electric Power Office
J. A. Heller

TRW ELECTROMECHANICAL DIVISION
THOMPSON RAMO WOOLDRIDGE INC.
CLEVELAND, OHIO

ABSTRACT

This report covers the mercury condensing development program at the Electromechanical Division of Thompson Ramo Wooldridge undertaken as part of the Sunflower I contract with the National Aeronautics and Space Administration (NAS 5-462). The work was performed between June 1960 and August 1962. The objective of this program was to provide a full-scale condenser-subcooler component suitable for integration into the Sunflower I power conversion system.

TABLE OF CONTENTS

TABLE OF CONTENTS (Cont'd.)

LIST OF ILLUSTRATIONS

LIST OF ILLUSTRATIONS (Continued)

LIST OF ILLUSTRATIONS (Continued)

LIST OF ILLUSTRATIONS (Continued)

LIST OF TABLES

Section 1.0
SUMMARY

33999

This report includes the initial analytical investigations necessary to establish the fluid dynamic design criteria for a mercury condenser capable of sustaining operation in a gravity field of zero to 1g in any direction. The effects of vapor velocity and gravity vector on drop size, drop acceleration, and drop velocity were specifically examined. The results of the analyses, together with their experimental verification, are included. The correlation used for the two phase condensing pressure drop prediction and methods of interface maintenance capable of operating under the system acceleration requirement were also experimentally investigated.

A modification of the conventional meteoroid protection model was developed and applied toward system armor.

The first condenser-subcooler design, CSC I-1, based on these analytical and experimental investigations is presented. The results and analysis of the full-scale component test are discussed.

Author

The redesign of the unit into CSC I-1A based on the analysis of operational problems encountered in the component test of the initial design is covered. Additional investigations were undertaken to verify the design integrity of the modified unit. These included quantitative determination of sensitive parameters affecting parallel tube two-phase condensing flow and natural convection-radiation heat transfer from fin/tube configurations in air and argon, the latter being the system operational environment.

The successful component test of the redesigned unit and the performance analysis is discussed. Two problem areas encountered in this second test, high operating pressure and the deteriorating effect of progressive mercury-tube wall wetting, are detailed.

Conclusions and recommendations applicable to the Sunflower condenser and also to space condensers in general are listed. The design compromise involved in designing condensers for wetting mercury is investigated analytically.

The reported work represents an advancement in the state of the art in space condensing especially in the area of multiple tube stability and design criteria as a function of system acceleration.

Section 2.0
CONDENSER-SUBCOOLER DESIGN REQUIREMENTS

2.1 SYSTEM DESCRIPTION

The Sunflower I Power Conversion System is designed to supply 3 kw of useful power to an earth orbital or interplanetary vehicle. Solar radiation is used as the prime mover and a mercury Rankine cycle employing a boiler/heat storage unit, turbo-alternator, condenser, and pump accomplishes the power conversion.

Briefly, a deployable parabolic collector 32 feet in diameter focuses incident solar radiation on a hemispherical boiler. A vehicle control system orients the collector toward the sun. The boiler/heat storage unit contains a through-flow mercury boiler tube which is immersed in a lithium hydride bath to provide the heat of vaporization during shade periods of orbital flight. From the boiler, the mercury vapor passes through a three-stage turbine on a common shaft with the alternator and condensate pump. From the turbine, the vapor is delivered to the condenser-subcooler which rejects the heat of condensation, subcools the condensate, and delivers it to the pump. The system is designed to operate for a year in space and to sustain operation under accelerations of 0 to 1g in any direction as a result of orbital transfers. An artist's drawing of the system is shown in Figure 2-1.

2.2 CONDENSER-SUBCOOLER REQUIREMENTS

As part of the Sunflower system, the condenser-subcooler component is required to accept a mercury mass flow rate of 13.72 lb/min at a quality of 95.2% from the turbine outlet, condense and subcool it to 400°F, and deliver it to the pump inlet at a NPSH of 3.8 psi. The back pressure imposed on the turbine is not to exceed 7.0 psia. In addition, the liquid mercury flow used to lubricate the rotating package bearings is subcooled in the condenser-subcooler and delivered to the pump inlet along with the condensate flow.

A final requirement specifies that, due to possible shifts in the boiler interface position, the condenser-subcooler component be capable of absorbing small perturbations in inventory.

The physical space available for the condenser-subcooler component when installed in the system structure is limited by the solar rays reflected from the collector to the boiler aperture. The resulting volume is a frustrum of a cone whose bottom radius is 4 feet, top radius is 2 feet, and height is 9 feet.

As a result of the operation in a space environment, it is necessary to consider the meteoroid hazard. A requirement of 99% probability of no meteoroid puncture in one year's operation was placed on the system. The necessary protection was investigated as part of the condenser-subcooler program.

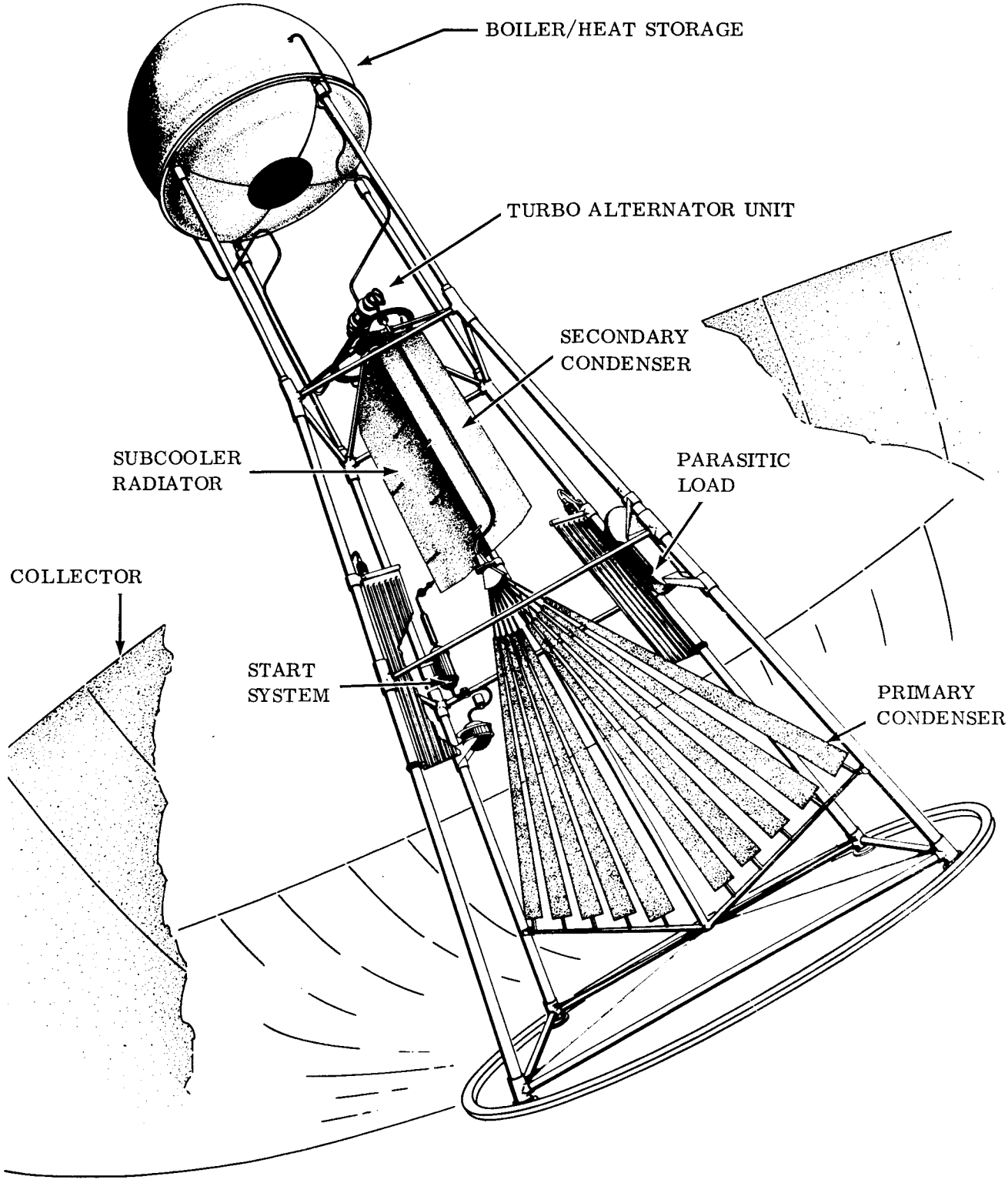

SUNFLOWER I SYSTEM

FIGURE 2-1

Section 3.0
CSC I-1

The condenser design is pressure-drop limited since high condenser pressure losses have an adverse effect on turbine output and/or pump NHSP. Complicating the situation is the Sunflower I system requirement that operation be sustained under accelerations from 0 to 1g in any direction. This requirement, combined with the high density of the mercury condensate, could create a strong destabilizing force tending to cause slugging, high pressure drop, and general maloperation of the condenser.

The acceleration requirement also has its effect on the subcooling portion of the component. To prevent cavitation in the low pressure subcooler lines due to static head losses in an adverse gravity orientation, the condensate line between the interface and pump must be maintained in close proximity to the interface. To provide adequate NPSH, the pump inlet itself must be located close to the interface.

The problem of subcooling in this acceleration environment can be adequately solved by a series of tube-in-tube exchangers coiled closely around the interface location. Cavitation of the pump or condensate lines can therefore be avoided in any gravity orientation and the boiler flow may be used as the coolant. This boiler flow could subsequently be cooled, as required, in a non-isothermal radiator with no cavitation problem since the fluid is at a high pressure.

The condensing portion of the component, however, presents a somewhat more difficult problem. Simple static tests show that the maintenance of multiple liquid/vapor interfaces in parallel tubes is very unstable if the gravitational force is such that the heavier condensate is "above" the vapor. This could be remedied by producing a large frictional pressure drop in the vapor, but a calculation shows that this pressure loss would substantially decrease system output.

Other possible solutions are the use of a spray condenser, an indirect condenser, or a single tube direct condenser. All of these result in a substantial weight penalty at the Sunflower I power level. One approach, however, that results in comparatively low weight and pressure drop is a combination of a multiple tube and single tube condenser. The majority of the condensing can be accomplished in a conventional tube array (light weight) and the remainder in a single tube (high stability) downstream from the multiple tubes. In both cases, the flow passages must be tapered to maintain the velocity of the vapor as the vapor weight flow decreases due to condensation. Maintenance of this velocity is necessary to insure that all the condensate droplets (dropwise condensation is assumed throughout this report) are carried to the interface and not allowed to accumulate.

3.1 ANALYTICAL INVESTIGATIONS

3.1.1 Fluid Dynamics

Analyses were conducted to evaluate the restrictions imposed on the condenser design as a result of the unique acceleration requirement. Specifically analyzed were the requirements for stable operation in the various gravity orientations under which the Sunflower condenser-subcooler is to operate. The following analysis which assumes dropwise condensation and no agglomeration will investigate the effect of vapor velocity on drop sizes, drop acceleration, and drop velocity.

Consider the mercury drop of Figure 3-1 hanging on a plane wall under the influence of gravity and surface tension at incipient movement where

β_m = mean contact angle with wall in degrees

$\pm\Delta\beta$ = distortion of contact angle at incipient movement, degrees

R = radius of spherical portion of drop

r_c = radius of contact circle

ρ_l = drop density

α = wall inclination to horizontal

DROP MODEL

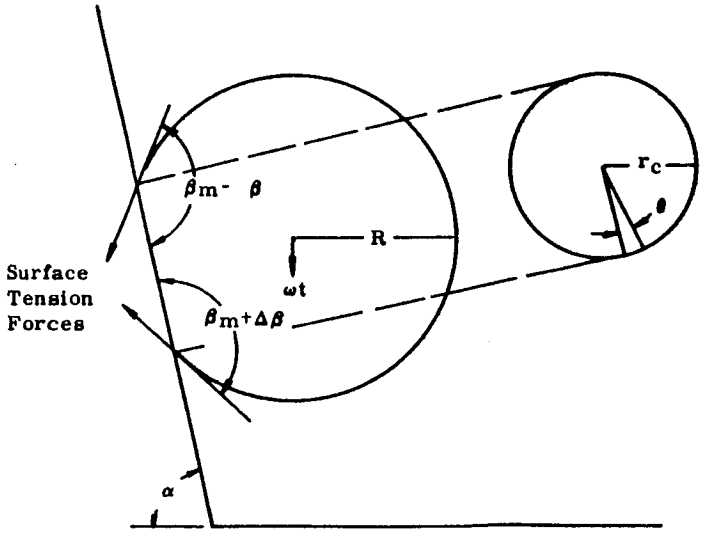

FIGURE 3-1

Summing the forces parallel to the wall at incipient movement:

$(\sin \alpha)$ x (weight) = surface tension forces

weight = (drop volume) x (density)

drop volume = (volume of sphere) - (volume of "cap")

$$= \frac{4}{3} \pi R^3 - \frac{1}{3} \pi h^2 (3R-h)$$

where h = cap height = $R - r_c \tan (\beta_m - 90)$

$$\text{Volume} = \frac{4}{3} \pi R^3 - \frac{1}{3} \pi \left[R - r_c \tan (\beta_m - 90) \right]^2 \left[2R + r_c \tan (\beta_m - 90) \right]$$

Neglecting the small effect of $\pm \Delta\beta$ on geometry and utilizing $r_c = R \cos (\beta_m - 90)$ yields

$$\text{Weight} = \frac{\rho l \pi R^3}{3} \left\{ 4 - \left[1 - \sin (\beta_m - 90) \right]^2 \left[2 + \sin (\beta_m - 90) \right] \right\}$$

$$F_w = n \sin \alpha \frac{\rho l \pi R^3}{3} \left\{ 4 - \left[1 - \sin (\beta_m - 90) \right]^2 \left[2 + \sin (\beta_m - 90) \right] \right\} \quad (1)$$

where $n = \frac{g_l}{g_c}$ $\quad g_l$ = local gravity

g_c = gravitational constant

F_w = weight component

Surface tension resultant (F_{ST}) can be expressed as (up is positive):

$$d F_{ST} \cong r_c \, d\theta \, \sigma \cos \theta \left\{ \left[- \cos (\beta_m + \Delta\beta) \right] - \left[- \cos (\beta_m - \Delta\beta) \right] \right\}$$

where σ = surface tension, liquid-gas

$$F_{ST} = 2 \int_0^{\pi/2} r_c \, d\theta \, \sigma \cos \theta \left[\cos (\beta_m - \Delta\beta) - \cos (\beta_m + \Delta\beta) \right]$$

$$F_{ST} = 2 \sigma r_c \left[\cos (\beta_m - \Delta\beta) - \cos (\beta_m + \Delta\beta) \right]$$

$$F_{ST} = 4 \sigma R \cos (\beta_m - 90) \sin \beta \sin \Delta\beta \quad (2)$$

since $r_c = R \cos (\beta_m - 90)$

Equating equations (1) and (2):

$$n \sin \alpha \; \frac{\rho_l \pi R^3}{3} \left\{ 4 - \left[1 - \sin (\beta_m - 90) \right]^2 \left[2 + \sin (\beta_m - 90) \right] \right\} = 4 R \sigma \cos (\beta_m - 90) \sin \beta_m \sin \Delta \qquad (3)$$

which expresses the force balance at incipient movement of a drop under the influences of weight and surface tension.

Reference 1 presents data which show that the distortion of the contact angle with a mercury droplet on a glass plate was $\approx \pm 10°$ at incipient movement as the plate was tilted. Using

$\beta_m = 141°$

$\Delta\beta = 10°$

σ = 0.0326 lb/ft (This value is for ambient temperatures; it is somewhat lower for higher temperatures. See reference 2.)

$\rho_l = 800 \text{ lb/ft}^3$

and plotting R versus sin α yields the curve of Figure 3-2. The experimental data of Reference 3, which is in good agreement with equation (3), is also plotted.

It is interesting to compare this same data with an approach found in Reference 4. Here the sine of the angle of tilt of the plate at incipient movement of a drop on the plate is given as

$$\sin \alpha = \frac{(\cos \beta_R - \cos \beta_A)}{(\rho / \sigma) C} V^{-2/3}$$

where $C = AV^{-2/3}$

β_R = receding contact angle

β_A = advancing contact angle

V = drop volume

A = area of the section cut by the plane of symmetry through the drop

DROP RADIUS AT INCIPIENT MOVEMENT MERCURY ON GLASS

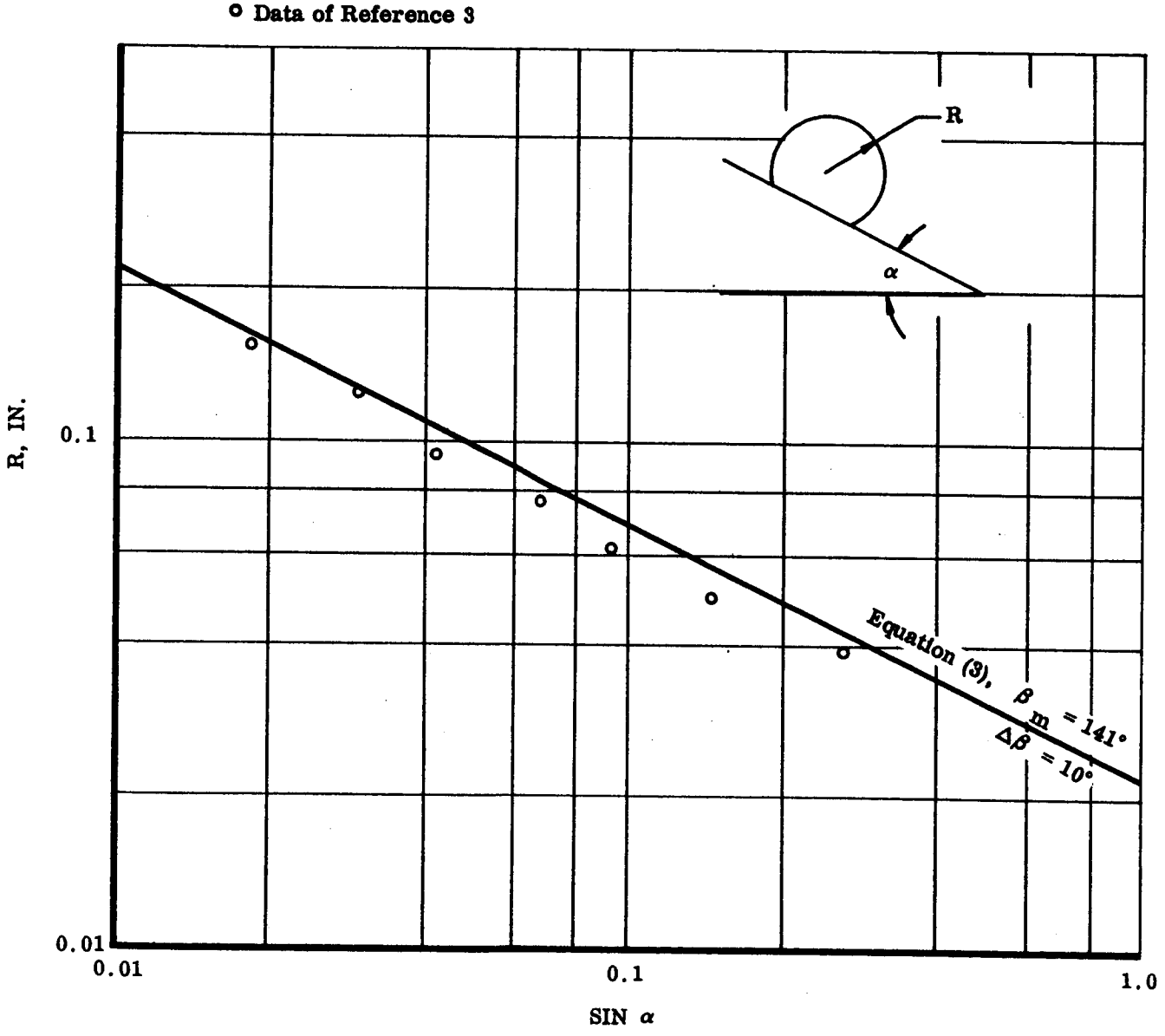

FIGURE 3-2

The authors of Reference 4 experimentally verified this relationship with a wetting fluid. However, if B_R and B_A are evaluated for mercury (a non-wetting fluid) as proposed in this report by subtracting and adding 10° to the mean contact angle, respectively, good agreement is obtained between the theory in Reference 4 and the data of Reference 3 (see Figure 3-3). This agreement lends some confidence to the assumption of a ± 10° deflection of the contact angles at incipient drop movement that is made in the analysis of this section.

This analysis considers no R/D effect where D is the tube diameter. However, at the tube diameter to be used in the Sunflower condenser, this ratio is small enough to use the flat plate analogy. Reference 3 justifies this assumption by experimental data similar to Figure 3-2 for drops in tubes of various diameters.

Next, the drag of the vapor on the condensing drop as it occurs in an actual condenser will be considered. This term in the force balance can be expressed as:

$$F_D = \frac{\rho_v V_v^2}{2 g_c} C_D Ap \qquad (4)$$

where

F_D = drag force

ρ_V = vapor density

V_V = vapor velocity

C_D = drag coefficient

A_p = projected area

Here the value of C_D must be evaluated. Reference 3 suggests that based on values of C_D for spheres, drops, and freely rising vapor bubbles, an average value of 1.0 may be used, especially in the 100 to 200 range of drop Reynolds numbers expected in the Sunflower application.

Evaluating Ap as a function of β_m results in (see Figure 3-1)

$$A_p = \frac{\beta_m}{180} (\pi R^2) + r_c^2 \tan (\beta_m - 90)$$

$$A_p = R^2 \left[\frac{\pi \beta_m}{180} + \sin (\beta_m - 90) \cos (\beta_m - 90) \right]$$

COMPARISON OF REFERENCES 3 AND 4 - MERCURY DROPS ON PLATE

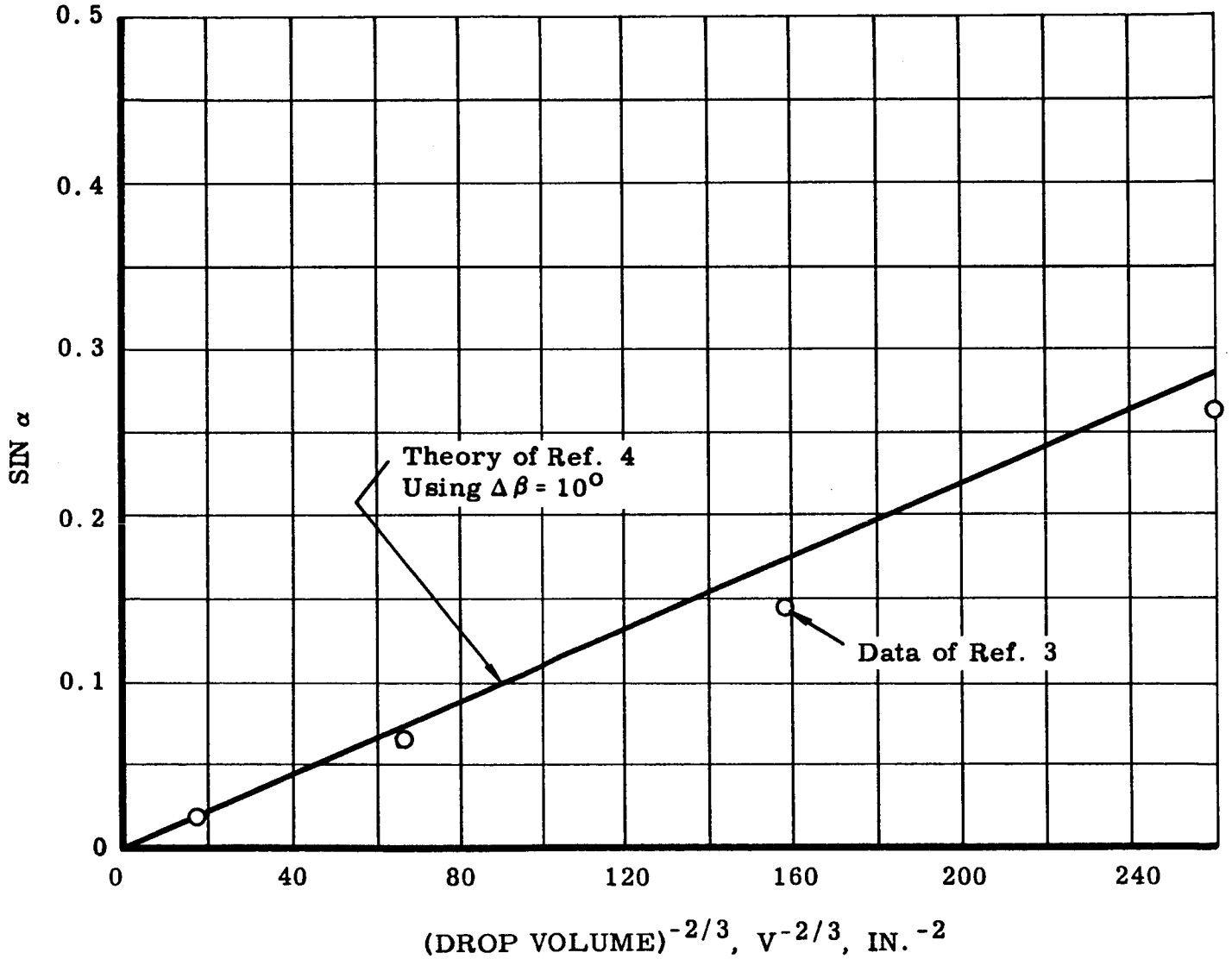

FIGURE 3-3

where β_m is in degrees. Finally,

$$F_D = \frac{\rho_V V_V^2 C_D}{2 g_c} R^2 \left[\frac{\pi \beta_m}{180} + \sin (\beta_m - 90) \cos (\beta_m - 90) \right] \quad (5)$$

The general equation of a drop in a mercury condenser, about to be swept (or fall) off a tube wall, may be written

Drag + weight component ± surface tension resultant = 0

$$\frac{\rho_V V_V^2 C_D}{2 g_c} R^2 \left[\frac{\pi \beta_m}{180} + \sin (\beta_m - 90) \cos (\beta_m - 90) \right] + n \sin \alpha \frac{\rho_l \pi R^2}{3} \left\{ 4 - \left[1 - \sin (\beta_m - 90) \right]^2 \left[2 + \sin (\beta_m - 90) \right] \right\} \pm 4 \sigma R \cos (\beta_m - 90) \sin \beta_m \sin \Delta\beta = 0 \quad (6)$$

To evaluate the drop diameters at the extreme conditions, four cases will be assumed. In Case I, flow is in opposition to gravity (assume in all cases that vapor velocity is in the positive direction) and the drop is about to be torn off the wall by the vapor drag against the forces of weight and surface tension (n = -1, α = 90°, $\Delta\beta$ = 10°, surface tension sign is negative). In Case II, flow is in the direction of gravity and the drop is about to be torn off the wall by drag and weight and retarded by surface tension (n = 1, α = 90°, $\Delta\beta$ = 10°, surface tension sign is negative). In Case III, zero gravity exists (n = 0, $\Delta\beta$ = 10°, surface tension sign is negative), and in Case IV flow is in opposition to gravity and the drop is about to fall off the wall back toward the condenser inlet against the forces of drag and surface tension (n = -1, α = 90°, $\Delta\beta$ = 10°, surface tension sign is positive). Case IV is the unstable case. Using the Sunflower I operating level, plots of the diameter of equivalent spherical drops versus vapor velocity for the four cases are shown in Figure 3-4.

Also plotted in Figure 3-4 are data from Reference 5. These data were obtained by accurately measuring the diameter of a mercury drop in a glass tube and then flowing nitrogen through the tube at a constantly increasing velocity until the drop was torn off and transported downstream. The data were taken with horizontal gas flow and should presumably match the zero g curve or Case III. The nitrogen pressure and temperature during these tests was such that the nitrogen density was essentially that of mercury vapor at 600°F. The close agreement of this independently obtained data is an additional verification of the analytical approach presented in this section.

From the graph, it is evident that the most critical case occurs when the flow is in opposition to 1g; i.e., a vapor velocity of at least 45 ft/sec is needed throughout the condenser to assure that all the condensate will be delivered to the interface when flow is against gravity (Case I rather than Case IV).

DROP SIZE AS A FUNCTION OF VAPOR VELOCITY AND GRAVITY ENVIRONMENT

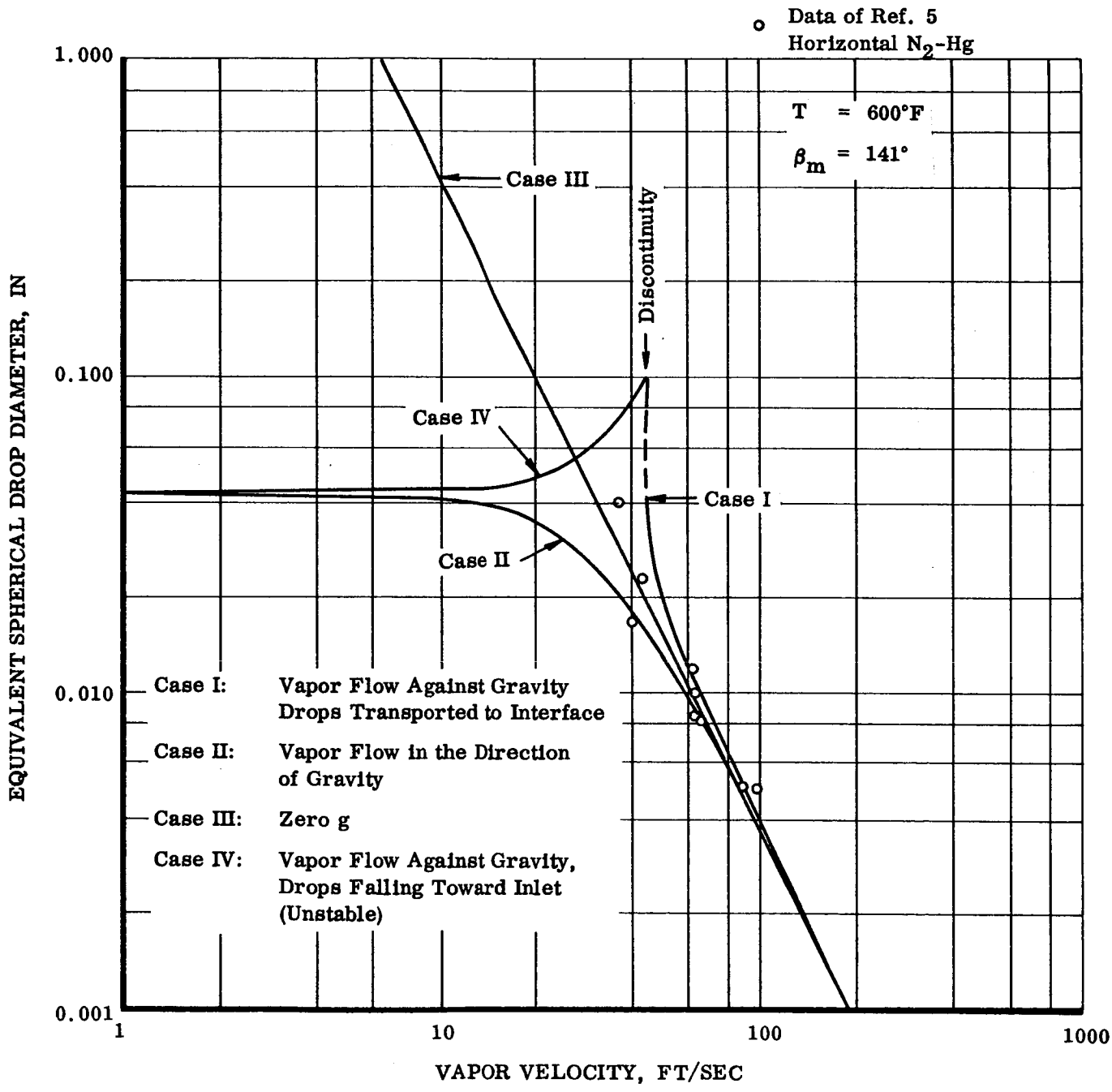

FIGURE 3-4

Furthermore, it is important that the drops have sizeable accelerations when torn off the wall to avoid high liquid hold-up and agglomeration. Once a drop is torn off the wall, its acceleration can be calculated. Initial drop acceleration for Cases I, II, and III are shown in Figure 3-5. Here the drop is assumed to have the same volume as it did when torn off and its shape is a sphere. The accelerating force is then the drag + weight, with the appropriate sign.

From examination of Figures 3-4 and 3-5, it appears that a vapor velocity of approximately 60 ft/sec is sufficient to make the sensitivity of the Sunflower I condenser-to-gravity orientation negligible. At this velocity, the drop diameters would vary from 0.0096 to 0.0116 inch with initial accelerations from 11 to 15g.

To gain greater insight into the operation of the condenser, it would be helpful to know drop velocity as a function of length of travel, assuming constant drop size during travel and no collisions with other drops or tube walls. The assumptions made limit the value of the following analysis, but consideration of these effects is difficult. The results of the analysis, therefore, should be examined with this reservation in mind.

Examine a condenser with vapor flow against gravity (previously determined as most severe case). The drop has been entrained and is on its unmolested way to the interface. Determine its velocity as a function of length.

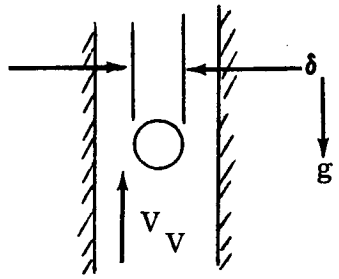

where

V_D = drop velocity

V_V = vapor velocity

δ = drop diameter

Assume V_V is a constant since it has been previously determined that vapor velocity will have to be maintained throughout the condenser with flow against gravity.

INITIAL DROP ACCELERATION VERSUS VAPOR VELOCITY

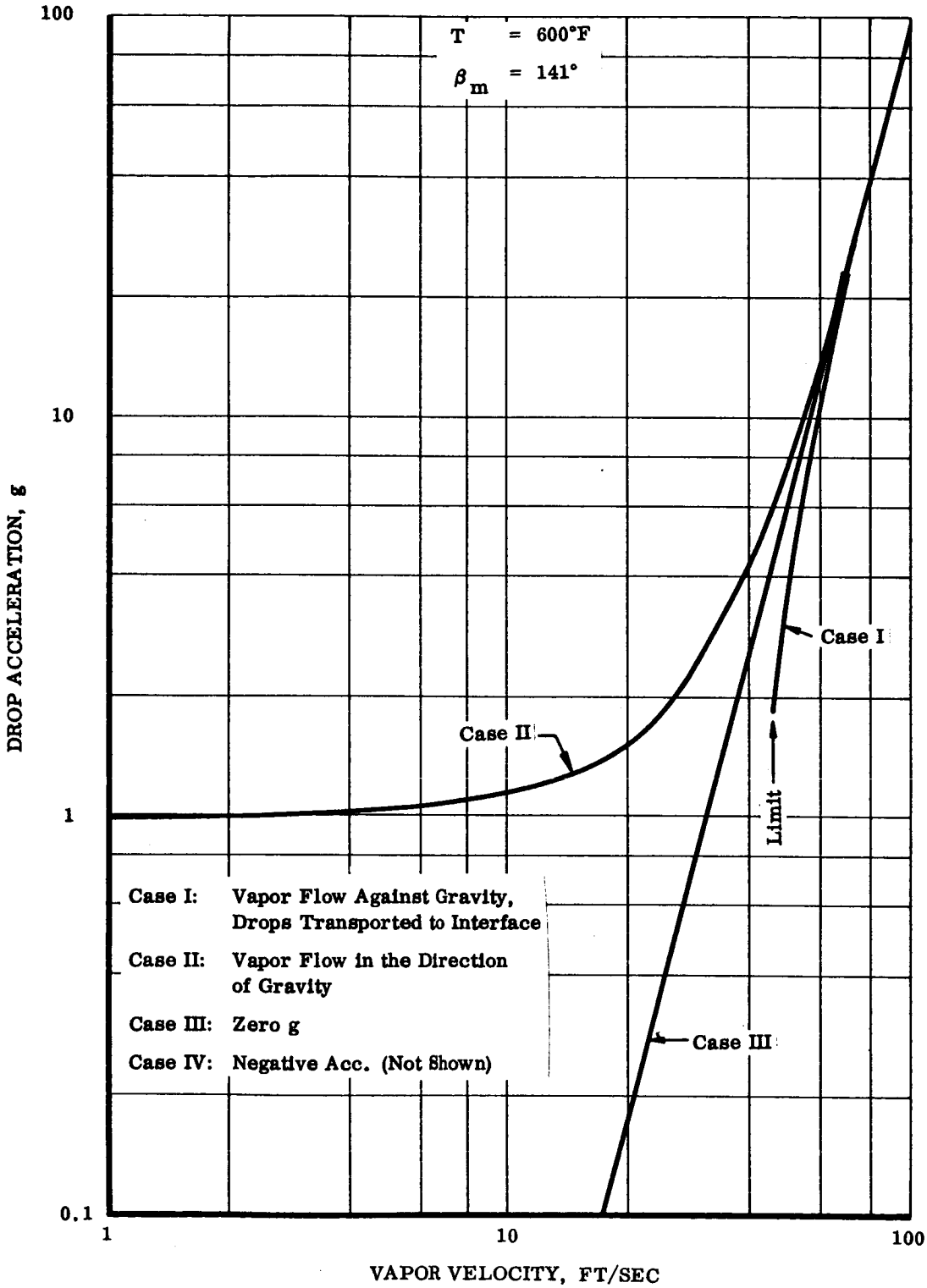

FIGURE 3-5

$$F = ma$$

$$\frac{C_D \pi \delta^2}{4} \frac{\rho_v (V_V - V_D)^2}{2 g_c} \pm \frac{n \pi \delta^3 \rho_l}{6} = \frac{\pi \rho_l \delta^3}{6 g_c} \frac{d^2 L}{d t^2} \quad (7)$$

let $\epsilon = \frac{V_D}{V_V}$, then $(V_V - V_D)^2 = V_V^2 (1 - \epsilon)^2$ and

$$\frac{d^2 L}{dt^2} = V_D \frac{dV_D}{d L} = V_V^2 \frac{\epsilon d \epsilon}{dL} \quad (V_V = \text{const.})$$

Re-writing equation (7) results in

$$\frac{\epsilon d \epsilon}{dL} = \left(\frac{3 C_D \rho_V}{4 \delta \rho_l} \right) (1 - \epsilon)^2 \pm \frac{n g_c}{V_V^2}$$

let $K_1 = \frac{3 C_D \rho_V}{4 \delta \rho_l}$ and $K_2 = \pm \frac{n g_c}{V_V^2}$

Integrating:

$$L = \frac{1}{2K_1} \ln \left[(\epsilon - 1)^2 - \frac{K_2}{K_1} \right] + \frac{1}{2 K_1 \sqrt{K_2/K_1}} \ln \left(\frac{\epsilon - 1 - \sqrt{K_2/K_1}}{\epsilon - 1 + \sqrt{K_2/K_1}} \right) + C \quad (8)$$

at $L = 0$, $\epsilon = 0$; then

$$C = \left[\frac{1}{2 K_1} \ln \left(1 - \frac{K_2}{K_1} \right) \right] + \frac{1}{2 K_1 \sqrt{K_2/K_1}} \ln \left(\frac{1 + \sqrt{K_2/K_1}}{1 - \sqrt{K_2/K_1}} \right) \quad (9)$$

Combining equations (8) and (9) yields the variation of ϵ with L from which the value of V_d with L may be obtained. Assuming a vapor velocity of 60 ft/sec, the drop size (δ) for operation against gravity for the Sunflower operating temperature is 0.0113 inch (from Figure 3-4). Using these and previously determined values of C_D, ρ_V, ρ_i, and n = -1, evaluation of the constants and determination of the variation in V_D with L results in the curve of Figure 3-6. Letting $L = \infty$ gives a limit on V_D where drag equals weight at 44.5 ft/sec. With an expected condenser tube length of $\approx$ 8 ft, it appears that the drop acceleration and resultant drop velocities from a vapor velocity of 60 ft/sec are sufficient for proper condenser operation. For instance, with an 8 ft condenser and linearly decreasing heat rejection, the mean length of drop travel would be 2/3 x 96 inches or 64 inches. This gives a mean drop velocity at the tube outlet of 35 ft/sec with flow against gravity.

DROP VELOCITY VS LENGTH OF TRAVEL
(β_m = 141°, T = 600°F, V_V = 60 fps against 1 g)

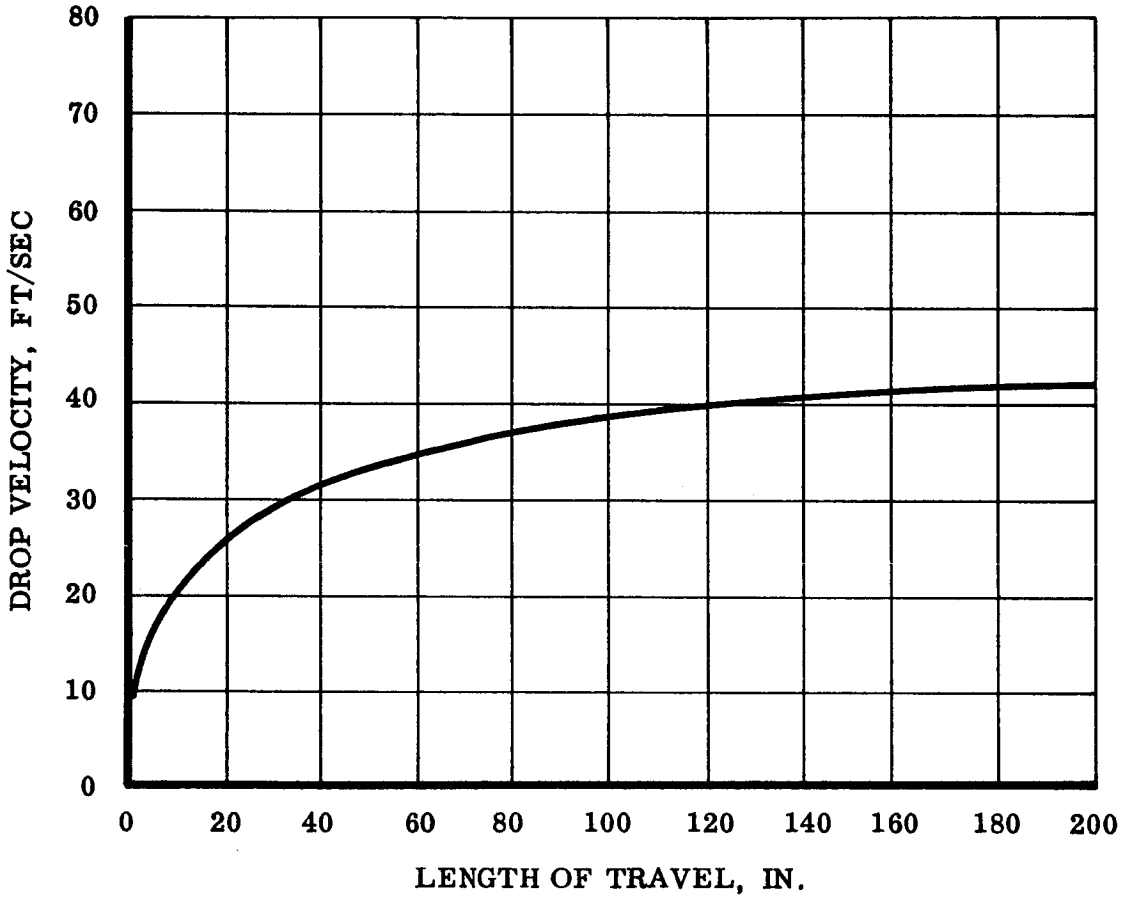

FIGURE 3-6

3.1.2 Meteoroid Protection

Upon initial investigation of the meteoroid protection requirements of the Sunflower I system, it became obvious that if the conventional conservative assumptions were used, an extremely heavy armor would result. For example, from Reference 6 (best data available at the time of the condenser design) Bjork proposed the following equation for meteoroid protection.

$$t_p = \frac{2.5 \times 10^{-4} \, KV^{1/3} \, (A\tau)^{3/10}}{\ln \left[(P_{(o)})^{3/10} \right]} \qquad (10)$$

where

t_p = protection thickness, cm

V_m = meteorite velocity, km/sec

A = vulnerable area in square meters

$P_{(o)}$ = probability of no penetration

τ = exposure time, sec

K = constant, 1.64 for aluminum and 0.908 for steel

Using V = 28 km/sec (velocity of important meteoroids) and the Sunflower requirements of τ = one year, or 3.15×10^7 seconds, and $P_{(o)} = 0.99$, the equation becomes

for steel $t_{ps} = 0.0942 \, A^{3/10}$

for aluminum $t_{pa} = 0.170 \, A^{3/10}$

where A is in ft^2

t is in inches

These curves are plotted on Figure 3-7.

Assuming a system vulnerable area of 50 ft^2 and steel protection yields a protection thickness of

$$t_{ps} = 0.0942 \, (50)^{0.3} = 0.304 \text{ in.}$$

METEOROID PROTECTION

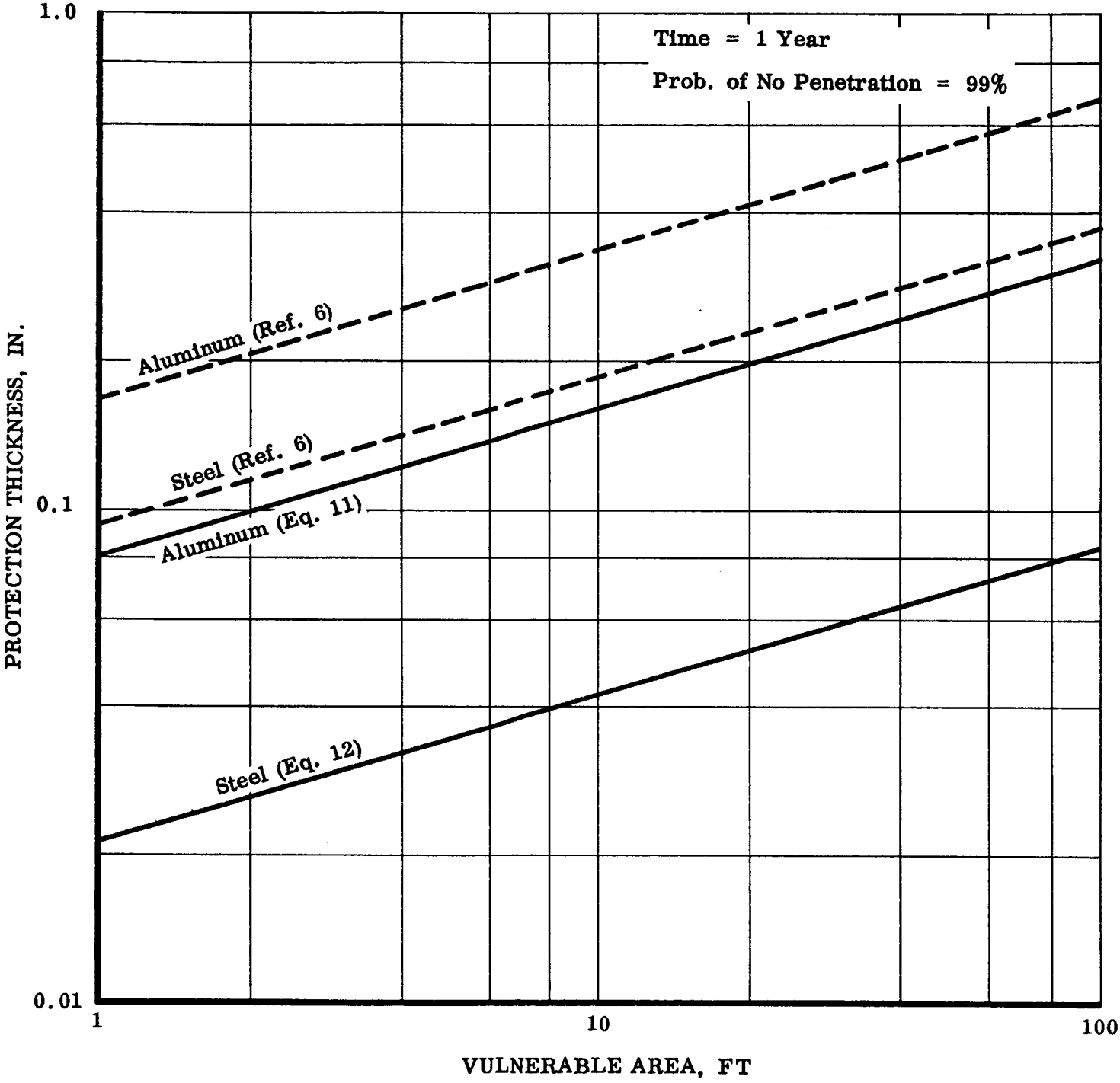

FIGURE 3-7

The approximate system protection weight should be

$$\text{Weight} = At_{ps}\rho = 632 \text{ lb}$$

or, if aluminum were used, the weight would be

$$\text{Weight} = 378 \text{ lb}$$

Aluminum, however, cannot be used for the complete system meteoroid protection. Steel must be used for all mercury and lithium hydride (boiler) contacting surfaces. In addition the steady state temperature of the boiler shell is too high for use of aluminum. At any rate, the meteoroid protection with this penetration model, exposure time, and probability consume between 400 and 600 lb or a significant proportion of the proposed system weight.

Equation (10) was derived assuming equal densities of the projectile or meteoroid and target or protection material. It is reasonable to assume, however, that there is some relationship between the protection thickness and densities of the target and projectile. There is speculation that the largest meteoroids have a density on the order of 0.05 gm/cc (roughly that of dust, due to their porosity) and the smallest that of stone or 2.8 gm/cc. Using these values for meteoroids of visual magnitude 1 and 30, respectively, and using a straight line interpolation results in a meteoroid density of $\sim$ 0.95 gm/cc (see Figure 3-8a) for the important meteroids, i.e., those with a high enough mass and high enough flux to seriously consider.

Summers and Charters (Reference 7) performed a series of tests impacting projectiles on copper and lead targets at velocities of 7000 ft/sec and found that penetration depth for copper targets, $\rho_t = 8.9$ gm/cc, varied as $(\rho_p / \rho_t)^{0.6}$, and for lead targets, $\rho_t = 11.3$ gm/cc, as $(\rho_p / \rho_t)^{0.3}$. Plotting these exponents against target density yields the curve of Figure 3-8b. Here the line is drawn asymptotic to 1.0 since a value of the exponent greater than one would give a decreasing protection thickness for a decreasing target density. The resulting values of the exponent of the (ρ_p / ρ_t) term are 0.70 for steel and 0.95 for aluminum. Multiplying Bjork's equations by the density ratios raised to the proper powers yields

$$t_s = 0.0213 \, A^{(0.3)} \tag{11}$$

$$t_a = 0.0816 \, A^{(0.3)} \tag{12}$$

These equations are also plotted in Figure 3-7 and were used to determine the meteoroid protection thickness for the Sunflower system.

To compare the weight of aluminum and steel protection (other materials with obvious advantages, such as beryllium, were not considered for the initial design due to cost and complexity of fabrication):

a. POSSIBLE METEOROID DENSITY VS VISUAL MAGNITUDE

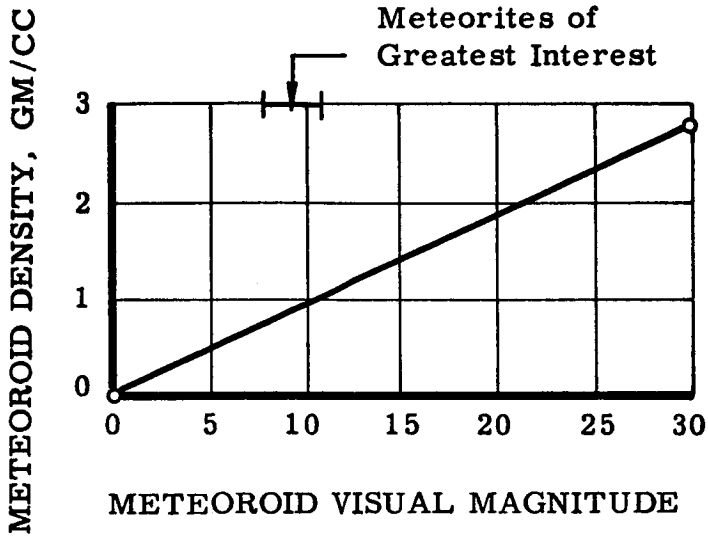

b. EXPONENT OF DENSITY RATIO TERM VS DENSITY OF PROTECTION MATERIAL

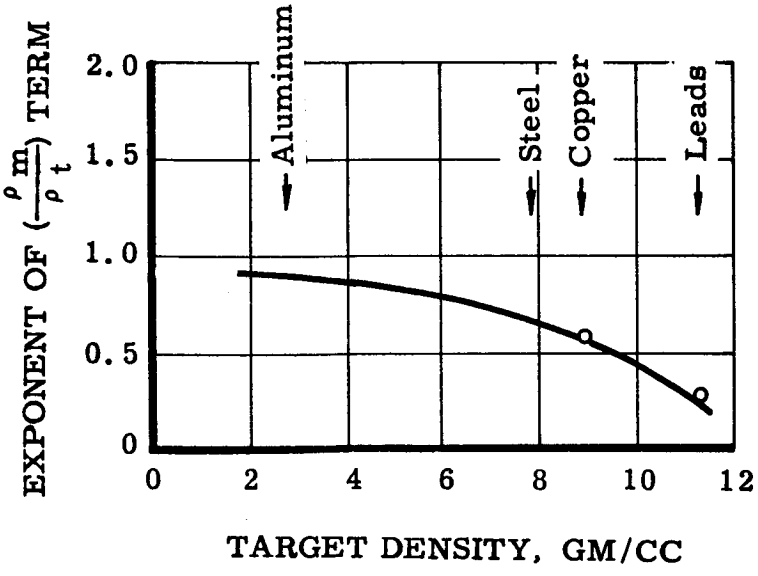

FIGURE 3-8

$$\frac{\text{steel protection wt}}{\text{aluminum protection wt}} \approx \frac{0.0214\, A^{0.3}\, \rho_s A}{0.0816\, A^{0.3}\, \rho_a A}$$

$$\approx 0.77$$

This indicates that using aluminum meteoroid protection affords no weight advantage over complete steel protection. Since steel must be used for all mercury contacting surfaces and for the boiler shell, its use for complete meteoroid protection is indicated. Bumper screen-type protection was not used for the condenser because of the uncertainty in its effect and its possible influence on condenser heat rejection. This concept might be used to protect the boiler, however, if its effect could be predicted.

The liberties taken in the analysis are realized, but the conservatism in making no correction whatsoever in Bjork's basic equation makes meteoroid protection for an approximately 50 ft^2 area with a probability of 99% of no puncture in one year prohibitive from a weight standpoint. The modifications made are predictions of the continuation of trends indicated by early experiments. Since aluminum is not used for meteoroid protection, the most glaring extrapolation is eliminated.

3.2 DESIGN PRESENTATION

3.2.1 Condenser

The Sunflower I system operating requirements (power level and environmental conditions) determined the basic condenser-subcooler configuration. At the Sunflower I power level, the condenser heat rejection is such that a flat plate parallel tube direct radiator was chosen for rejecting the heat of condensation because of its weight advantage over an indirect heat rejection system. Furthermore, due to the ± 1g operating requirement, it was necessary to maintain a relatively high vapor velocity throughout the condenser to assure delivery of all the liquid to the interface (see Secion 3.1.1). This necessitated the tapering of the inlet and exit headers to accommodate the addition or removal of vapor, and the tapering of the parallel condensing tubes due to the decreasing vapor flow rate as condensation occurs. The subcooler heat exchangers had to be kept close to the pump inlet to prevent static head losses from cavitating either the pump or the interface-to-pump line.

The flowing quality of the vapor-condensate mixture leaving the parallel tube portion of the condenser is an independent variable. From a weight standpoint, the lower this figure the lighter the condenser, realizing the heat must be rejected elsewhere if not in the parallel tube condenser. The proposed means of rejecting the residual latent heat was in a tube-in-tube heat exchanger just upstream of the interface chamber. The high pressure liquid-mercury intended to remove the heat of subcooling was used as a heat sink. A value of 1% was chosen based on the available heat capacity in the coolant. Although this value appears low at first examination, the density ratio of liquid to vapor is approximately 6700 to 1 at the condenser operating pressure, which makes the flowing volume fraction about 1/67 at 1% quality.

Another independent variable is the type of tube taper. Two types were considered: linear diameter taper and linear area taper. The former had a slight weight advantage and fit very well into the trapezoidally-shaped area available for the condenser, since, to maintain a constant vapor velocity in the tube, a decreasing rate of heat rejection with attendant decreasing fin width with length results. For example, assume a linear diameter tapered condenser tube.

$$D = D_0 \left(1 - \frac{L}{L_T}\right)$$

where D = the tube diameter at length, L

D_0 = the initial tube diameter

L_T = the length where the tube diameter would be zero. (Actually, the tube will end before this point at L_c.)

$$A = A_0 \left(1 - \frac{L}{L_T}\right)^2$$

where A = the tube cross sectional area at L

A_0 = the initial cross sectional area.

Furthermore, given constant vapor velocity and assuming constant vapor density:

$$\dot{m}_V = \dot{m}_{V0} \left(1 - \frac{L}{L_T}\right)^2 \tag{13}$$

where

$\dot{m}_V$ = vapor flow rate at any point

$\dot{m}_{V0}$ = initial vapor flow rate

but $$\dot{m}_V = \dot{m}_{V0} - \frac{1}{h_{fg}} \int_0^L q_{(L)}\, dL \tag{14}$$

where $q_{(L)}$ is the heat rejection per unit time and length along the tube

Equating (13) and (14)

$$\dot{m}_{V0} - \frac{1}{h_{fg}} \int_0^L q(L)\, dL = \dot{m}_{V0} \left(1 - \frac{L}{L_T}\right)^2$$

Differentiating:

$$q_{(L)} = \frac{2\, h_{fg}\, \dot{m}_{V0}}{L_T} \left(1 - \frac{L}{L_T}\right) \tag{15}$$

which indicates a linear decrease in $q_{(L)}$ along the tube.

Assuming now a constant area tapered tube and a constant vapor velocity,

$$A = A_0 \left(1 - \frac{L}{L_T}\right)$$

$$\dot{m}_V = \dot{m}_{V0} \left(1 - \frac{L}{L_T}\right) = \dot{m}_{V0} - \frac{1}{h_{fg}} \int_0^L q_{(L)}\, dL$$

$$\dot{m}_{V0} \left(-\frac{L}{L_T}\right) = -\frac{L}{h_{fg}}\, q_{(L)}$$

$$q_{(L)} = \frac{\dot{m}_{V_0}\, h_{fg}}{L_T}$$

which indicates a constant $q_{(L)}$. If the latter variations were used, the fin efficiency necessary at the small end of the trapezoidally shaped available space would have to be greater than 100%. The choice of linear diameter taper was thus determined.

With the available pressure drop between the turbine outlet and pump inlet of 3.2 psi, it was felt that a 1 psi two-phase condensing drop could be permitted in the condenser tubes. The remainder of the pressure drop would be consumed in friction and bend losses elsewhere. Based on the work of previous investigations conducted at TRW on mercury condensing pressure drops (Reference 2) the overall two-phase pressure drop in a condenser could be predicted based on the pressure drop that would exist in the condenser if only the vapor phase were present. This ratio, $\Delta P_{TF}/\Delta P_V$ or Φ_{INT}, has been plotted versus an inlet parameter for various condenser configurations and is shown in Figure 3-9. Included in this plot are constant diameter and tapered diameter condenser tubes, both horizontal and tilted. In all cases, however, the ratio Φ_{INT} is near 1.5 at values of $N_{Re0}\,(V_V/10)^{1.25}$ above 8000. Since, in this condenser design, the outlet quality will be 1%, its comparison with condensers of 0% outlet quality is reasonable. Some difference may admittedly exist in the Φ_{INT} value of a tapered tube

PRESSURE DROP TEST RESULTS FOR MERCURY CONDENSING IN GLASS TUBES

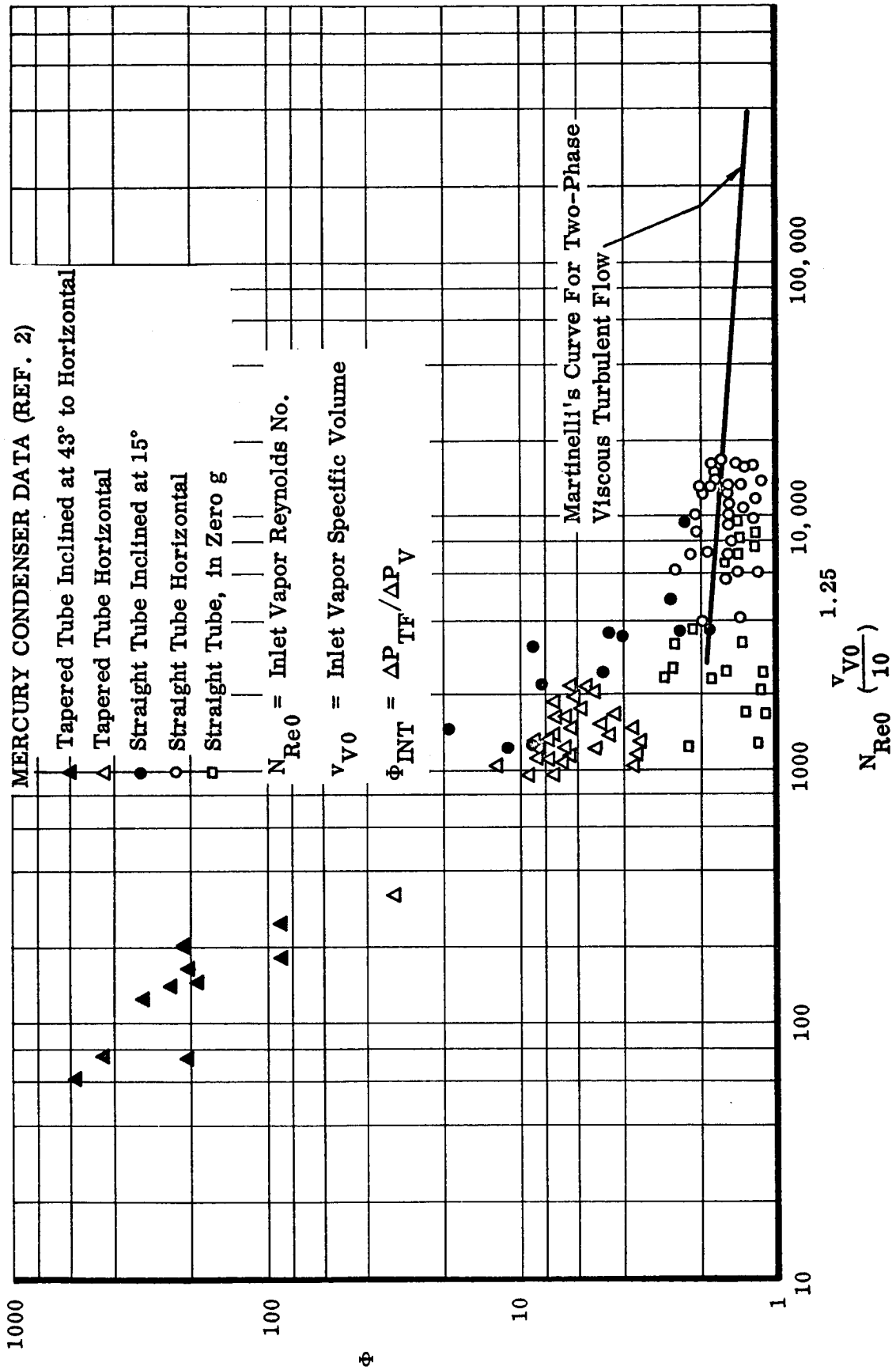

FIGURE 3-9

condenser when plotted versus an inlet parameter only. However, a single step-tapered condensing tube similar in geometry to a single tube in the full-scale prototype condenser was to be breadboard tested prior to condenser fabrication to verify the analysis conducted with respect to vapor velocity and pressure drop.

With a pressure drop, inlet and outlet conditions, meteoroid protection, and minimum values of sensitive parameters defined, a weight optimization can be conducted.

3.2.2 Condenser Weight Minimization

The basic unknowns to be determined are the length and number of tubes, tube diameters, and vapor velocity. The latter will be checked to meet the requirements of Section 3.1.1.

First, express the relationship of vapor velocity, tube length, and tube inlet diameter to the pressure drop.

$$dP_V = f_V \frac{\rho_V V_V^2}{2g} \frac{dL}{D}$$

where ρ = vapor density

V_V = vapor velocity

f_V = vapor friction factor

dL = incremental length

dP_V = incremental vapor pressure drop

but $\Delta P_{TF} = \Phi \Delta P_V$

and $\Delta P_s = \Delta P_{TF} \pm \Delta P_m$

where ΔP_s = static pressure drop

ΔP_m = momentum pressure gain or loss.

However, Section 3.1.1 showed that the drops will reach the end of the tube at varying velocities. Although the integrated effect of these velocities on the momentum pressure recovery could be calculated, a recovery of zero (all drops traveling at the vapor velocity) will be assumed as a factor of safety; i.e., if some of the drops do not reach vapor velocity at the end of the condenser tube, they would cause a pressure rise (since they were originally traveling as vapor at the vapor velocity) which would lower the pressure drop.

Therefore

$$\Delta P_s \approx \Delta P_{TF} = \Phi \Delta P_V$$

$$\Delta P_s = \Phi \int_0^{L_c} f_V \frac{\rho_V V_V^2}{2g} \frac{dL}{D}$$

where L_c = condenser length

but $N_{Rev} = \frac{\rho_V D V}{\mu_V}$ (ρ_V assumed constant)

and $f_V = \frac{0.316}{(N_{Reo})^{1/4}}$ (smooth tube)

V_V = constant

$D = D_0 (1 - \frac{L}{L_T})$

If the outlet quality is to be 1%, from equation (13)

$$L_c = 0.9 L_T$$

$$\Delta P_s = \Phi \int_0^{0.9 L_T} \frac{0.316 \mu^{1/4} \rho_V V_V^2 dL}{\rho_V^{1/4} \left[D_0 (1 - \frac{L}{L_T}) \right]^{1/4} V_V^{1/4} D_0 (1 - \frac{L}{L_T})}$$

$$\Delta P_s = \frac{3.12 \Phi (0.316) \mu^{1/4} \rho^{3/4} V_V^{7/4} L_T}{D_0^{5/4} 2g}$$

Given (for Sunflower condenser conditions):

$\Phi = 1.5$

$\mu = 0.367 \times 10^{-4}$ lb/ft-sec

$\rho_V = 0.120$ lb/ft^3

$g = 32.2$ ft/sec

$\Delta P_s = 144$ lb/ft^2

results in

$$\frac{V^{7/4} L_T}{D_0^{5/4}} = 4.53 \times 10^5 \qquad (16)$$

V in ft/sec

L_T in ft

D_0 in ft

Also from continuity

$$\dot{m}_{V0} = \rho_0 V_V A_0 N$$

where $\dot{m}_{V0}$ = inlet vapor weight flow

A_0 = cross sectional area of tube at inlet

N = number of tubes

resulting in

$$V_V D_0^2 N = 2.68 \text{ ft}^3/\text{sec}$$

The vulnerable area of the condenser tubes is

$$A_V = \pi D_{AVG} L_c N$$

and the tube weight is

$$\text{tube weight} = \int_0^{L_c = 0.9 L_T} \frac{\pi \left[(D + 2 t_p)^2 - D^2 \right] dL \, N \rho_t}{4}$$

t_p = prot. thickness

ρ_T = tube material density

$$\text{tube weight} = t_p N \rho_t \pi L_T (0.495 D_0 + 0.9 t_p) \qquad (19)$$

The header vulnerable areas will be taken as $\pi D_{AVG} L$ and the weight as $\pi D_{AVG} t_p L \rho_{HDR\ MAT}$. Other items in the condenser subcooler component will not be considered in weight optimization (i.e., the inlet tube from turbine exhaust to condenser inlet header, the outlet tube from the condenser to subcooler, and the subcooler itself) since their vulnerable area is fixed and not affected by the condenser configuration. Their presence, of course, will be considered when determining vulnerable area and overall condenser-subcooler weight. Fins will be sized in accordance with Reference 8.

The tube and header material for the prototype condenser was 347 stainless steel. Choice was based on compatibility with mercury, adequate strength at moderate temperature, ease of fabricating (welding), and moderate cost. Fin material was chosen as 1100-0 aluminum for its high thermal conductivity. Its poor strength was not a factor because the fins were not relied upon for load carrying capability.

The fin coating chosen for this unit was a high emissivity ($\epsilon \approx 0.85$), high temperature enamel. The unit was to be used as a ground unit only although it was designed for space operation by being weight minimized, relying on radiation to space for heat rejection, and operating in any gravity orientation. Therefore, money and time were saved by deferring the choice and application of a space coating to a later unit.

One last input prior to a weight optimization is the physical space available for the condenser. Limited by the solar rays reflected from the inner edge of the collector to the boiler cavity, this area was a frustrum of a cone with 8 ft and 4 ft diameter bases and a 9 ft height.

The independent parameters then are number of tubes, tube length (less than 9 ft), total inlet header length (less than 8 ft), and total outlet header length (less than 4 ft).

Starting with an assumed length of 8 ft, inlet header of 8 ft, and outlet header of 1.5 ft, the variation of weight with number of tubes is shown in Figure 3-10a. An eighteen tube condenser appears to result in near minimum weight. The small advantage in a twenty tube condenser is not justified due to the increased fabrication difficulty and decreased reliability.

By varying the condenser length, inlet header length, and outlet header length from these values, results in the weight variations shown in Figures 3-10b and 3-11. The weight optimized condenser then contains 18 parallel tubes arranged in a trapezoid with bases of 8 and 1.5 ft and a height of 8 ft.

This optimization also fixed the condensing tube inlet diameter at 0.598 in. and the exit diameter at 0.0598 in. The resulting condensing tube vapor velocity was a constant 60 ft/sec as compared to the minimum entrainment velocity in a 1g environment of 45 ft/sec (see Section 3.1.1). The resulting value of the parameter $N_{Re}(W_O/10)^{1.25}$ was 9100 which was acceptably above the design minimum of 8000 for a Φ_{INT} of 1.5. In order to provide equal vapor flow to each tube, the inlet header was step-tapered to produce constant static pressure in the header. Assuming a 70%

a. CONDENSER WEIGHT AS A FUNCTION OF THE NUMBER OF CONDENSER TUBES

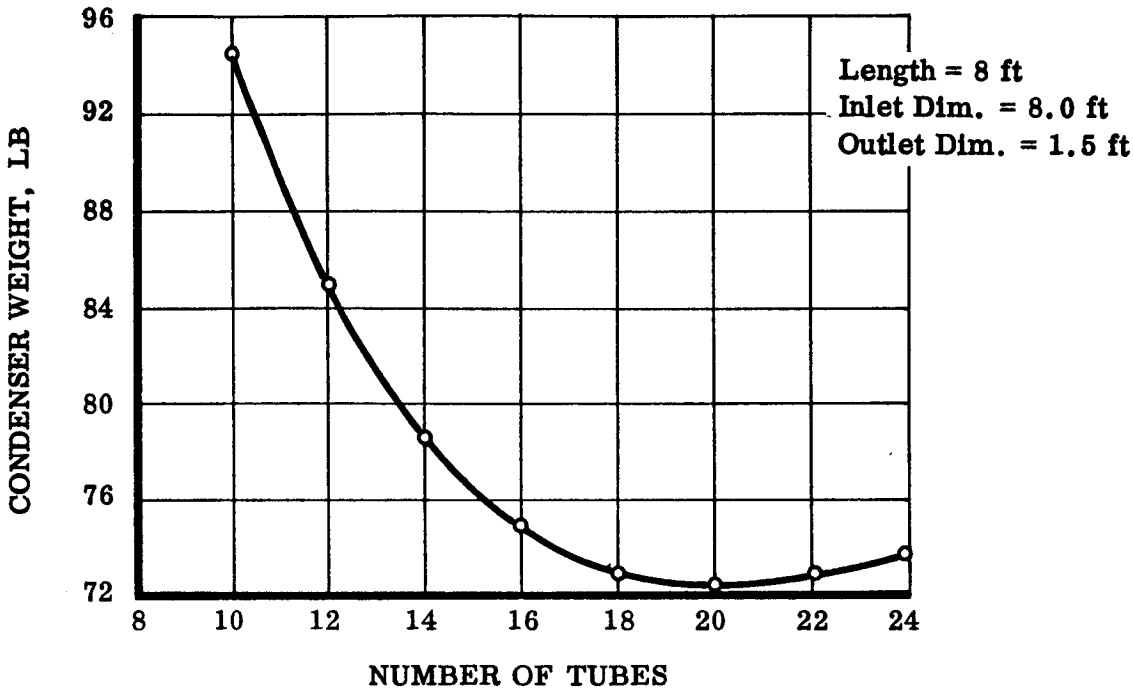

b. CONDENSER WEIGHT AS A FUNCTION OF TUBE LENGTH

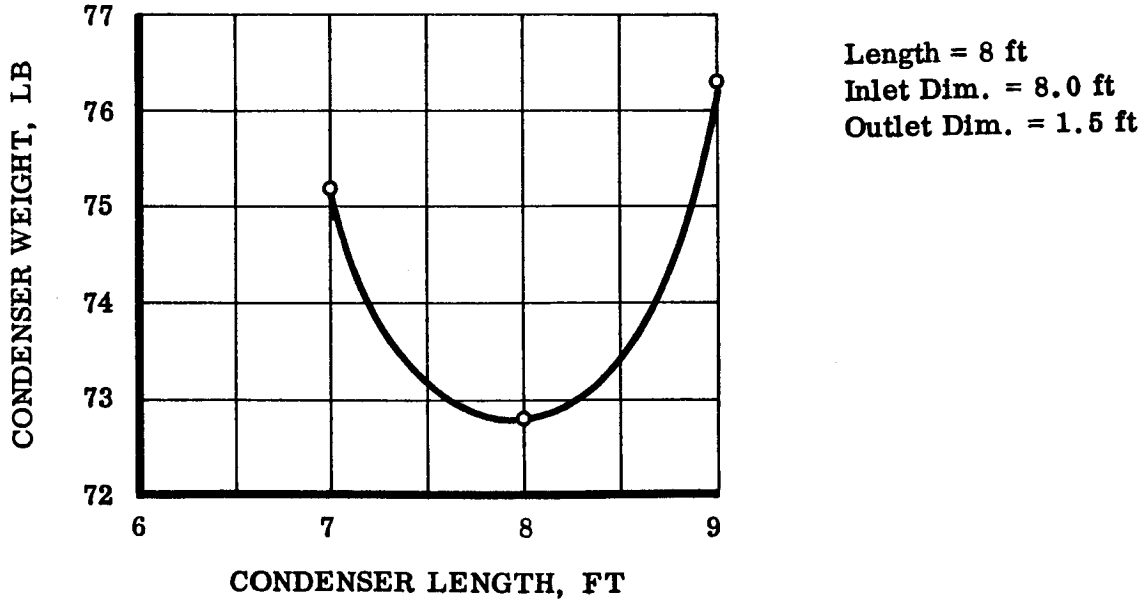

FIGURE 3-10

a. CONDENSER WEIGHT VERSUS OUTLET DIMENSION

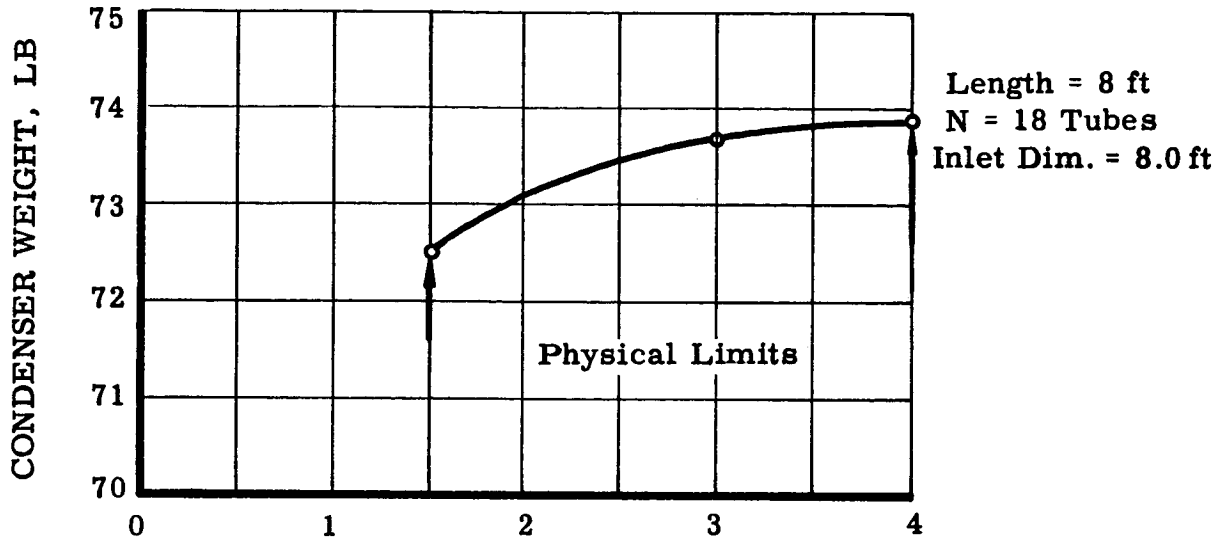

b. CONDENSER WEIGHT VERSUS INLET DIMENSION

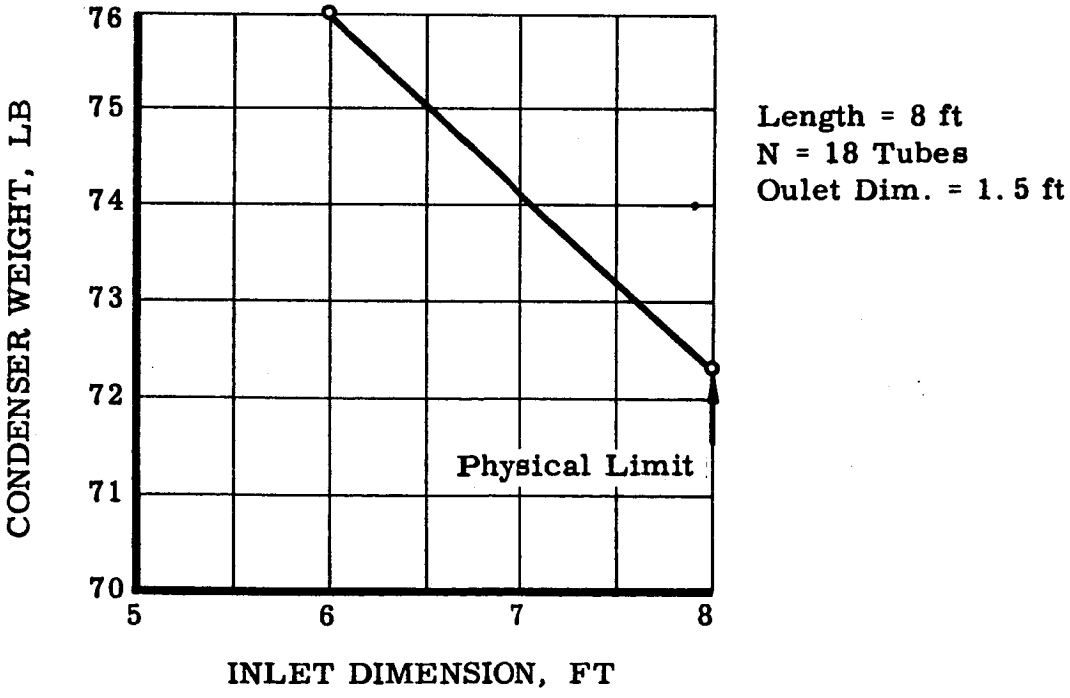

FIGURE 3-11

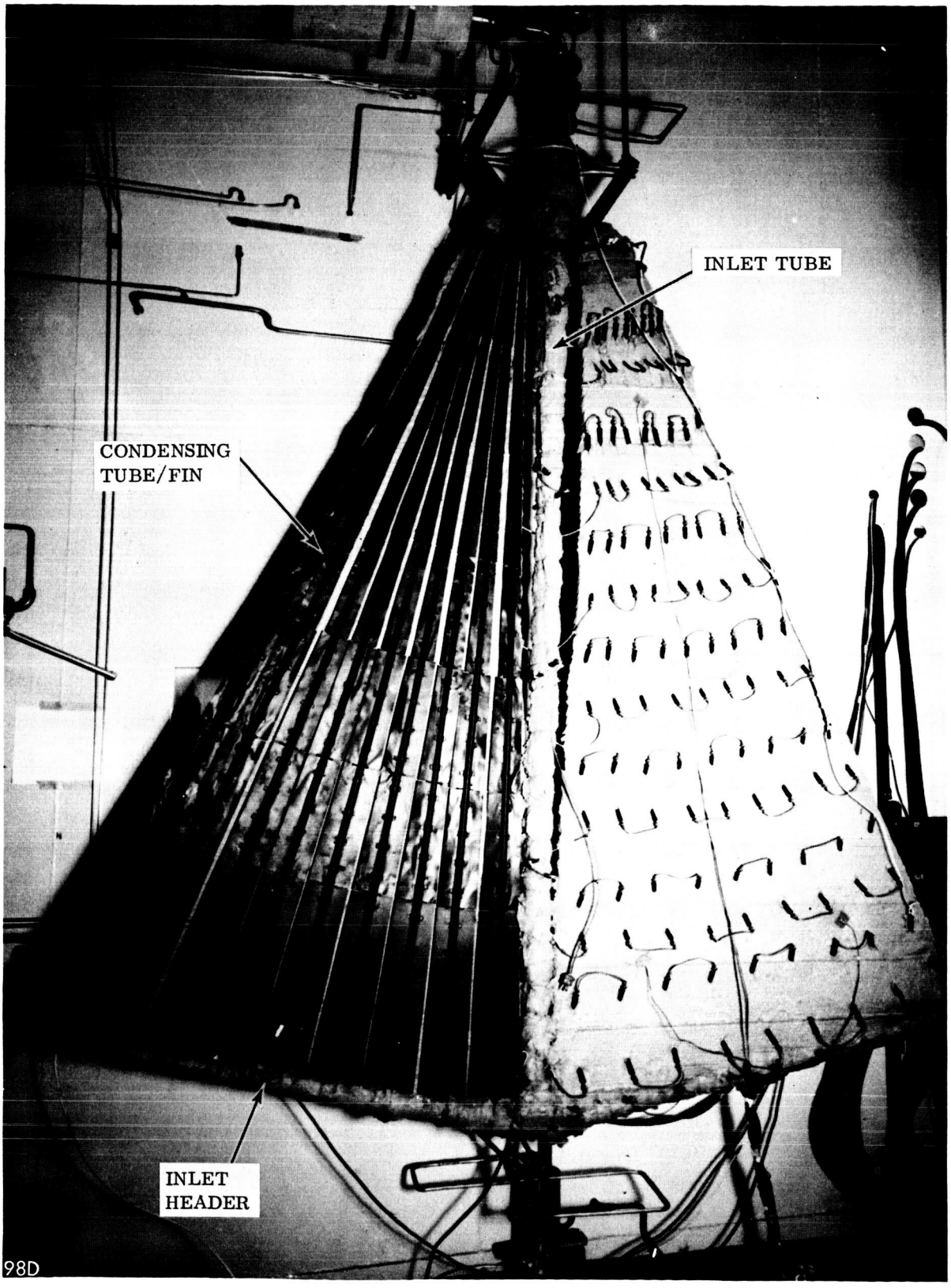

CSC 1-1 INSTALLED IN TEST BOOTH

FIGURE 3-12

CSCI-1 CONDENSER - SUBCOOLER TEST SCHEMATIC

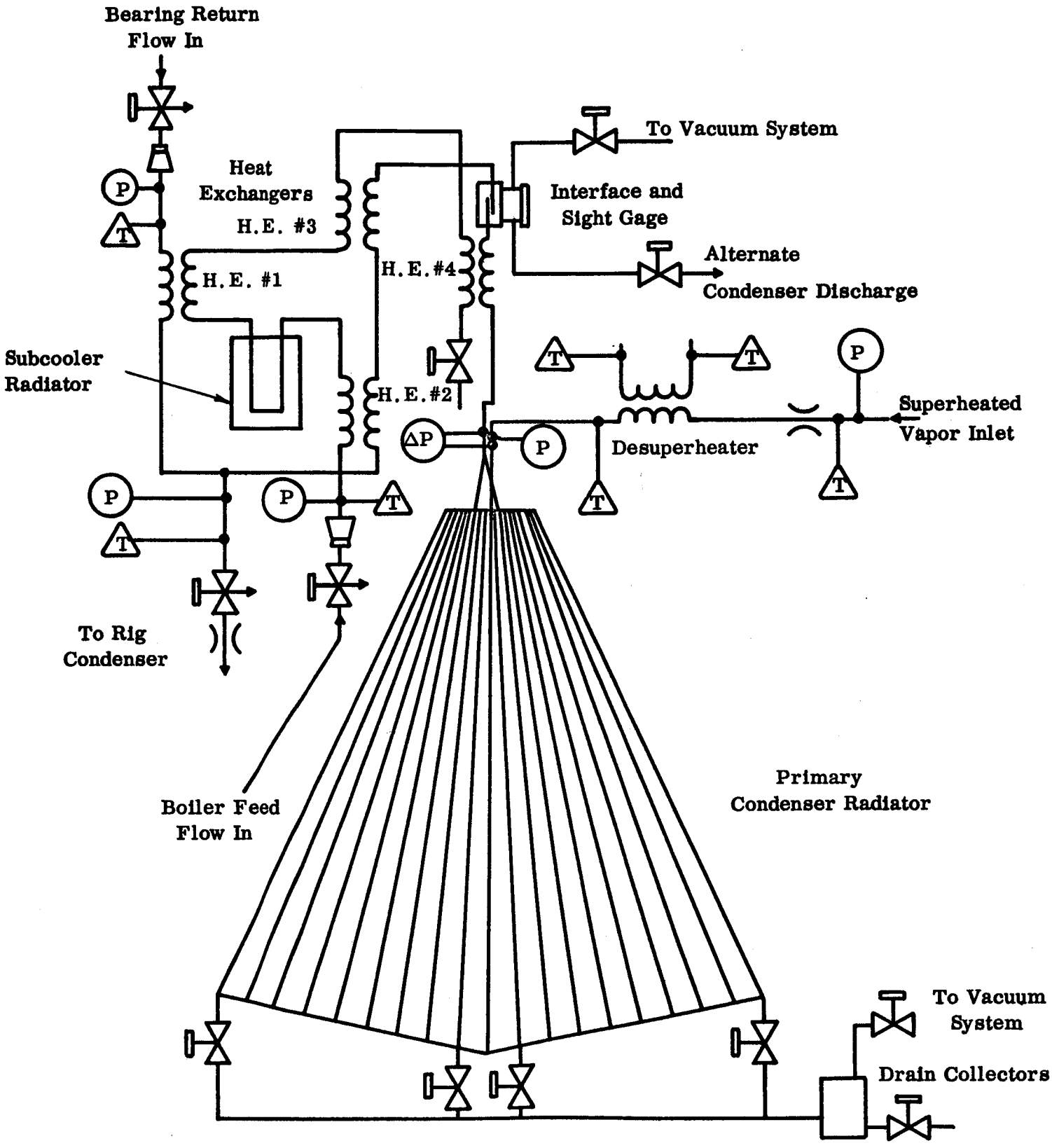

FIGURE 3-13

Ten linear equations in ten unknowns describing the heat balance of the heat exchangers were solved. The U values in the exchangers were allowed to vary ± 50% from the design (to allow for design tolerance) and the effect on the critical subcooler temperatures noted. The most critical temperature, the pump inlet, was affected as shown in Figure 3-14. Realizing the dangers of pump cavitation in the event of an underdesign in these exchangers, they were oversized 25% for a factor of safety. This resulted in a negligible weight penalty.

Using the high pressure pump flow as coolant, the heat exchanger lengths were determined using Figure 3-15. (Curve 6 was used due to the similarity of the experimenter's apparatus to the subcooler heat exchangers.) Using 5/16 inch tubes inside 1/2 inch tubes, the lengths of these heat exchangers were 15.3 inches, 11.9 inches, 3.63 inches, and 1.63 inches for heat exchangers 1 through 4, respectively. This included the 25% safety factor. The heat gained by the coolant flow was rejected in a non-isothermal radiator sized in accordance with Reference 8. The subcooler heat exchanger bundle is shown in Figure 3-16. Its compactness, as specified in Section 3.0, is evident in this photograph.

3.2.4 Pressure Drop Summary

The overall condenser pressure drop was distributed as follows.

Turbine to inlet header (friction)		0.243 psi
Inlet header (bend and friction)		0.071
Outlet header (bend, expansion, and friction)		0.041
Condenser to subcooler (friction)		0.449
Subcooler (liquid friction)		0.144
Subcooler static head (worst case)		0.642
		1.590 psi
Condenser tubes (design)		1.000
	Total	2.590 psi
Turbine outlet		7.000 psia
Condenser overall drop		2.590 psi
Pump inlet		4.410 psia
Vapor pressure at 400°F		0.386
	NPSH	4.024 psi (3.8 req'd)

THE EFFECT OF ERRORS IN SUBCOOLER HEAT EXCHANGER DESIGN ON PUMP INLET TEMPERATURE

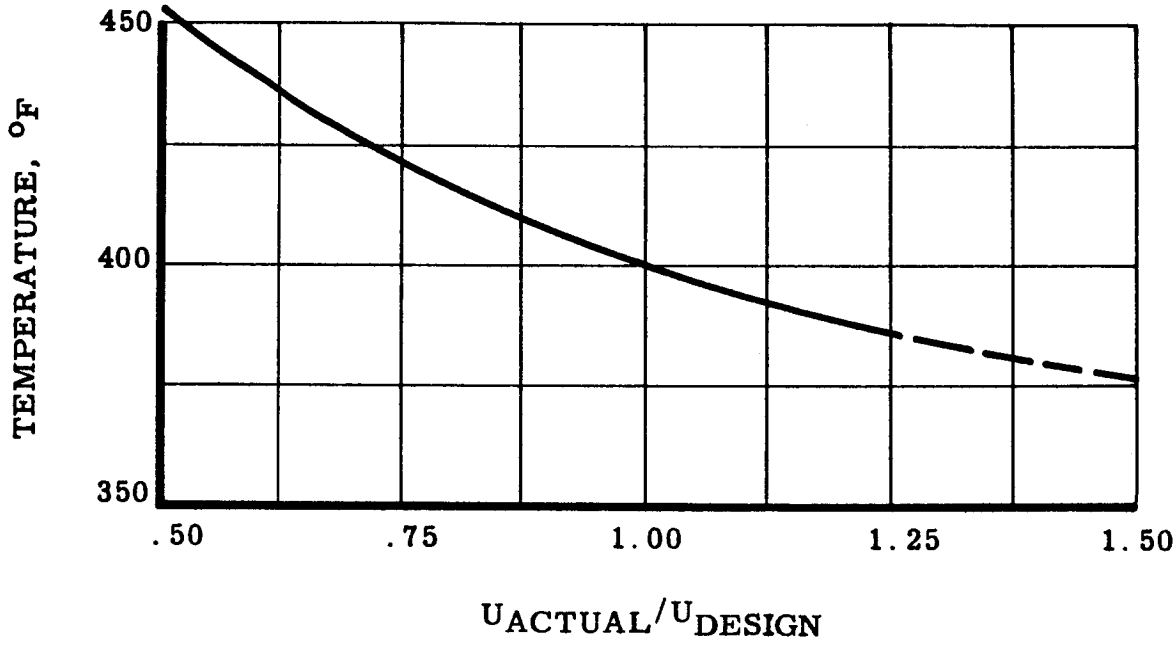

FIGURE 3-14

LITERATURE SEARCH, LIQUID MERCURY HEAT TRANSFER

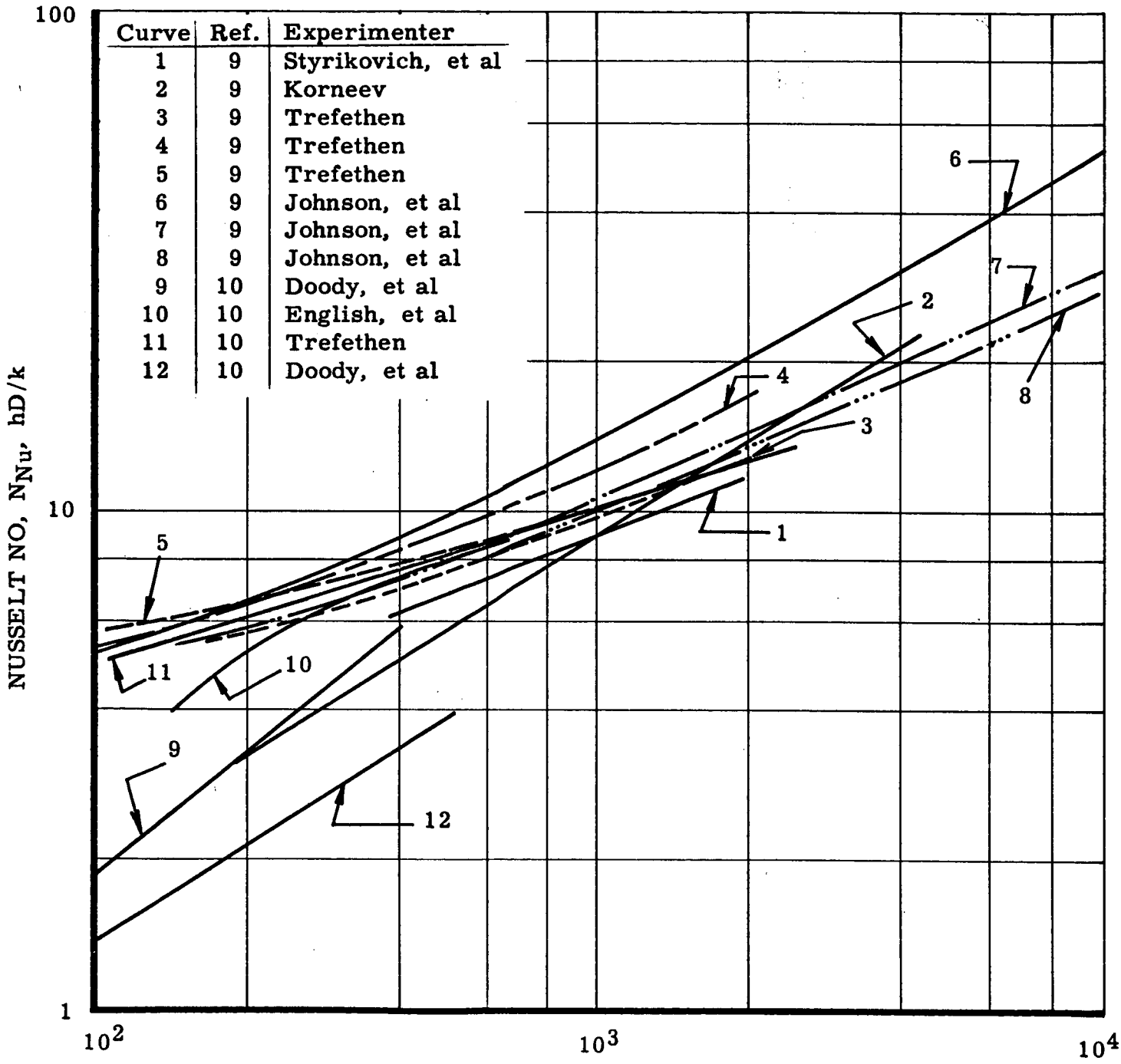

Curve	Ref.	Experimenter
1	9	Styrikovich, et al
2	9	Korneev
3	9	Trefethen
4	9	Trefethen
5	9	Trefethen
6	9	Johnson, et al
7	9	Johnson, et al
8	9	Johnson, et al
9	10	Doody, et al
10	10	English, et al
11	10	Trefethen
12	10	Doody, et al

FIGURE 3-15

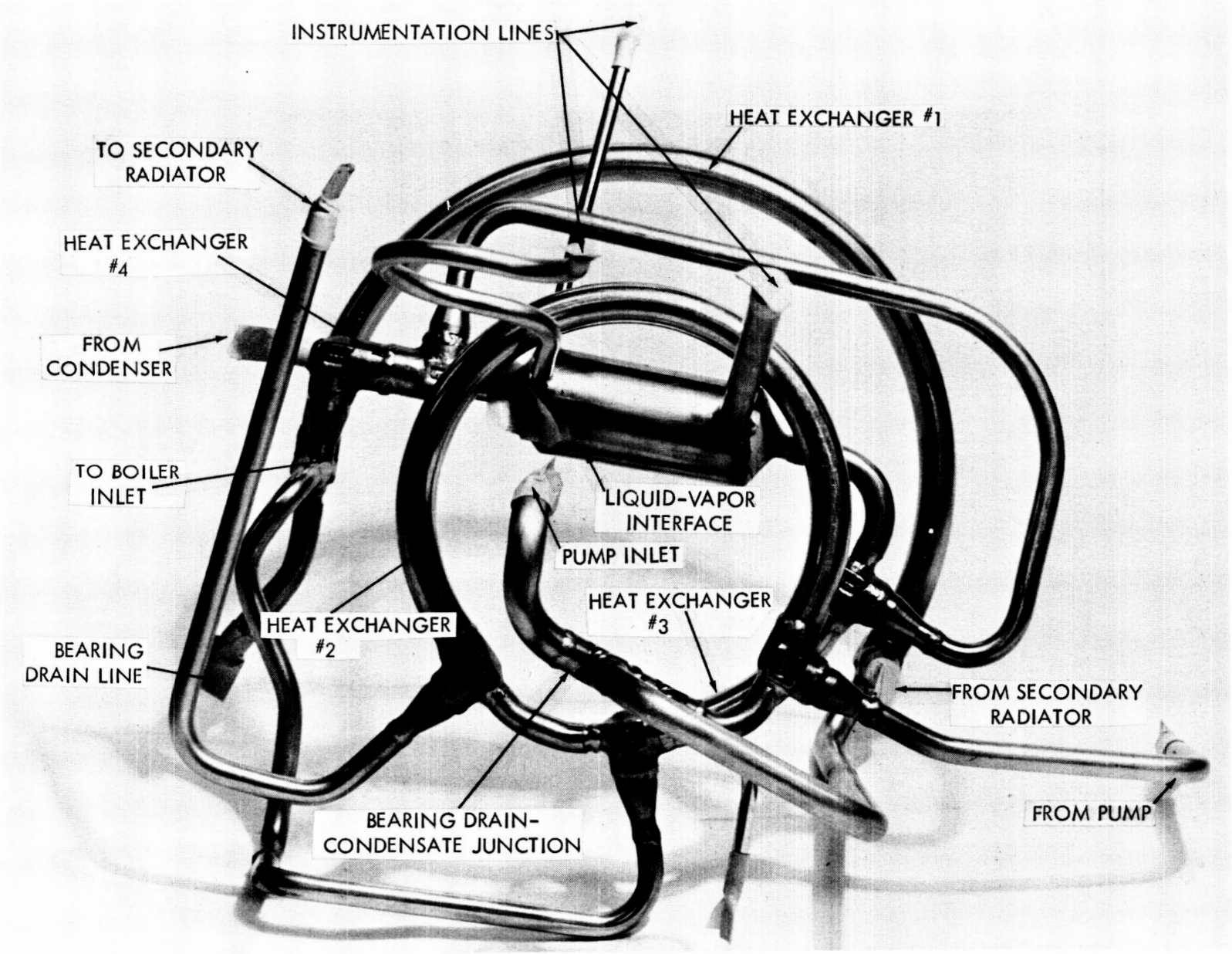

COMPACT HEAT EXCHANGER ASSEMBLY

FIGURE 3-16

3.2.5 Weight Summary

The system vulnerable area was broken down as

Inlet tube	5.12 ft^2
Inlet header	2.33
18 condenser tubes	12.37
Outlet header	0.05
Subcooler and Miscellaneous	1.34
Boiler	30.20
Total	51.41 ft^2

Using this area and the analysis of Section 3.1.2 results in a steel armor 0.069 inch thick. This results in the following condenser-subcooler weight breakdown.

Inlet tube	11.1 lb
Inlet header	9.5
Condensing tubes	41.3
Outlet header	0.2
Subcooler	3.2
Fins	7.2
Total	72.5 lb

3.3 EXPERIMENTAL INVESTIGATIONS

3.3.1 Single Tapered Tube Breadboard

To substantiate the velocity requirements for stable condensing flow against gravity and to verify the two-phase pressure drop prediction, a full-scale Pyrex glass condensing tube was fabricated and tested. The tube contained eight steps of decreasing diameter to approximate the continuous taper of the prototype condenser tubes. The test section was made of glass to permit observation of the flow phenomenon and to gain greater insight into the mechanism of condensing.

The test was performed first with flow against gravity; then the entire apparatus was inverted and data with flow in the direction of gravity were taken. The extremes of the effect of gravity on condenser operation were felt to be achieved by such testing. A schematic of the apparatus with flow in opposition to gravity is shown in Figure 3-17, and a photograph is shown in Figure 3-18.

Basically, the operation and data taken were the same for both orientations. Vapor was generated in the stainless steel boiler using contact strip heaters; the vapor was allowed to condense in the glass test section. The boiler and test section were joined by a Kovar seal. The presence of high quality vapor at the test section inlet was assured by boiler baffling and by guard heating the line between the boiler and test

SINGLE TUBE BREADBOARD SCHEMATIC

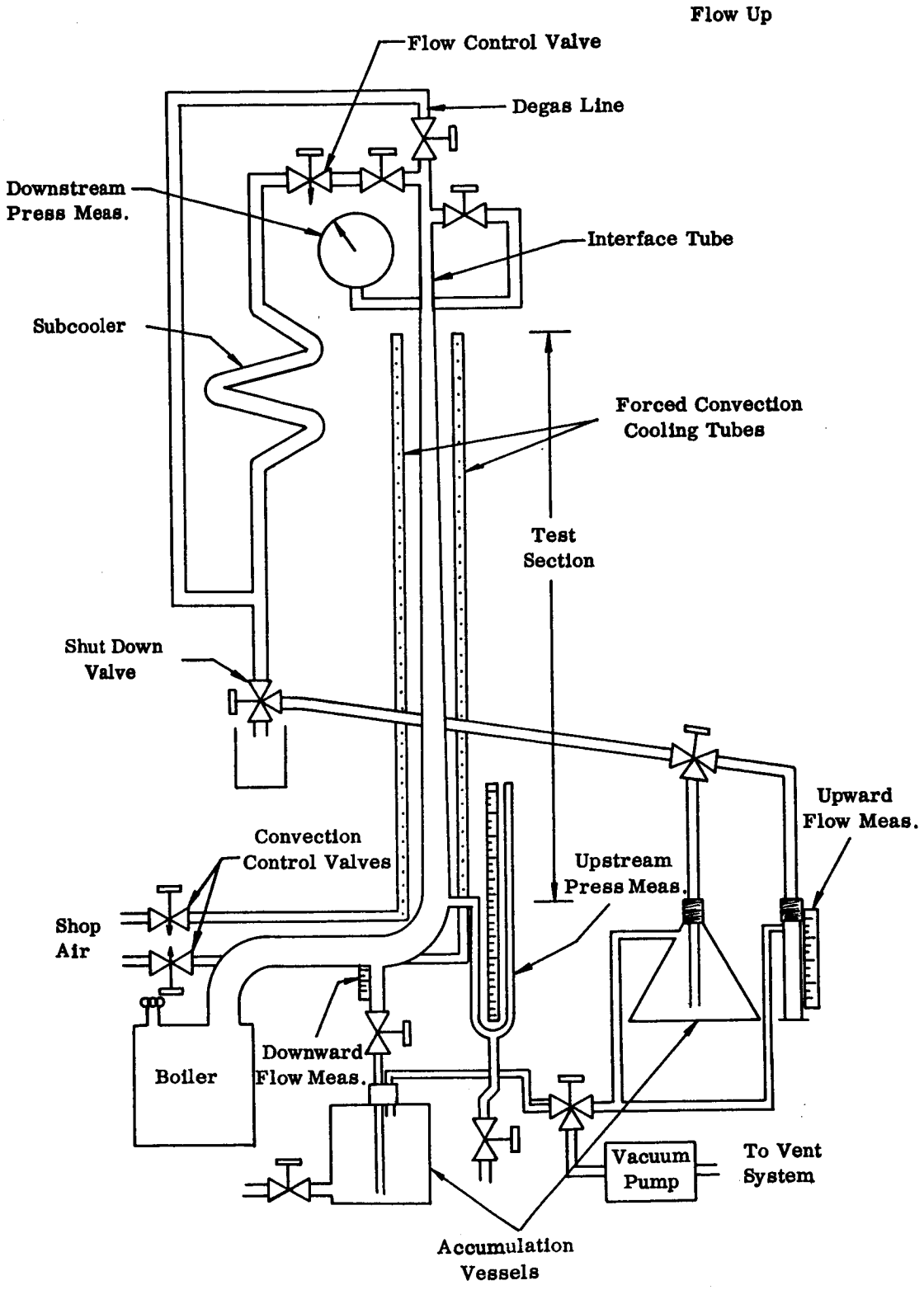

FIGURE 3-17

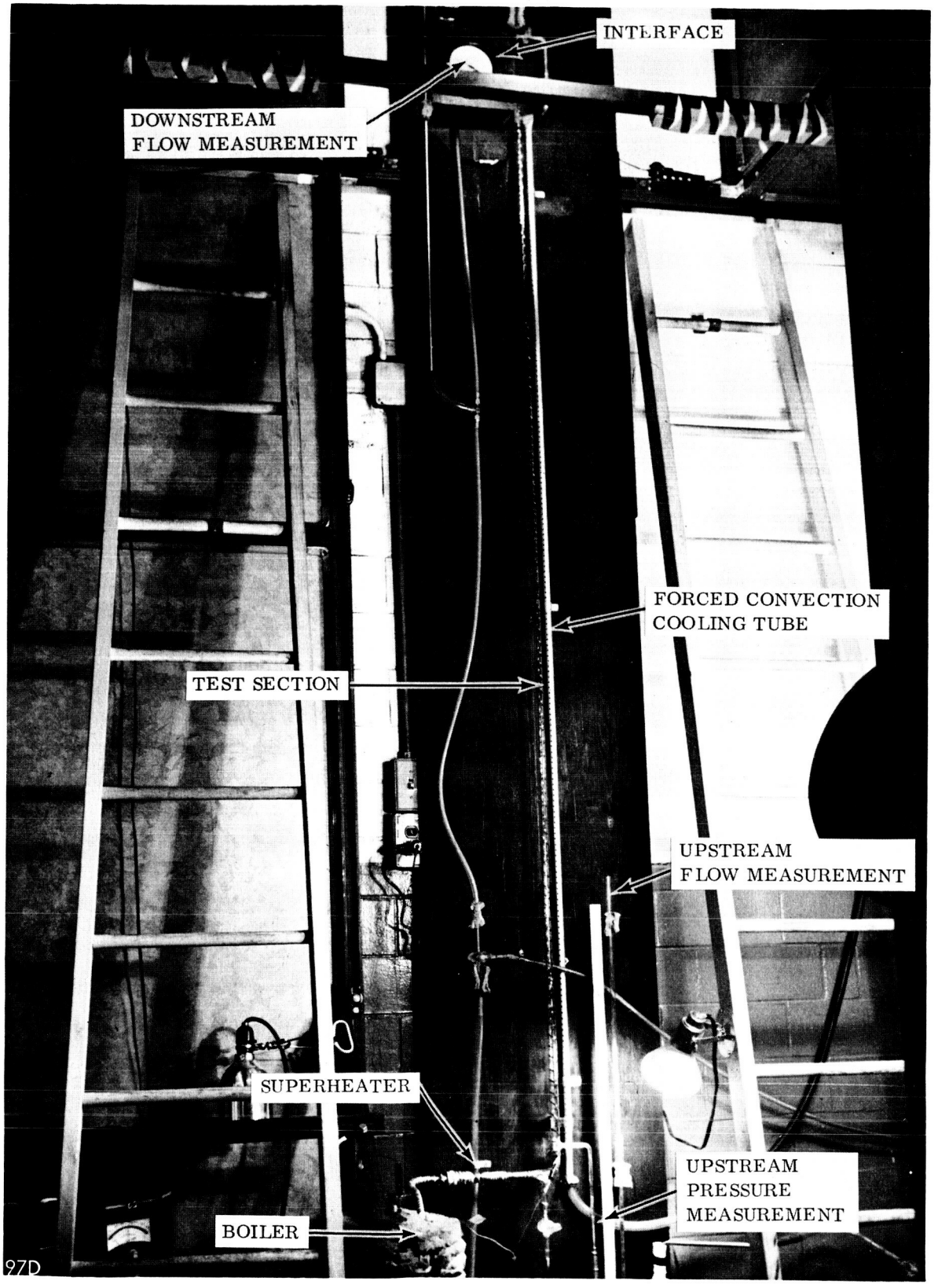

SINGLE TUBE BREADBOARD

FIGURE 3-18

section. The generation of high quality vapor by the boiler was borne out by observation of the flow just upstream of the test section; the tube appeared clear with vapor flowing.

Depending on the operating point desired, air was sometimes blown over the test section to reduce operating pressure. The interface was maintained downstream of the test section in a less-than-critical diameter* tube and its position maintained by modulating the flow control valve. The interface was positioned so that the quality of the mixture leaving the test section was the design value of 1%. This could be done by ratioing the latent heat rejection area downstream of the test section to the total latent heat rejection area. If this ratio is 1/100 and q/a is constant throughout the condensing area (it is, approximately, due to the relatively constant condensing temperature), then the quality leaving the test section is 1%, assuming the quality coming in is 100%.

Upstream pressure measurement was accomplished with a simple U-tube mercury manometer which was run with the leg toward the test section full to minimize extraneous condensation and error. Downstream pressure measurement was made with a sensitive bourdon tube gage. The use of a low displacement pressure measurement was necessary here since a manometer would be statically and dynamically unstable to pressure fluctuations with flow against gravity if tapped into the liquid downstream of the test section and would condense too high a portion of the remaining vapor

---

*Texts such as Hydrodynamics by Lamb and Theoretical Hydronamics by Milne-Thompson have discussed interfacial stability. If two fluids at rest and of different densities are superposed, wave motions can take place on the interface between them. For the case where a liquid is above its vapor, the wavelength is

$$\lambda = 2\pi\sqrt{\frac{\sigma}{(\rho_2 - \rho_1)\, g}}$$

where λ = wavelength
ρ_1 = density of vapor
ρ_2 = density of liquid
σ = surface tension
g = gravitational acceleration

and a stable interface between two parallel vertical plates exists if the spacing between the plates is less than $\lambda/2$, as discussed by Lamb. For the three dimensional case of mercury in a glass tube, the maximum tube diameter is expected to be of the same order of magnitude. Experiments at TRW have shown a critical diameter of 0.168 inch for mercury in a 316 stainless steel tube. This topic is investigated and discussed in Reference 3.

(causing experimental error) if tapped into the vapor-condensate stream at the end of the test section. The bourdon tube gage was calibrated daily to insure accuracy of the pressure measurement. Weight flow was obtained by allowing the condensate to accumulate in a graduated cylinder for a measured time. In the flow-against-gravity orientation, the velocity was sometimes too low to transport all the condensate to the interface. In these instances a "downflow" measurement was made and added to the flow reaching the interface to obtain total flow. A photograph of the breadboard installed with vapor-flow against gravity is shown in Figure 3-18.

To aid in determination of the variation in heat rejection along the test section, thermocouples were installed every 12 inches on the outside surface of the tube. By calculating the variation in heat rejection along the tube (based on the tube area and temperature) the local vapor flow rate can be found and the "vapor only" pressure drop calculated.

The experimental two-phase friction pressure drop can be obtained from the measured pressure drop (manometer reading minus bourdon tube gage reading corrected for static head to read interface pressure) by the following method.

Consider a section dL along a tapered tube

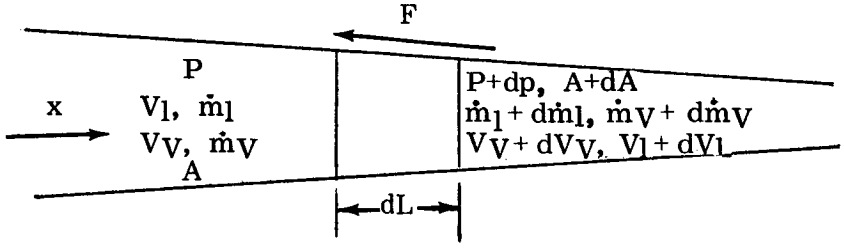

$$\Sigma F_x = PA - (P + dP\ (A + dA) - (P + \frac{dP}{Z}) \left[(A - A + dA) \right] - F$$

$$\Sigma F_x = - AdP - F \qquad (16)$$

From momentum:

$$\Sigma F_x = (\dot{m}_l + d\dot{m}_l)\ (V_l + dV_l) + (\dot{m}_V + dM_V)\ (V_V + dV_V) - \dot{m}_l V_l - M_V V_V$$

$$\Sigma F_x = d\ (\dot{m}_l V_l) + d\ (\dot{m}_V V_V) \qquad (17)$$

Therefore equating equations (16) and (17)

$$-AdP - F = d(\dot{m}_l V_l) + d\ (\dot{m}_V V_V)$$

Define

$$F \equiv dP_{TF}\,(A + \frac{dA}{2}) \cong Ad\,P_{TF}$$

Then

$$-AdP - AdP_{TF} = d\,(\dot{m}_l\,V_l) + d\,(\dot{m}_V\,V_V)$$

Using the values entering the test section and those at the interface results in

$$P_1 - P_2 = \Delta P_{meas} = \Delta P_{TF} - \frac{\rho_{V1}\,V_{V1}^2}{g}$$

and

$$\Delta P_{TF_{(\text{inlet to interface})}} = \Delta P_{meas} + \frac{\rho_{V1}\,V_{V1}^2}{g}$$

but

$$\Delta P_{TF_{(\text{test section})}} = \Delta P_{TF_{(\text{inlet to interface})}} - \Delta P_{TF_{(\text{exit to interface})}}$$

The last term, however, turns out to be negligible so

$$\Delta P_{TF_{(\text{test section})}} = \Delta P_{meas} + \frac{\rho_{V1}\,V_{V1}^2}{g}$$

In plotting the results of the testing, the correlation found in earlier condensing work at TRW was used. A value Φ_{INT} was defined as $\Delta P_{TF}/\Delta P_V$ where ΔP_V is the pressure drop that would result if only the vapor phase were flowing. This Φ_{INT} value was plotted versus the parameter $N_{Re0}\ (v_{V0}/10)^{1.25}$ and is shown for both upward and downward condensing in Figure 3-19 along with the results of other experiments conducted at TRW. The scatter in these data is a result of the difficulty in accurately determining the heat rejection variation and consequently ΔP_V and the normal problems experienced in two-phase pressure drop measurement.

These data agree with the previous work: Φ_{INT}, as defined, is approximately 1.5 for values of $N_{Re0}\ (v_{V0}/10)^{1.25}$ greater than 8×10^3. Thus, it was verified that the value of Φ_{INT} used in the condenser design was valid for flow in the direction of and in opposition to the gravity vector, provided the value of $N_{Re0}\ (v_{V0}/10)^{1.25}$ in the full scale condenser is above 8×10^3.

Φ_{INT} VS $N_{Re0}\left(\frac{v_{V0}}{10}\right)^{1.25}$
FOR FLOW VERTICALLY UP AND VERTICALLY DOWN
MERCURY CONDENSING IN A STEP-TAPERED TUBE

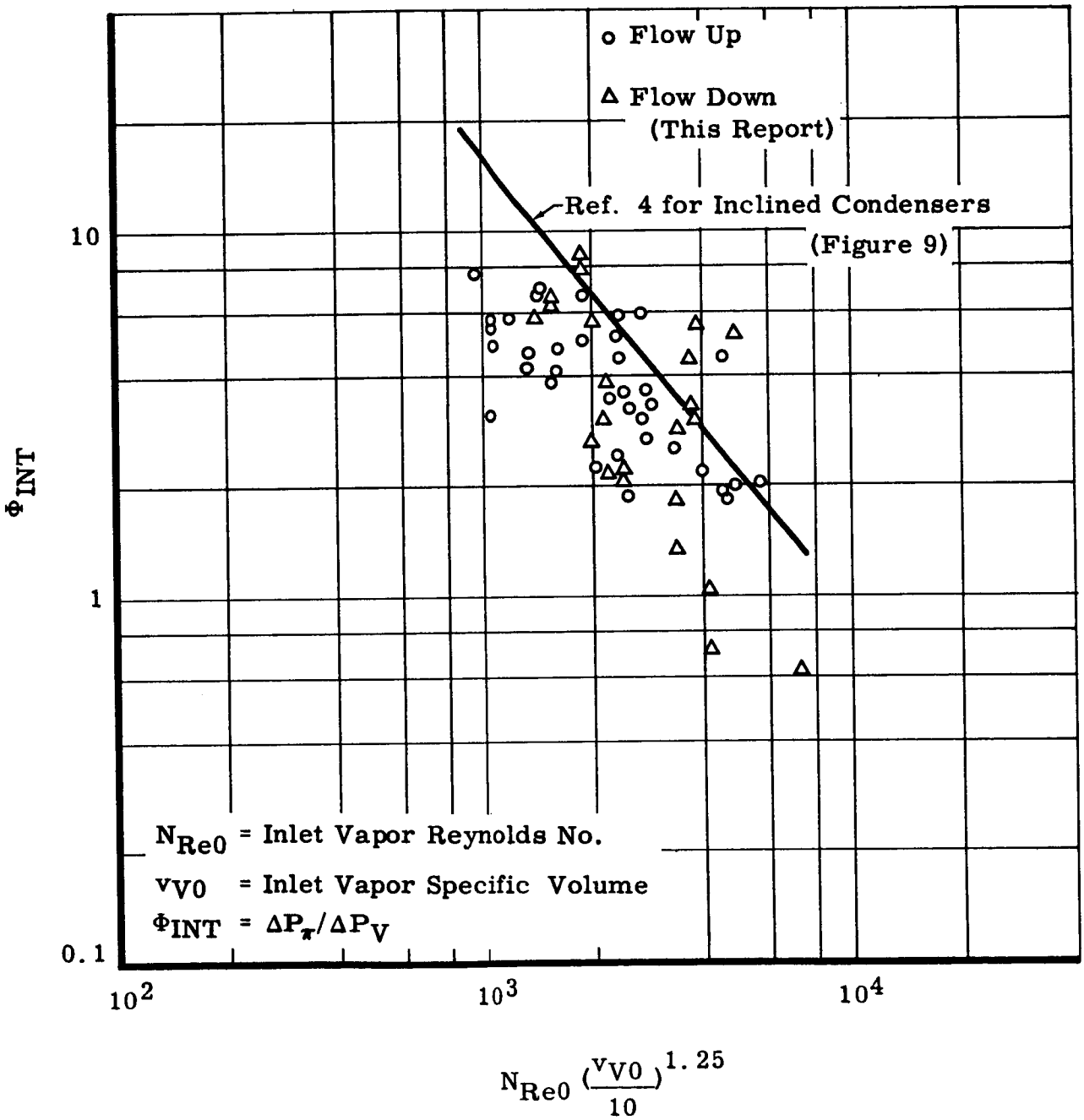

FIGURE 3-19

The minimum velocity necessary for flow against gravity was also investigated. Unfortunately, the heat rejection of the glass tube was limited by its ability to sustain high ΔT's through the wall without breakage, so consequently the range of operation was not as great as intended. However, data were obtained from the breadboard with flow in opposition to gravity on the minimum velocity necessary to transport all the condensate to the interface (no downflow). These data are plotted in Figure 3-20 as a function of vapor density. The theoretical relationship from equation (6) is also plotted using $\eta = -1$, $\alpha = 90°$, and the coefficient of the surface tension term as negative (Case I). Good agreement is noted with the vapor density having a slightly greater effect than predicted by the equation. Some of the discrepancy may be attributed to a C_D other than 1.0.

Therefore, the single tube breadboard quantitatively verified the pressure drop correlation of Section 3.2 and the minimum velocity requirement of Section 3.1.1. The following were further concluded as a result of the testing.

1. Single tube start-up with flow in opposition to gravity is no problem providing the tube is sufficiently preheated.

2. Interfacial stability in a single tube whose diameter is less than the critical diameter is not only possible, with flow against gravity, but quite easily obtained.

3. The mechanics of mercury condensing are essentially those outlined in Reference 3 with the exception that drop collision and agglomeration occur, especially at low vapor velocities. Their significance was not determined.

3.3.2 Interface Problem

Maintenance of a stable liquid/vapor interface under the conditions specified by system requirements posed several problems. Specifically, the requirements of the method of interface maintenance are

1. To provide the pump with a continual supply of vapor-free condensate.

2. To compensate for transient differences between inlet mass flow from the condenser and outlet mass flow to the pump.

3. To have a comparatively low pressure drop.

4. To operate in a gravity field of up to 1g in any direction.

5. To be tolerant of the small amount of non-condensables that might be present in the system.

MINIMUM VAPOR VELOCITY NECESSARY TO TRANSPORT ALL CONDENSATE TO THE INTERFACE WITH FLOW AGAINST 1g

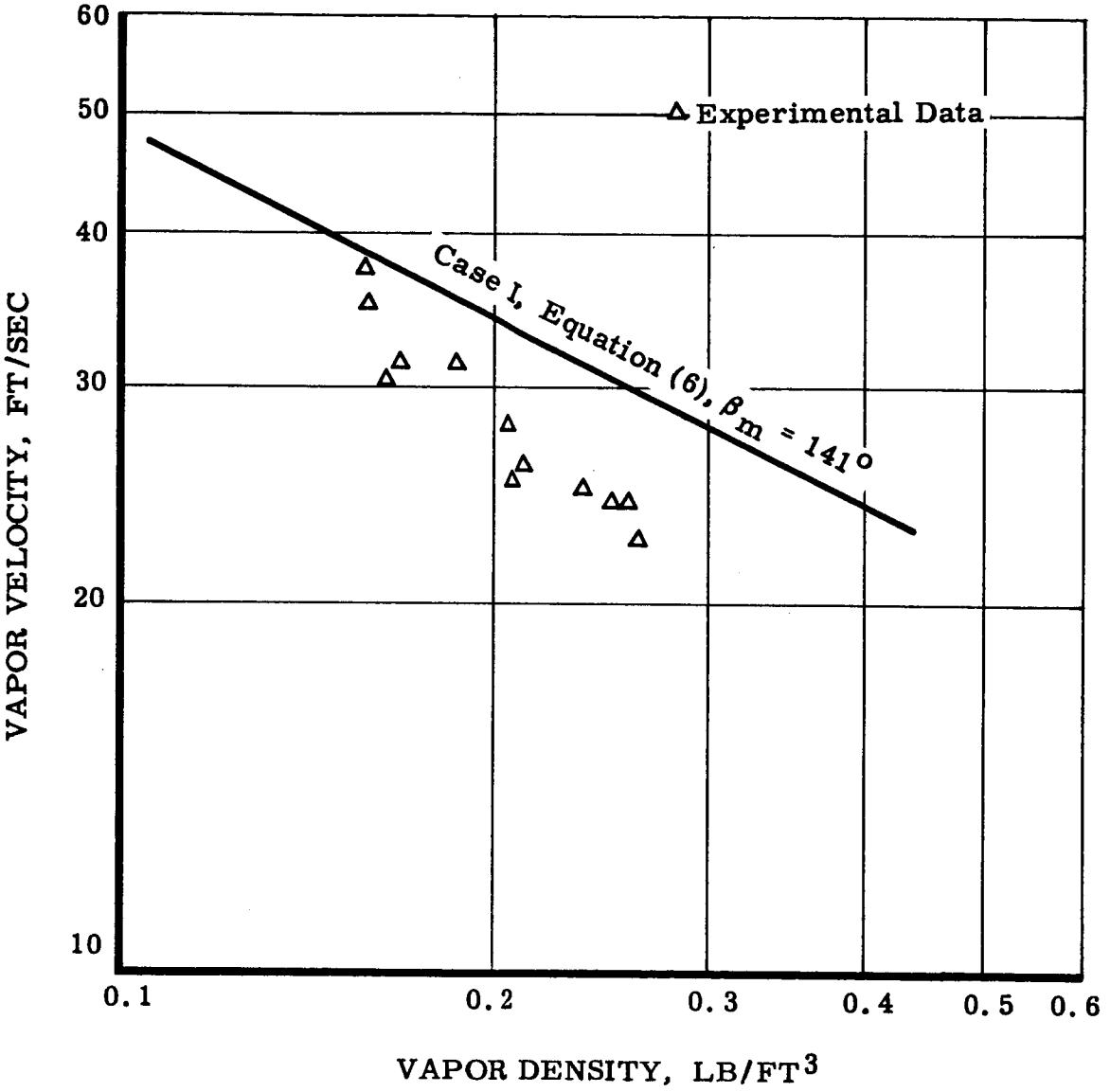

FIGURE 3-20

A single critical diameter tube would have too high a pressure drop to satisfy (2) above. In addition, multiple tube interfaces in an inverted condenser, i.e., flow against gravity, are unstable in most cases, as shown in the following analysis.

Assume the following condenser.

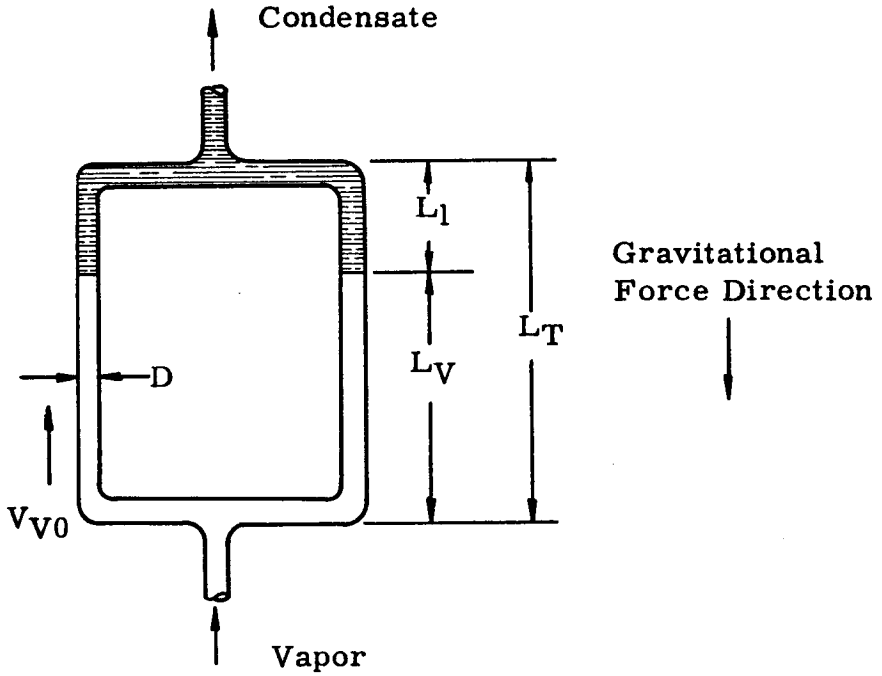

$$\Delta P_s = \Delta P_{TF} - \Delta P_M + \Delta P_{\text{liquid static head}}$$

$$\Delta P_s = \bar{\Phi}_{INT} f'_V \frac{L_V}{D} \frac{\rho_V V_{V0}^2}{2 g_c} - \frac{\rho_V V_V^2}{g_c} + L_l P_l N \qquad (19)$$

where

$\Phi_{INT} = \Delta P_{TF}/\Delta P_V$

f_V' = integrated vapor friction factor based on inlet vapor velocity

ρ_V = vapor density

V_{V0} = inlet vapor velocity

ρ_l = condensate density

$\eta = g_L/g_c$

also $$q\,L_V = \dot{m}_{V0}\,h_{fg} = \frac{\pi D^2}{4}\,G_0\,h_{fg} \qquad (20)$$

where q = heat rejection per unit length

$\dot{m}_{V0}$ = inlet vapor mass flow

G_0 = inlet vapor mass flow rate per unit area.

Combining equations (19) and (20) results in

$$\Delta P_s = \Phi f' \frac{\pi D G_0^3 h_{fg}}{8 q g_c \rho_V} - \frac{G_0^2}{\rho_V g_c} + \left(L_T - \frac{\pi D^2}{4}\frac{G_0 h_{fg}}{q}\right)\rho_l n$$

Differentiating:

$$\frac{d\,\Delta P_s}{d\,G_0} = \Phi f' \frac{\pi D h_{fg} 3 G_0^2}{8 q g_c \rho_V} - \frac{2 G_0}{\rho_V g_c} - \left(\frac{\pi D^2 h_{fg} \rho_l n}{4q}\right)$$

Substituting

$$\frac{\pi D^2}{4}\quad\frac{h_{fg}}{q}\quad\frac{L_V}{G_0}$$

This results in

$$\frac{d\,(\Delta P_s)}{d\,G_0} = \left(\frac{\Phi f' L_V}{D} - \frac{4}{3} - \frac{2 L_V \rho_l n \quad \rho_V}{3 G_0^2}\right)\frac{3 G_0}{2 g_c \rho_V}$$

From Reference 11,, a necessary condition for the avoidance of flow excursions is that d $(\Delta P_s/dG_0)$ is positive. Reference 12 shows that stable flow oscillations may occur even at this condition of positive slope depending on the shape of the ΔP_s vs G_0 curve (especially in boilers), but in any event the requirement of Reference 11 appears to be a prerequisite if stable hydrodynamics are to be expected.

Therefore

$$\frac{\Phi f' L_V}{D} > \frac{4}{3} + \frac{2 L_V \rho_l n g_c \rho_V}{3 G_0^2} \qquad (21)$$

Substituting values from the Sunflower condenser into equation (21) results in

$$2.70 \not> 4/3 + 66.7$$

or the condenser would not be stable to excursions. Any attempt to satisfy the stability criterion would result in a higher pressure drop which cannot be tolerated. The single exception is a decrease in the local gravitation. The equation indicates stability at g levels below 0.02. This, however, is not consistent with the system acceleration specification.

Many devices which contained the interface in a single location were considered for the solution to this problem and the more promising were dynamically tested. Only two, however, appeared to have merit. One was a centrifugal separator which would receive the low quality mixture tangentially along the edge of a cone near the apex. The condensate would then be forced to the base of the cone as shown below.

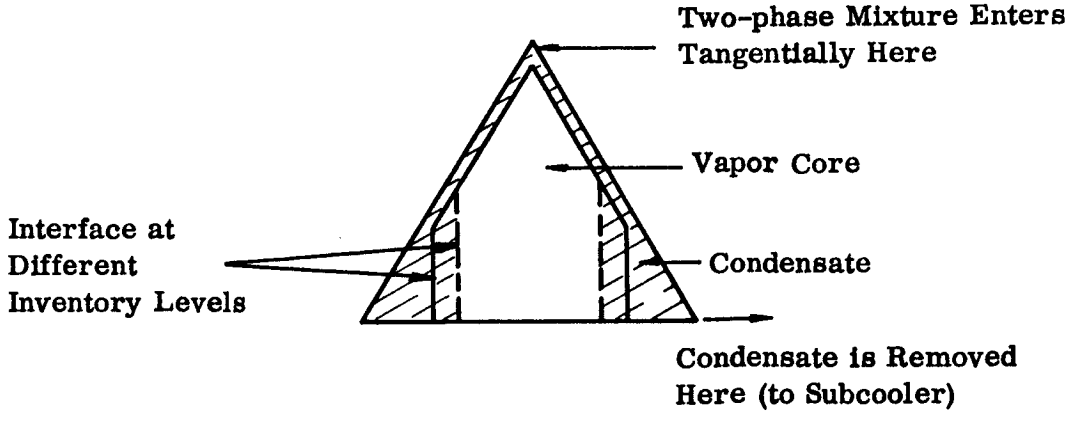

This is in contrast to a normal cyclone liquid-vapor separator where a small liquid inventory is driven to the apex of the cone by the pressure gradient in the boundary layer of the vapor.

It can be seen from the sketch that variations in system inventory can be absorbed by the increase or decrease of the volume fraction of the liquid in the separator. Also, if sufficient velocities were maintained, an artificial gravity would be created that would make operation insensitive to external gravity forces. A plastic model of such a separator was built and tested with single phase flow (liquid mercury) to determine its mode of operation in different orientations of a 1g environment (Figure 3-21).

Liquid was admitted tangentially through a 0.050 inch orifice near the apex of the cone. The cone had a base diameter of 2-3/8 inches and a height of 2 inches. The liquid was then removed tangentially near the base of the cone. The 'core' of the separator was vented to atmopshere to allow for inventory changes without building up pressure in the separator. Throttling valves in the liquid line upstream and downstream of the separator allowed changes in liquid inlet velocity and liquid inventory to be made.

It was found that if the inlet liquid velocity was kept above 40 ft/sec the separator maintained a stable cylindrical "vapor" core no matter what the gravity orientation. In addition, the transient response to flow and steady-state operation with various amounts of inventory (approximately 5% to 100% liquid volume fraction) were investigated and found to be satisfactory. It was thus shown that further investigation of the scheme was warranted, probably a two-phase adiabatic experiment (H_g and N_2) and then a dynamic experiment using a two-phase condensing flow.

The second scheme which appeared to have merit for the solution of the interface problem was the device shown in Figure 3-22. In this scheme, a two-phase mixture would be admitted to a chamber (probably a sphere) through one tube which terminated near the chamber wall and liquid would be removed through another tube terminating at the center of the chamber. If the chamber were kept more than 50 per cent full of liquid, it can readily be visualized that the liquid line feeding the pump would always be flooded in a 1g field, no matter what the orientation.

Short term zero g tests have been performed with mercury in spheres; these are reported in Reference 13. The analytical and experiment conclusion drawn is that the equilibrium configuration for mercury in zero g is "one in which the liquid vapor surface of the mercury is a surface of constant curvature and the mercury remains in contact with the walls of the sphere at the same contact angle as was observed in the 1g environment." If this is true and the sphere were again kept at least 50% full of liquid (condensate), it can readily be visualized that the center of the sphere (pump inlet line) would continually be flooded.

EXPERIMENTAL CENTRIFUGAL SEPARATOR

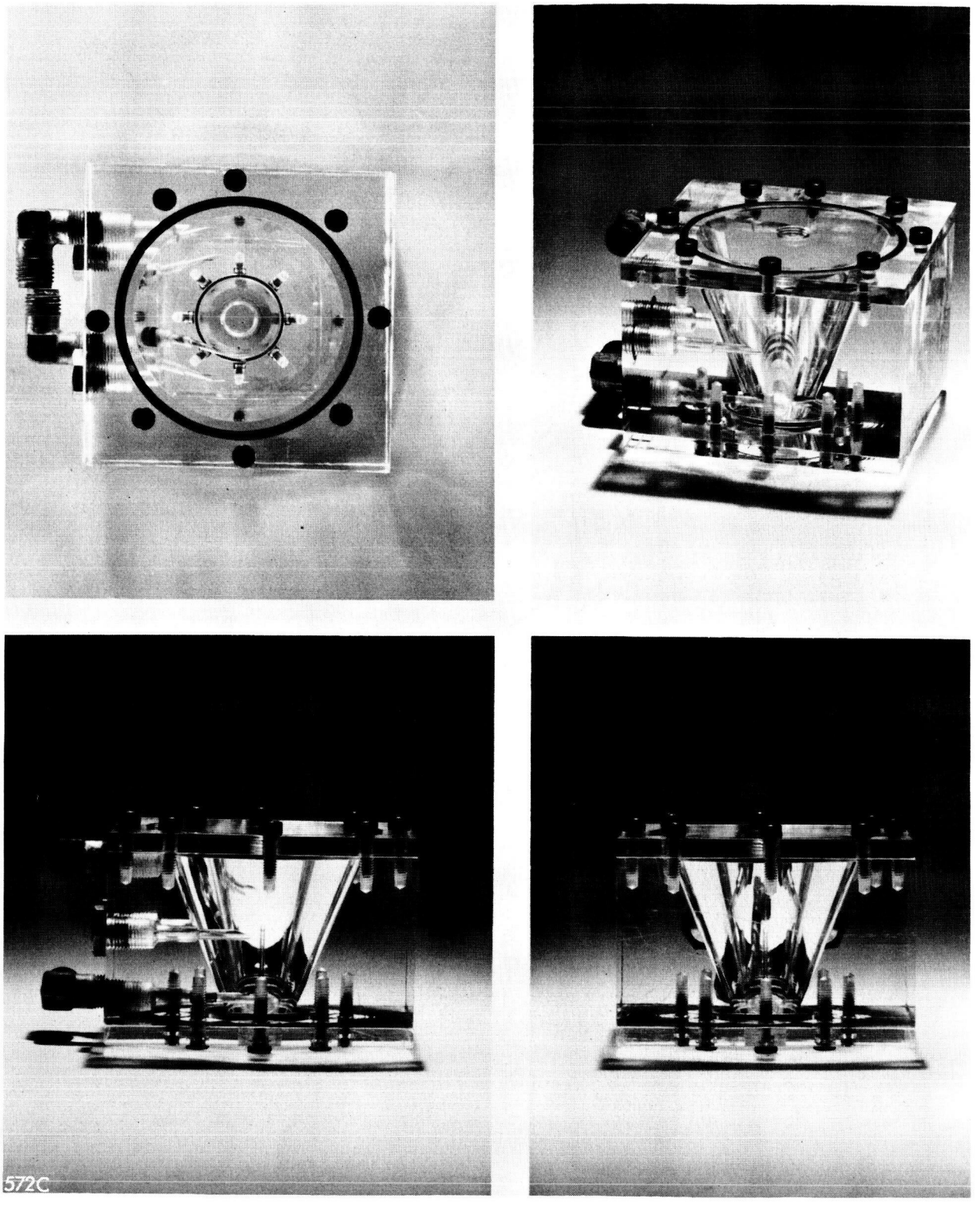

FIGURE 3-21

INTERFACE CHAMBER SCHEMATIC

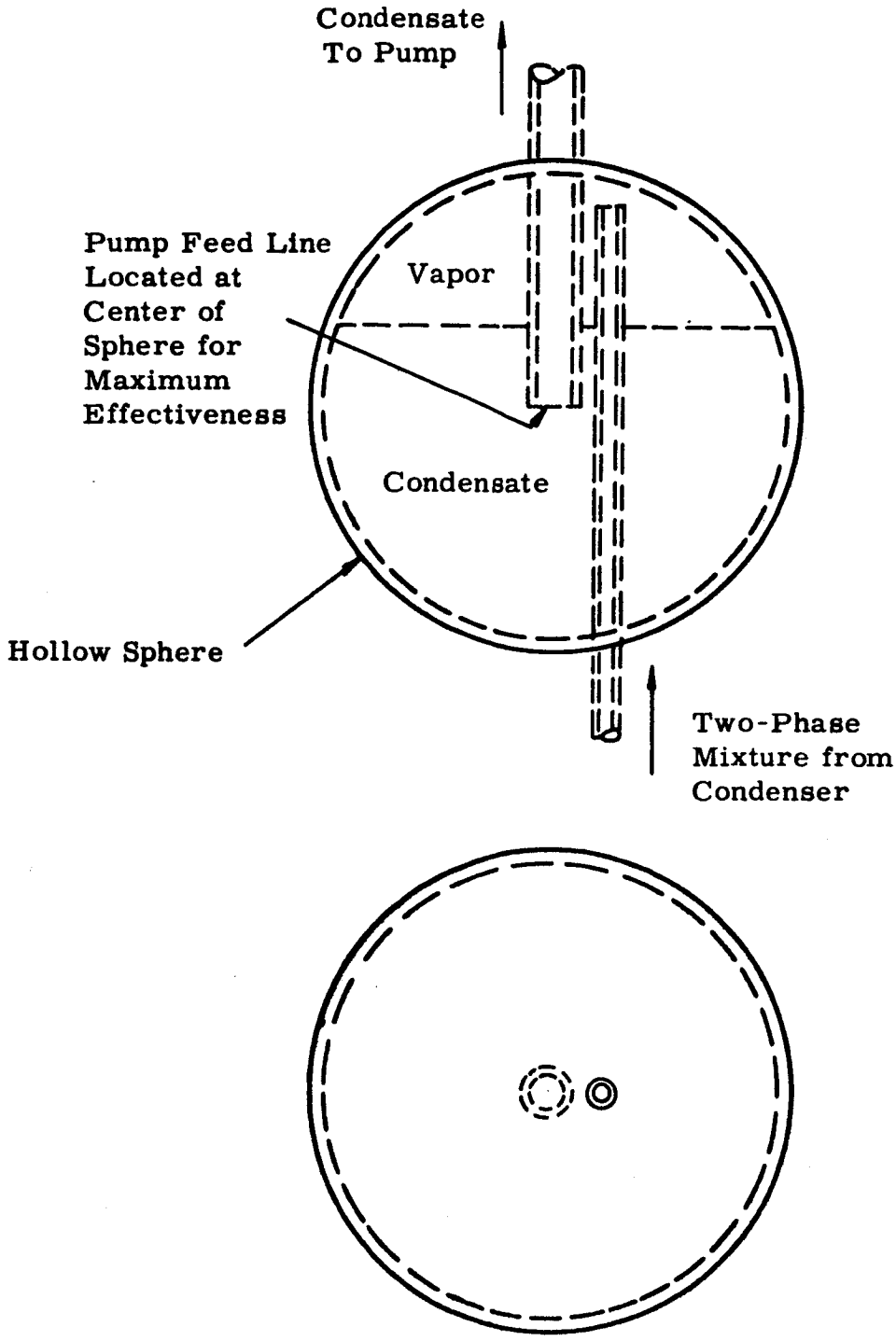

FIGURE 3-22

Not considered in the static analysis above, however, is the turbulence created by the dynamic nature of the process during operation. This effect would probably be greatest in a zero g environment where there is no gravity to restore the liquid to stability.

In considering the approach to solve the interface maintenance problem in the CSC I-1 design, the unit shown in Figure 3-22 was chosen. The I-1 unit was to be operated on the ground only, with flow in opposition to gravity. The testing, development, and proof of the operation in a gravity environment of this latter device was felt to involve much less time and money than the centrifugal separator. The major developmental effort for the simple chamber lies in the zero g operation, whereas the operation of the centrifugal separator under a gravity environment was felt to be the more difficult mode to prove. The simple chamber in the I-1 design was thought, therefore, to be advantageous while evaluating the two methods for space application. Before this method was incorporated into full-scale hardware, its operation under dynamic conditions was checked in a 1g environment. A test apparatus and glass model of the interface were built and operated to check out performance with flow in the direction of and opposed to the gravity vector.

The apparatus used for the upward condensing tests is shown in Figure 3-23. The chamber is shown in the upward orientation with respect to gravitational acceleration.

The main components of the test apparatus were the steel pot boiler which supplied mercury vapor, the stepped steel condenser tube which rejected heat from the vapor to provide low quality vapor to the test section, and a glass test section which included the interface device to be tested. Bourdon tube pressure gages were located at the test section inlet and outlet.

The tests were conducted by supplying heat to the boiler with electric heaters and by rejecting heat from the condenser and test section by convection and radiation from the condenser tube wall. A fan was used at times to circulate air over the condenser tube to lower condenser pressure level.

As low quality mercury vapor entered the glass test section and condensed, the flow control was closed and the liquid inventory was allowed to build up in the sphere. When the proper liquid level was attained, the flow control valve was opened and set to maintain the desired level.

One object of the test was to determine whether liquid was continually removed through the liquid outlet with all vapor and non-condensable gases (if present) remaining in the interface sphere. These observations could be made by looking through the walls of the glass test apparatus.

Another phenomenon which was observed and recorded was the pressure drop through the test section. These recordings were made from the bourdon tube pressure gages

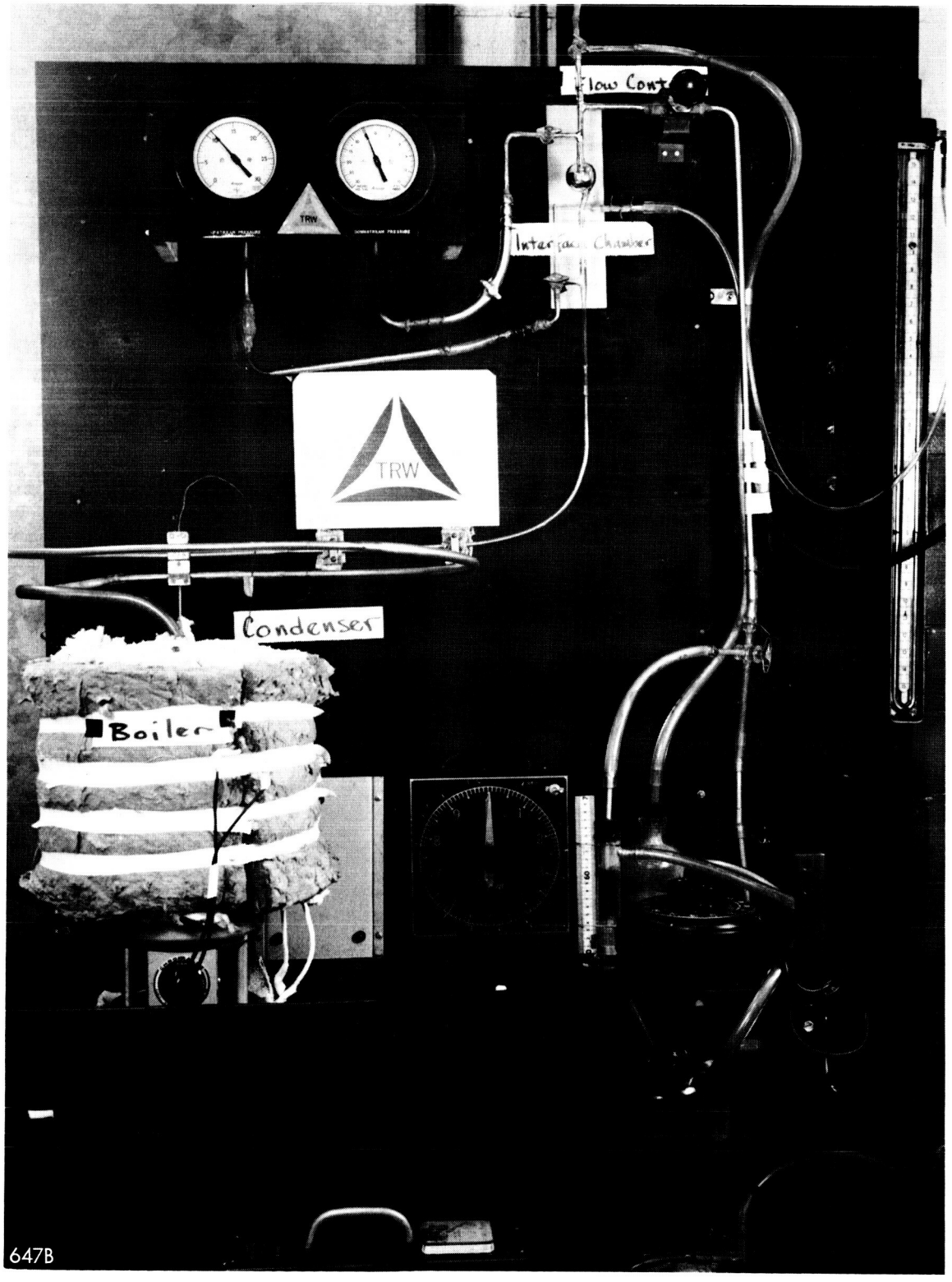

INTERFACE CHAMBER TEST RIG

FIGURE 3-23

which indicated the fluid static pressure. The flow rate was measured by collecting the condensate removed from the test section during a measured period of time. These pressure drops were then corrected for the effect of the liquid leg from the liquid-vapor interface to the downstream pressure tap.

No problem was observed with upward condensing operation as long as the liquid covered the liquid outlet tube; there was no evidence of non-condensable gas or mercury vapor in the liquid line.

The only problem observed during operation with downward condensing was with mercury vapor traveling into the liquid line when the liquid level was lowered close to the liquid outlet tube. This occurred most often when there were few or no non-condensable gases present and a great deal of bubbling and turbulence was observed as vapor passed through the mercury condensate in the sphere.

It was concluded from this test that operation of the device was satisfactory for incorporation in CSC I-1. All of the previously determined requirements were met in the test, except the zero g application.

The requirement for further development of this device and of the centrifugal separator prior to their incorporation into flight hardware is recognized.

3.4 COMPONENT TEST

3.4.1 Test Description

The purpose of the test was to determine the condenser operating characteristics, verify design inputs, and determine if any problem areas were present prior to integration into the system. The test procedure was to include steady-state operation at design and off-design conditions during start-up and step changes in vapor flow rate.

The condenser-subcooler was installed in the test booth with vapor flow against the gravity vector as a demonstration of condenser operation in the most adverse orientation of the Sunflower I acceleration requirement. Since the condenser heat rejection was designed for space, the heat transfer capabilities were too great for ground operation and it was necessary to fit one side of the condenser with permanent insulation. Removable insulation was applied to the other side to be used only during preheat. The necessary preheating was obtained by attaching heaters to the inlet tube, inlet header, and condensing tubes.

A schematic diagram showing the condenser-subcooler installed in the test rig is shown in Figure 3-13. The condenser inlet quality was controlled and measured with a liquid-mercury-cooled desuperheater. By varying the coolant flow rate and its inlet temperature the heat removed from the vapor could be varied and a heat balance written to determine the inlet quality. In addition to the instrumentation

shown in Figure 3-13, surface thermocouples were attached to the condensing tubes to monitor condenser and individual tube performance. Any condensed mercury collected in the inlet header could be drained into the illustrated collector pot.

The desired simulated liquid flow conditions for the subcooler heat exchangers were obtained by metering and heating liquid mercury flow. Since non-condensables could present a problem during operation, a de-gas line leading to a vacuum manifold was supplied at the liquid-vapor interface. This line should be used only intermittently in the event of slight system leakage.

3.4.2 Results

Completely successful operation of the condenser portion of this unit was never obtained. Although the incoming vapor was completely condensed, approximately half of the condensate remained in the lower portions of the condenser, decreasing the effective heat rejection area and causing high operating pressures which necessitated shutdown. A complete presentation of the results of this test are contained in Reference 14.

Typical tube temperature profiles during attempted operations are shown in Figure 3-24. Figure 3-24a presents Section 1 (first foot) condensing tube temperatures as a function of time. It can be seen that liquid accumulation and tube blockage is progressive, beginning with the outermost tube (#9) and working inward. Figure 3-24b shows tube temperature profiles just prior to shutdown. Liquid accumulation in tubes 7 and 9 is indicated by the lower-than-saturation temperatures. As the condensing tubes became blocked, the vapor condensed and dropped back into the inlet header where it was swept to the header ends, resulting in progressive tube and header blockage as condensate accumulated.

Added to this problem was the vapor recirculation from the inner to outer tubes through the outlet header, as shown in Figure 3-24b (higher temperatures at upper ends of tubes 7 and 9 than in the middle).

Thermal unbalance due to the difference in sensible heat contained in each tube, the result of uneven preheat, presented another problem during start-up attempts. Careful insulation application improved, but did not eliminate, this problem.

The subcooler tube-in-tube heat exchanger operation was satisfactory, although the values of overall heat transfer coefficient were somewhat lower than predicted. The device used to maintain a stable liquid-vapor interface under dynamic conditions functioned as expected.

a. FIRST SECTION TUBE TEMPERATURES VS TIME

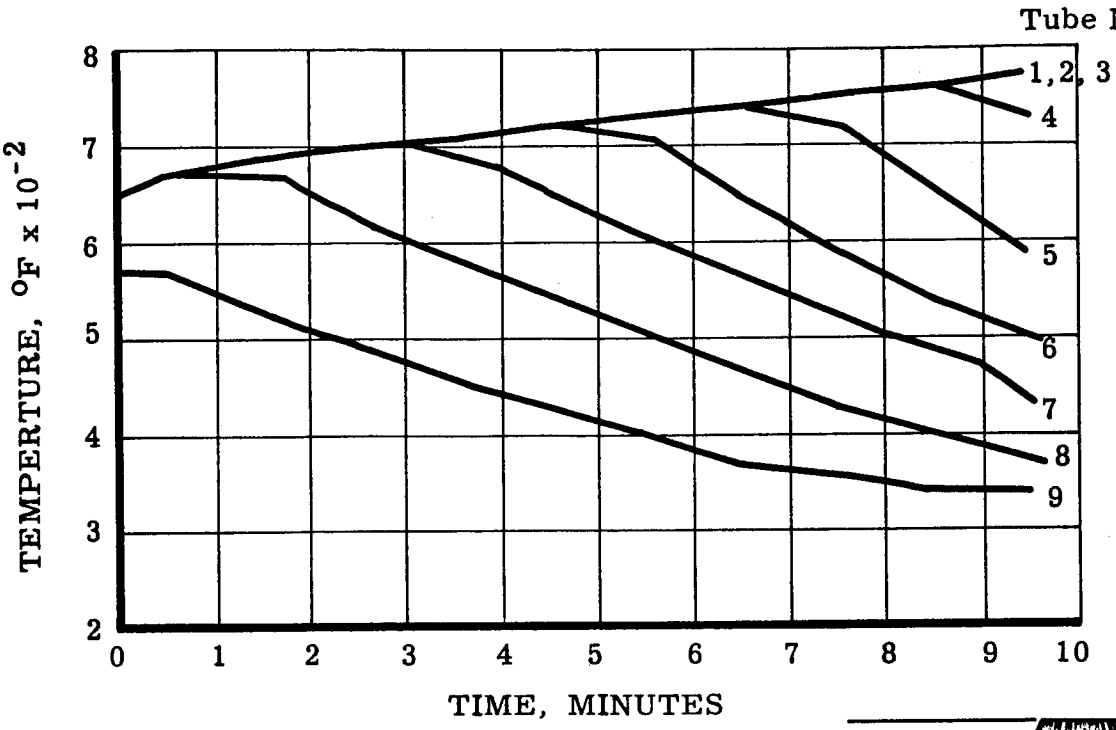

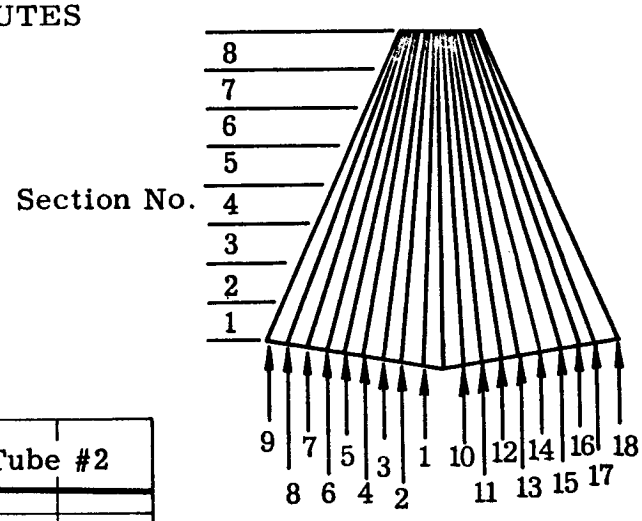

b. TUBE TEMPERATURE PROFILE AT SHUT-DOWN

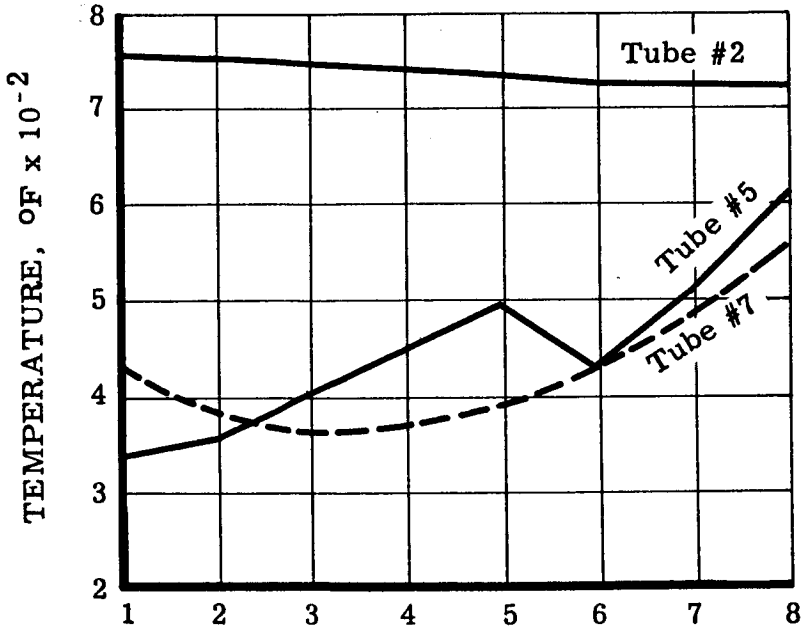

FIGURE 3-24

Section 4.0
CSC I-1A

4.1 CSC I-1 TEST ANALYSIS

The design exit quality of one percent from the parallel portion of condenser CSC I-1 required that tube-to-tube thermal unbalances be small since a greater heat rejection capability in one tube can reduce the quality at the exit end of that tube to zero. If the tube diameter at the downstream sections is less than the critical diameter (see the footnote in Section 3.3.1), condensate will bridge the tube and block further vapor flow. The only way to clear the tube when this occurs is to produce a pressure drop in a parallel tube greater than the liquid head of the trapped slug. This problem is magnified in tapered tubes where a small slug is continuously lengthened as it is lifted toward the exit, requiring an increasing pressure.

The low design outlet quality thus permitted a relatively small unbalance in the thermal and/or geometric characteristics of the tubes to drop the vapor velocity in some tubes below a level necessary for drop transport; at this point the drops agglomerated and bridged the less-than-critical diameter tube and could not be removed since a sufficient pressure drop in a parallel tube could not be created. This was then accompanied by tube-to-tube recirculation, increasing liquid hold-up in the tubes and inlet header, and increasing pressure level.

In parallel tube condensers designed for zero or micro-gravity environments, the liquid vapor interface(s) may be held in each individual tube. Consequently, unbalances can be compensated for by shifting the interface positions in the tube as shown by the following analysis.

Consider the two-tube condenser below operating in zero or micro-gravity.

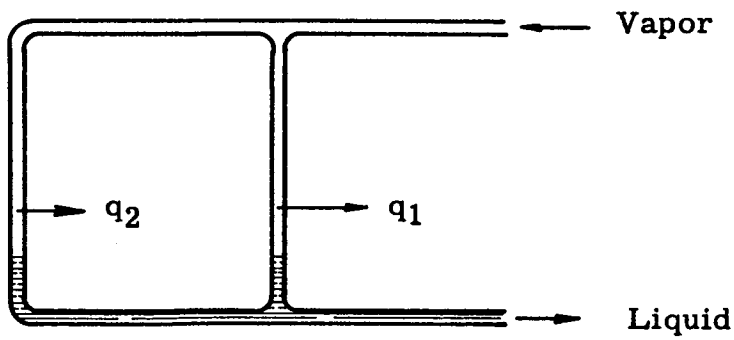

If the heat rejection capability per unit length of tube No. 1 becomes greater than tube No. 2,

$$q_1 > q_2$$

and

$$\dot{m}_{V1} > \dot{m}_{V2} \qquad \text{(vapor mass flow rates)}$$

This means that the pressure drops are unequal.

$$\Delta P_1 > \Delta P_2$$

However, since the tube inlet pressures are equal (assuming negligible header pressure drop), the interface pressures are unequal, which is not a stable condition. Therefore the unbalance is compensated for by adjustment of the interface location until

$$\Delta P_1 = \Delta P_2 \text{ at which } l'_{c2} > l'_{c1} \text{ and } \dot{m}_{V1} > \dot{m}_{V2}$$

where l'_c are the respective condensing lengths

However, for the Sunflower condenser designed for lg in any direction, the interface cannot be held in the tubes (as previously shown) and thermal and geometric unbalances can be compensated for only by changes in exit quality. Obviously the design exit quality must be sufficiently large to compensate for the unbalances without allowing the vapor velocity to drop below that value required for drop transport. Nor does one want to have too high an outlet quality because of the weight penalty involved. The minimum exit quality to meet the above requirements can be approximated assuming reasonable geometric and thermal unbalances.

Assuming a tapered condenser tube with a constant vapor velocity and neglecting the small momentum recovery which results, the following analysis investigates the necessary outlet quality (based on 100% inlet quality) for parallel tube stability.

Friction:

$$dP_s = \Phi f_V \frac{(G_x)^2}{\rho_V 2 g_3} \frac{dL}{D} \qquad (22)$$

Thermal Balance:

$$dL = -\frac{G h_{fg}}{q} \frac{\pi D^2}{4} dX \qquad (23)$$

Combining equations (22) and (23) gives

$$dP = \Phi f_V \frac{(GX)^2}{\rho_V 2_{gs}} - \left(\frac{Gh_{fg}\,\pi D^2}{4Dq}\right) \qquad dX$$

$$dP = C_1 \frac{G^3 X^2 D}{q} \quad dX \qquad (24)$$

where

$$C_1 = \frac{\Phi f \pi h_{fg}}{8 \rho_V g_s} \quad \text{(assumed constant)}$$

Φ_{int} = ratio of two-phase to vapor-only pressure drop (see Section 3.2)

f_V = vapor phase friction factor

G = total (vapor + condensate) weight flow per unit area

X = local quality

h_{fg} = heat of vaporization

D = average tube diameter

ρ_V = vapor density

g_s = local gravitational constant

q = heat rejection per unit length

The assumption that Φ_{int} and f are constant will not affect the answer greatly since two condensing tubes will be compared and these values will change very little from tube to tube over the quality ranges to be examined. The use of an average D rather than an integrated one should also have little effect since the pressure drop of one tube is to be compared to another rather than the absolute value obtained.

Integrating equation (24)

$$\int_{P_1}^{P_e} dP = C_1 \frac{G^3 D}{q} \int_{X_0=1}^{X_e} X^2 dX$$

$$P_e - P_1 = C_1 \frac{G^3 D}{q} \left[\frac{X_e^3}{3} - \frac{1}{3} \right]$$

$$P_1 - P_e = C_1 \frac{G^3 D}{q} \left[\frac{1 - X_e^3}{3} \right] \qquad (25)$$

where

P_1 = inlet pressure

P_e = exit pressure

Integrating and solving for G

$$\int_0^L dL = - \frac{G h_{fg} \pi D^2}{4q} \int_{X_0=1}^{X_e} dX$$

$$L = - \frac{G h_{fg} \pi D^2}{4q} \left[X_e - 1 \right]$$

$$G = \frac{4Lq}{\pi D^2 h_{fg} \left[1 - X_e \right]} \qquad (26)$$

Combining equations (25) and (26)

$$P_1 - P_e = C_2 \frac{q^2}{D^5} \frac{\left[1 - X_e^3 \right]}{\left[1 - X_e \right]^3} \qquad (27)$$

$$C_2 = C_1 \frac{1}{3} \left[\frac{4L}{\pi h_{fg}} \right]^3$$

Equation (27) provides an expression for tube exit quality as a function of tube geometric and thermal characteristics. This can now be applied to two parallel operating tubes as shown in the following sketch.

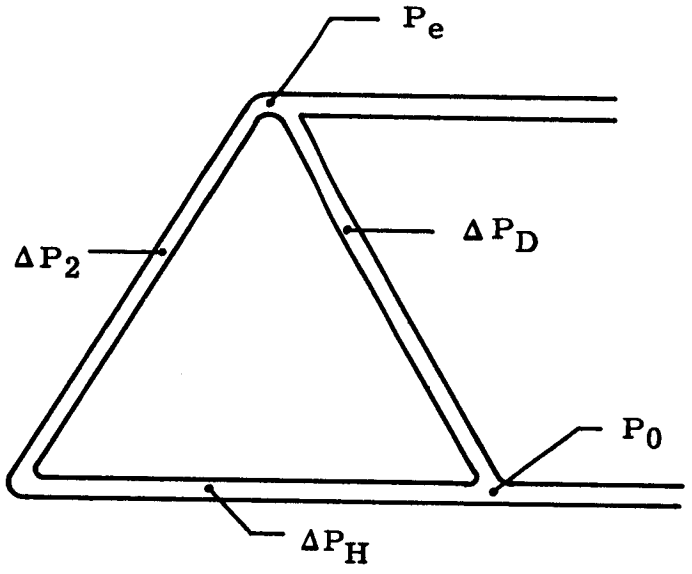

It can be seen that

$$\Delta P_2 + \Delta P_H = \Delta P_D$$

where

ΔP_H = the header friction loss

With the higher design vapor velocities required for parallel tube stability (as will be shown later), the design condenser tube pressure drop will be on the order of 2 psi for CSC I-1A (redesign of CSC I-1) while ΔP_H will remain about 0.1 psi.

Therefore

$$\Delta P_D = 2.0 \text{ psi}$$

$$\Delta P_2 = 1.9 \text{ psi}$$

Allow tube D to operate at design conditions and tube 2 to deviate from design to the extent that

$$q_2 = \epsilon_q \, q_D$$

$$D_2 = D_D / \epsilon_D$$

$$X_{e2} \quad \alpha X_{eD}$$

where

subscript D = design conditions
subscript 2 = actual conditions

Then, using equations (27) and (28) and cancelling

$$\frac{\Delta P_D - \Delta P_H}{\Delta P_D} = \frac{1.9}{2.0} = \frac{\left[1 - (\alpha X_{eD})^3\right]\left[1 - X_{eD}\right]^3}{\left[1 - (\alpha X_{eD})\right]^3\left[1 - X_{eD}^3\right]} \epsilon_q^2 \, \epsilon_D^5 \qquad (29)$$

Equation (26) then expresses the effect of thermal, geometric, and fluid dynamic unbalances between tubes (for CSC I-1A conditions) on the design outlet quality necessary to maintain the vapor velocity greater or equal to α times the design exit vapor velocity. Equation (26), however, still has two unknowns, α and X_{eD} or design outlet quality, even after ϵ_D and ϵ_q are determined. However, these two numbers are related since

$$\frac{X_{ez}}{X_{eD}} = \frac{V_{ez}}{V_{eD}} = \alpha$$

and from Figure 3-4 the minimum value of V for operation in opposition to gravity is 45 ft/sec. Therefore

$$V_{e2} = \alpha V_{eD} \geq 45 \text{ ft/sec}$$

$$V_{eD} = \frac{X_{eD} \; \dot{m}_t}{\rho_v A_e} = \frac{45}{\alpha}$$

Based on the desire to maintain a reasonable pressure drop in the CSC I-1A while using the same shortened tubes as in CSC I-1, it was felt that a 90 ft/sec velocity could be tolerated, making $\alpha \approx 1/2$.

A plot of X_{eD} using an α of one-half and equation (29) is shown in Figure 4-1. This plot shows the required outlet quality as a function of ϵ_D and ϵ_q. The deviations assumed in the figure are accumulative, i.e., ϵ_q & ϵ_d do not tend to compensate for one another.

DESIGN OUTLET QUALITY AS A FUNCTION OF ϵ_q AND ϵ_D
FOR $\alpha = 1/2$

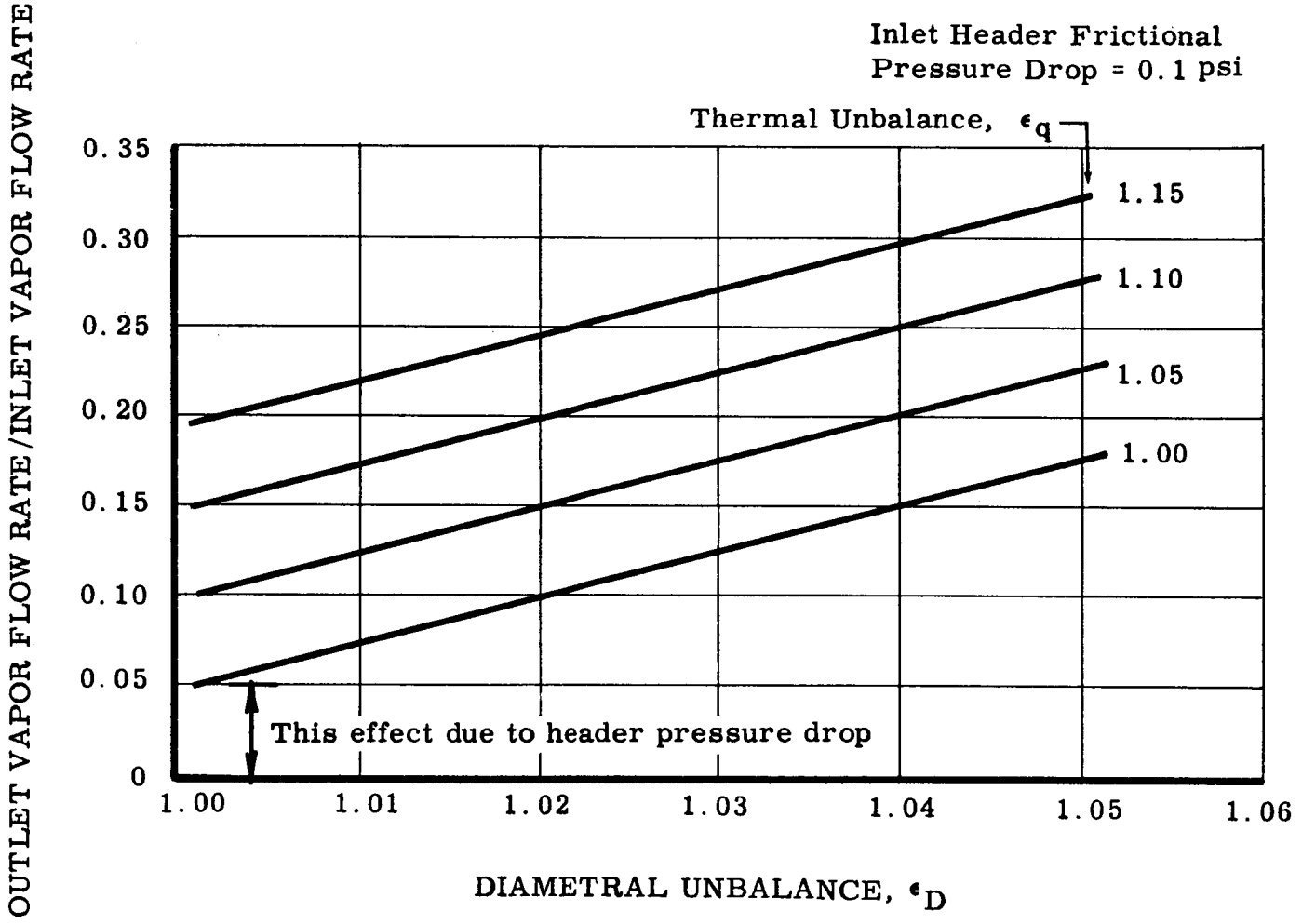

FIGURE 4-1

Based on drawing tolerances, an ϵ_D of 1.01 is maximum and an estimated value of ϵ_q is 1.05. These values yield an $\dot{m}_{Ve}/\dot{m}_{V0}$ of 0.126 or based on a 0.952 inlet quality, an exit quality of 12.0 percent. As a factor of safety 12.6 percent will be used in the redesign.

To summarize, with a 0.1 psi inlet header pressure drop, 2 psi condensing tube drop, unbalances in q and D less than or equal to 5 percent and 1 percent respectively, and a 90 ft/sec design vapor velocity, the outlet velocity in the unbalanced tube will not drop below 45 ft/sec if the design outlet quality is 12.0 percent.

4.2 DESIGN PRESENTATION

4.2.1 Primary Condenser

Based on a re-evaluation of the overall Sunflower I program, it appeared advisable, at this time, to design condenser-subcooler CSC I-1A as a developmental ground operating unit. This eliminated the need for optimization and made hardware from CSC I-1 available for the redesign; consequently, a saving of time and money was effected. The items utilized were the long lead time, high cost parts: the step-tapered inlet header and tapered condensing tubes. With the unit being designed for ground operation only, convection as well as radiation could be relied upon for heat rejection. Also, since 1g will be present at all times in a specific direction and because utilization of CSC I-1 hardware made the condenser pressure drop somewhat of a dependent variable, the interface was located above the pump inlet assuring adequate net positive suction head at all times.

Realizing that parallel tube stability and a less-than-critical diameter at the tube exit had been the major problem with CSC I-1, the redesign attempted to eliminate these problems and provide an increased stability margin. Using the unbalance analysis of the previous section it can be seen that the exit quality, and hence the exit vapor velocity, must be increased if stability margin is to be increased. Accordingly, a velocity of approximately 90 ft/sec was selected which allows the exit quality to decrease to less than half of its design value before the minimum entrainment velocity of 45 ft/sec is reached. Allowing for a heat rejection variation of 5 percent and a diametral deviation of 1 percent results in a design exit quality of 12.6 percent (see Figure 4-1).

With these design inputs fixed, the condenser geometric configuration could be determined. Based on 13.72 lb/min mass flow and 95.2 percent quality, it was determined that a constant vapor velocity of 94 ft/sec was obtained with ten condensing tubes available from the CSC I-1 design. This works in well with the inlet header since every other tube of the CSC I-1 unit could be omitted. The design exit quality of 12.6% is reached at a tube diameter of 0.231 inch with constant vapor velocity yielding a condensing length of 61.56 inches.

Removing alternate condensing tubes from the step-tapered inlet header changed the velocity variation and consequently static pressure distribution. However, the effect is

negligible when compared to the allowable 0.1 psi pressure drop assumed in the unbalance analysis.

The outlet header was redesigned based on the assumption that bends in low quality regions should be eliminated to reduce the possibility of flow separation and agglomeration. The resulting outlet header was trapezoidally-shaped and accepted the flow from the ten condensing tubes and delivered it to the secondary condenser (condenses outlet quality of parallel tube condenser) free of bends. A sketch of this header is shown in Figure 4-2. To eliminate fin interference it was necessary to add an 8 inch adiabatic section to each condensing tube, which in turn was connected to the outlet header.

1100-0 aluminum fins were furnace-brazed to the stainless steel tubes to reject the heat of condensation. These fins were resized in accordance with equation (15); the fin test results are presented in Section 4.3.2. A constant 0.090 inch thick, continuous fin of varying width was used on each tube. Heaters were added to preheat the entire condenser to the design operating temperature with the tapered condensing tubes and fins being the only uninsulated part of what will be called the primary condenser. Figure 4-3 is a photograph of the primary condenser during fabrication.

4.2.2 Secondary Condenser

The 12.6 percent primary condenser exit quality must be reduced to ~0.6 per cent prior to entering the interface chamber. It was decided to use a single tapered tube direct condenser at this time with an indirect condenser to be investigated later as a possible weight or pressure drop saving. A 64.6 inch condensing length was used, which brings the condenser, physically, to just below the subcooler-heat exchanger bundle and pump inlet. The tube diameter was tapered from a 0.210 inch by 2.052 inch rectangular cross-section to a 0.210 inch diameter tube with the 1100-0 aluminum fin sized to maintain a constant 94 ft/sec vapor velocity.

With the interface to be positioned above the pump inlet it was necessary to add a 21 inch long, 0.210 inch inside diameter 347 stainless steel line. This line, referred to as the low quality vapor line, was used to deliver the mixture from the secondary condenser to the interface chamber. An 1100-0 aluminum fin was sized to reject only sensible heat.

4.2.3 Inteface Chamber

The interface chamber was a 4 inch high, 1-1/2 inch inside diameter vessel with glass viewing slots for visual observation of the interface during condenser operation. The 0.6 per cent quality mixture enters at the top and condensate is removed from the bottom. AMS 4000 aluminum fins are attached to the 316 stainless steel chamber and used to reject the final quality. A schematic diagram of the interface chamber is shown in Figure 4-4.

CSCI-1A PRIMARY CONDENSER OUTLET HEADER

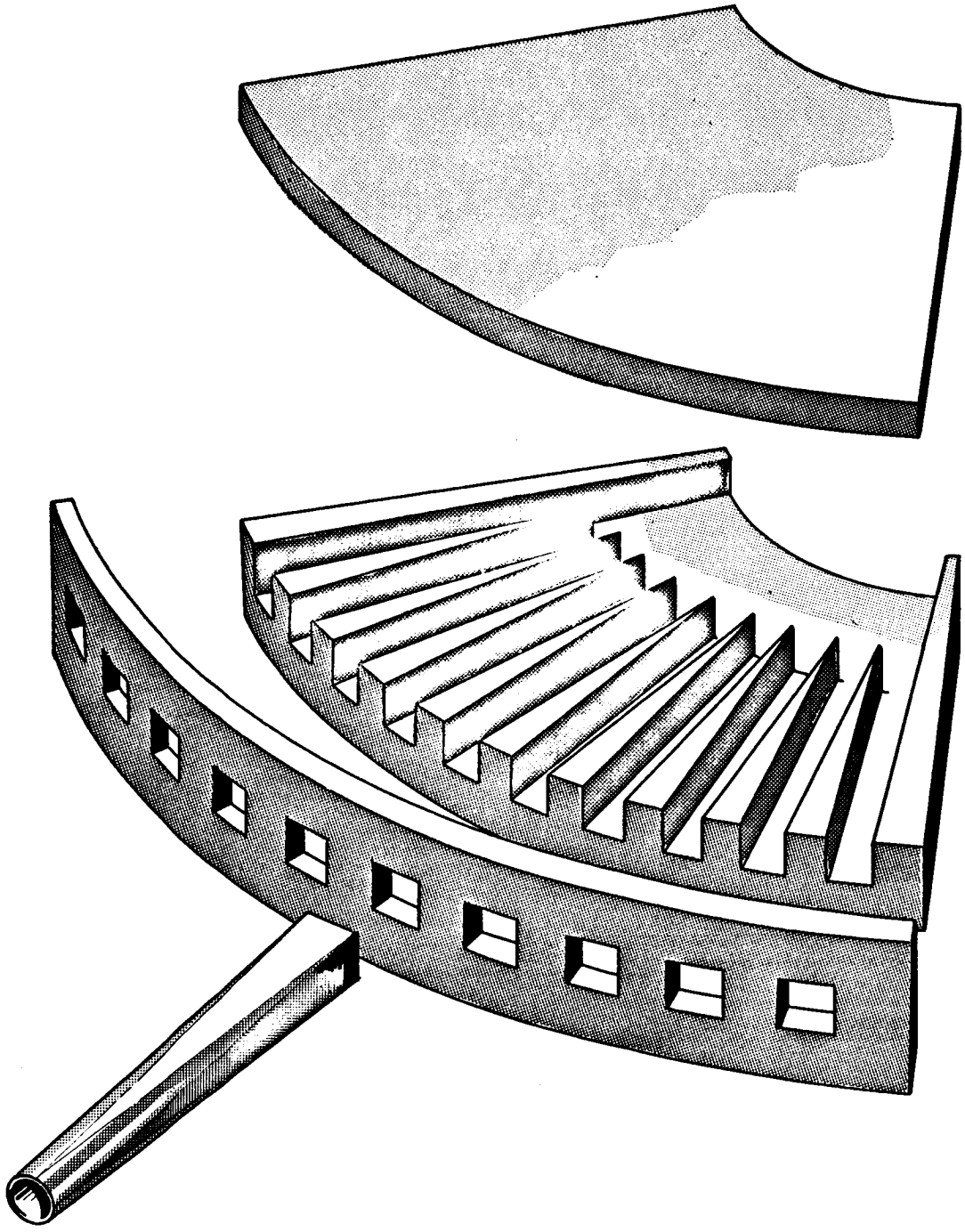

FIGURE 4-2

PRIMARY CONDENSER DURING FABRICATION

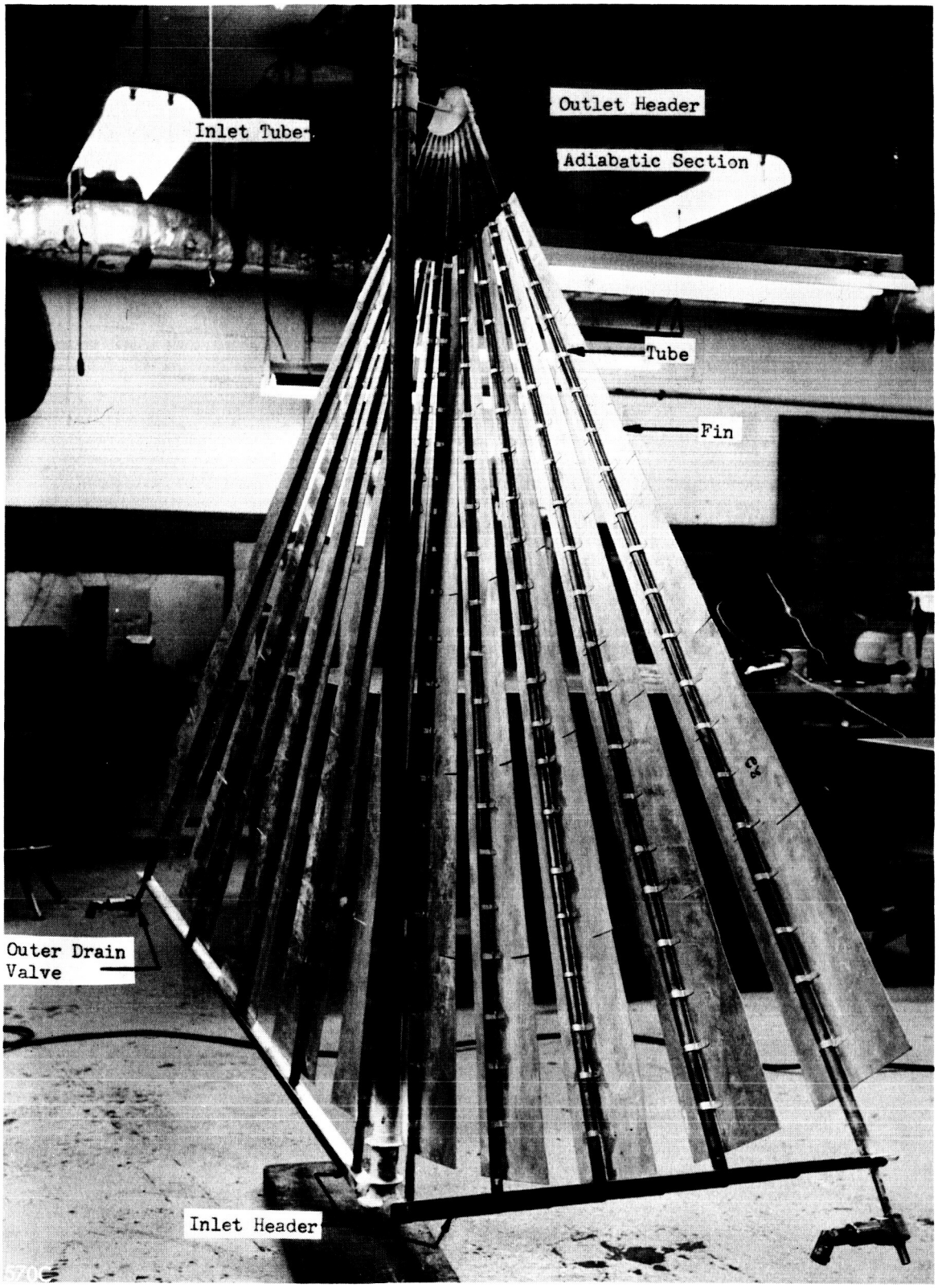

FIGURE 4-3

LIQUID-VAPOR INTERFACE CHAMBER SCHEMATIC

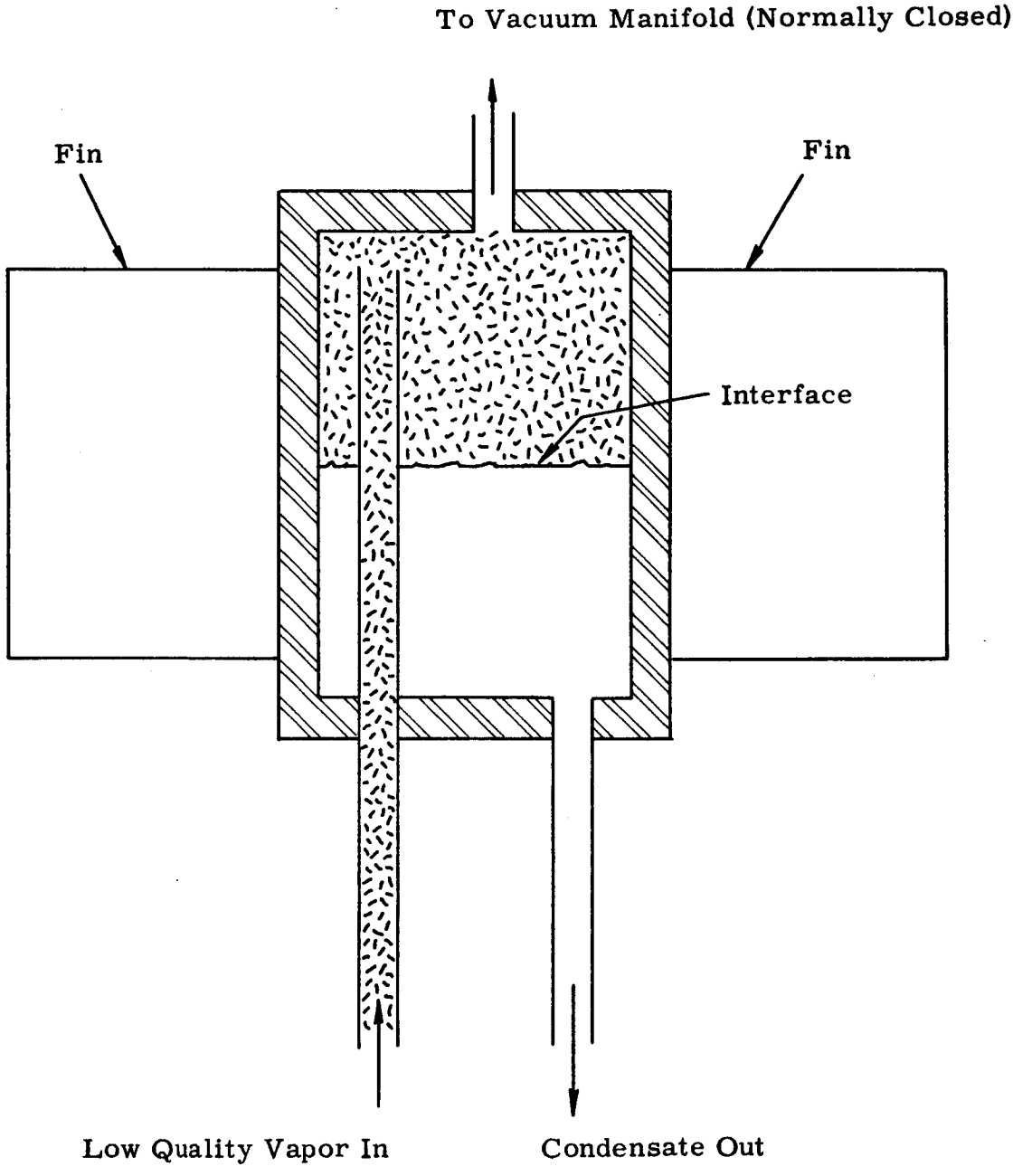

FIGURE 4- 4

4.2.4 Subcooler Heat Exchangers

The modifications to the CSC I-1 subcooler-heat exchanger design included removing the tube-in-tube heat exchanger upstream of the interface chamber and resizing the subcooler radiator from the CSC I-1 test results. The three remaining tube-in-tube heat exchangers are used to subcool the condensate and bearing return flows. They are made of 316 stainless steel tubing 1/2 inch and 5/16 inch outside diameter. The high pressure boiler feed flow is again used as coolant. The subcooler heat exchanger (installed in the test rig) is shown in Figure 4-5.

Since the turbo-alternator unit bearing flow requirements had not been finalized at this time, it was necessary to determine the effect of variation of this flow on the heat exchanger temperatures. Specifically, the pump inlet temperature would be directly affected which would in turn affect the pump net positive suction head and bearing lube supply temperature. To this end, a computer program was set up and the effect of three different bearing flows analyzed. The results are shown below. As can be seen, the effect on the pump inlet temperature was negligible and no heat exchanger modifications were necessary.

Bearing Flow lb/min.	Pump Inlet Temperature °F
16.0	368
22.0	375
28.0	382

The non-isothermal subcooler radiator cools the high pressure boiler feed flow used as coolant in the subcooler heat exchangers. It is a 1/4 inch OD 316 stainless steel tube, 91 inches long, brazed to a 0.040 inch 1100-0 aluminum fin coated with high emissivity enamel.

4.2.5 Pressure Drop Summary

The calculated condenser pressure drop is as follows.

Inlet tube	0.55 psi
Header	0.38
Condenser tubes (primary	1.25
Outlet header (including adiabatic section)	0.61
Condenser tube (secondary)	0.63
Low quality vapor line	1.94
Subcooler (liquid)	0.14
Static head (interface to pump)	5.3 ± 0.7 (pressure rise; depending on interface position)
Total drop	0.2 ± 0.7 psi

SUBCOOLER HEAT EXCHANGERS AND LOW
QUALITY VAPOR LINE

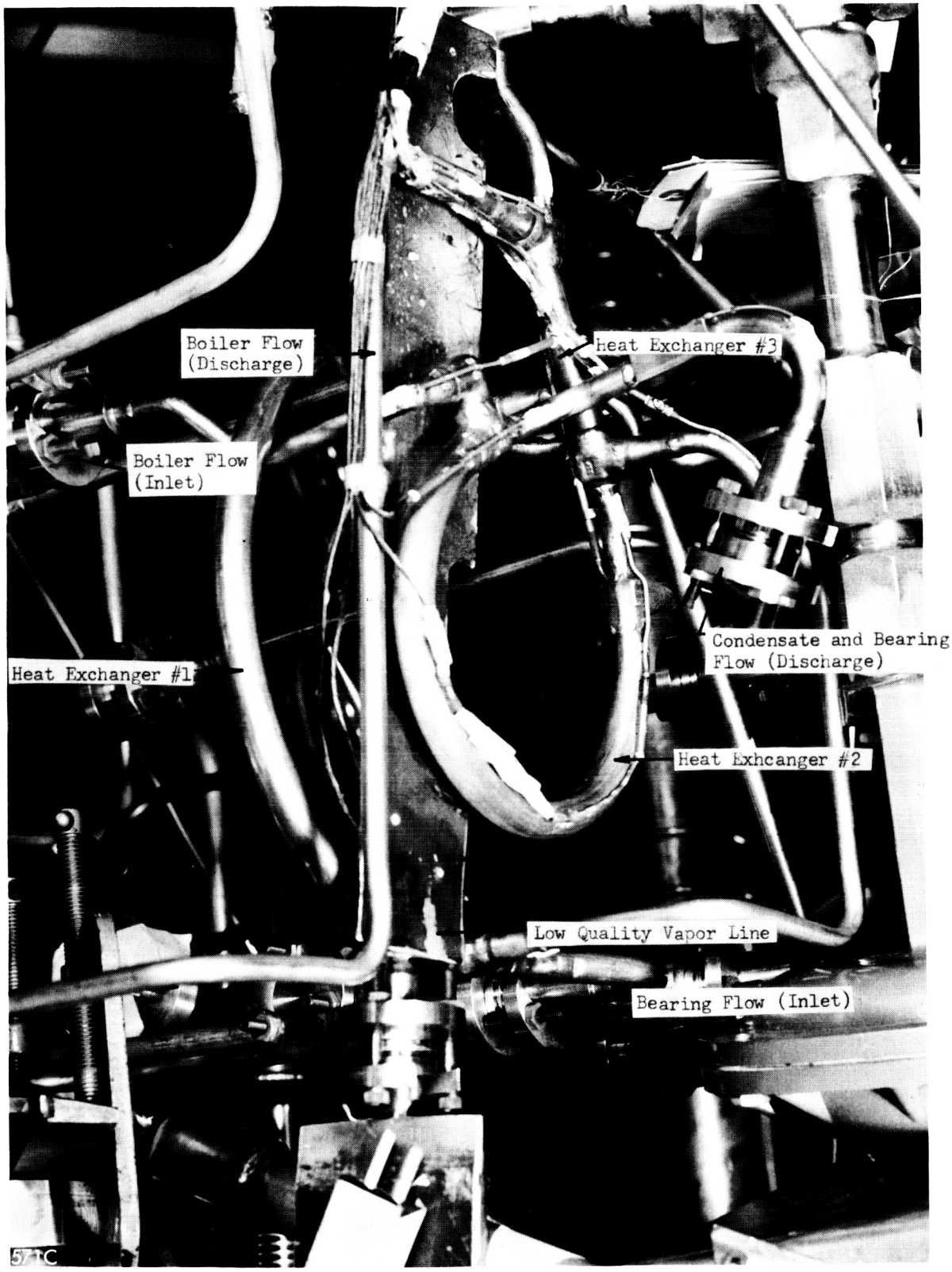

FIGURE 4-5

Turbine outlet	7.0 psia
Pump inlet	6.8 ± 0.7 psia
Vapor pressure 400°F	0.39 psia
NPSH	6.4 ± 0.7 psia

In these calculations the correlations of Section 3.3.1 and Reference 15 were used.

4.3 EXPERIMENTAL INVESTIGATIONS

4.3.1 Multiple Tube Breadboard

It was felt that experimental verification of the analysis conducted with regard to parallel tube unbalance, design vapor velocity necessary for stability (Section 4.1), and feasibility of parallel tube start-up with flow against gravity was necessary. To this end, a three-tube glass condensing appratus was built and operated. A schematic diagram of this breadboard is shown in Figure 4-6 and a photograph is given in Figure 4-7.

The breadboard was designed to operate in air with mass flow limited by the output of the small pot boiler available from the single tube breadboard testing. The mass flow capability of this boiler with three parallel tubes requires a less than critical diameter to achieve greater than 23 ft/sec exit velocity at a nominal quality of 10 per cent. At first glance this velocity appears to be in direct violation of the 45 ft/sec specified in Section 3.1.1. However, the minimum entrainment velocity is heavily dependent on vapor density (Figure 3-18) and at the expected breadboard operating pressure this velocity was near the required entrainment velocity.

Since a specific conclusion of the preprototype testing was to avoid critical diameters, and the objective of this test was limited to determination of the conservativism of the design criteria, these outlet velocity limitations were accepted. This explains the low velocities noted in the data.

All tests were conducted with the multiple tube flow vertically upward. The test section itself was designed for constant static pressure at the inlet of the three condensing tubes (by the static regain method). The condensing tubes were step-tapered to maintain vapor velocity for operation in opposition to 1g.

To operate, the glass tubes were preheated to approximately 600°F and the boiler heated at atmospheric pressure until boiling started. The system was then evacuated, increasing the boiling rate and initiating vapor flow through the condenser. Valve No. 1 (Figure 4-6) was then shut and the interface allowed to proceed upstream in the interface tube. As this occured, the quality at the exit of the multiple tubes is decreased by the shift in relative condensing heat transfer area upstream and downstream of this junction. This relation is the basis of primary condenser exit quality calculations.

In the steady state stable flow tests, the interface could be readily stopped and held in a fixed position by modulating valve No. 1. This facilitated accurate steady state

MULTIPLE TUBE BREADBOARD SCHEMATIC

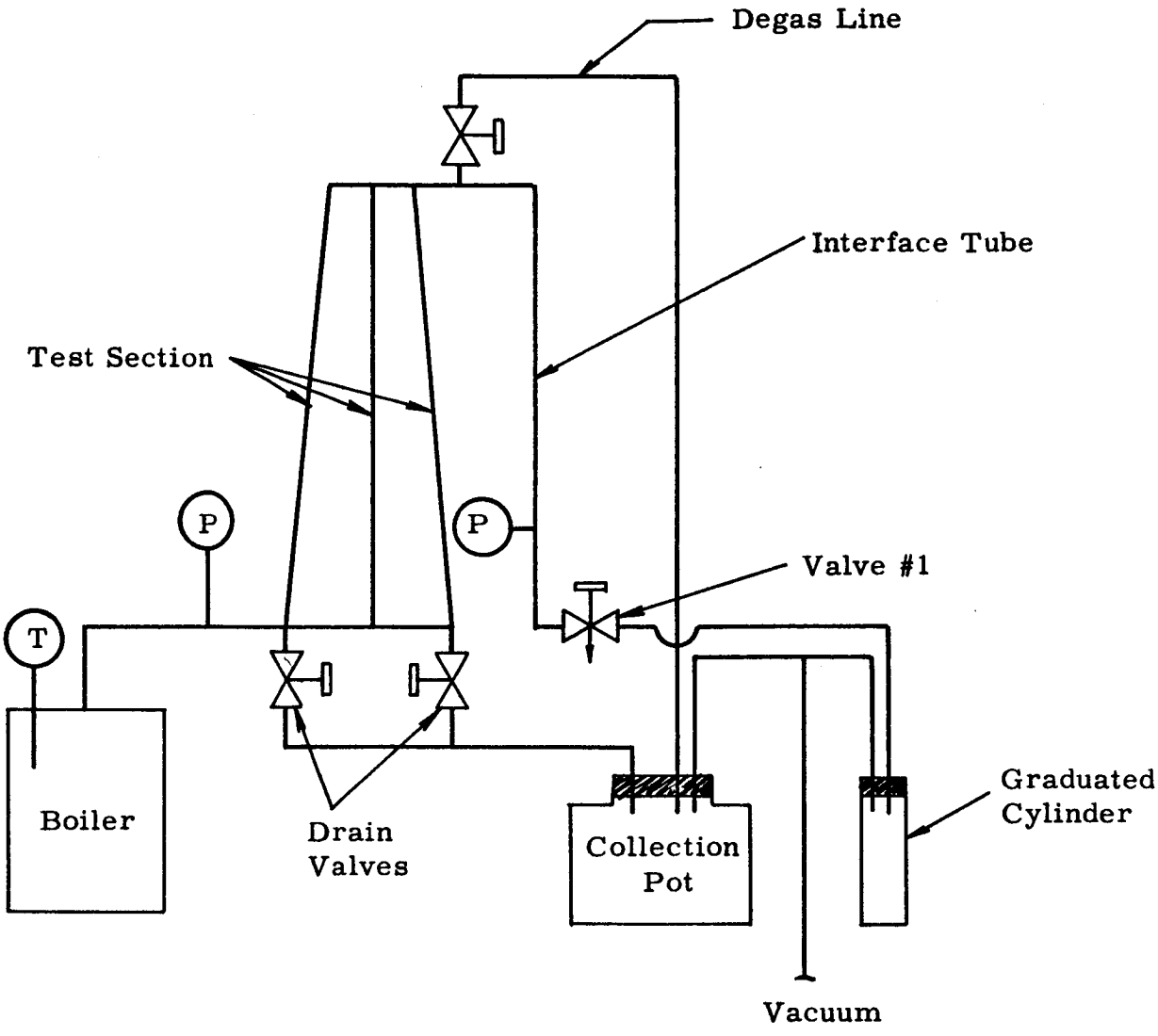

FIGURE 4-6

MULTIPLE TUBE BREADBOARD

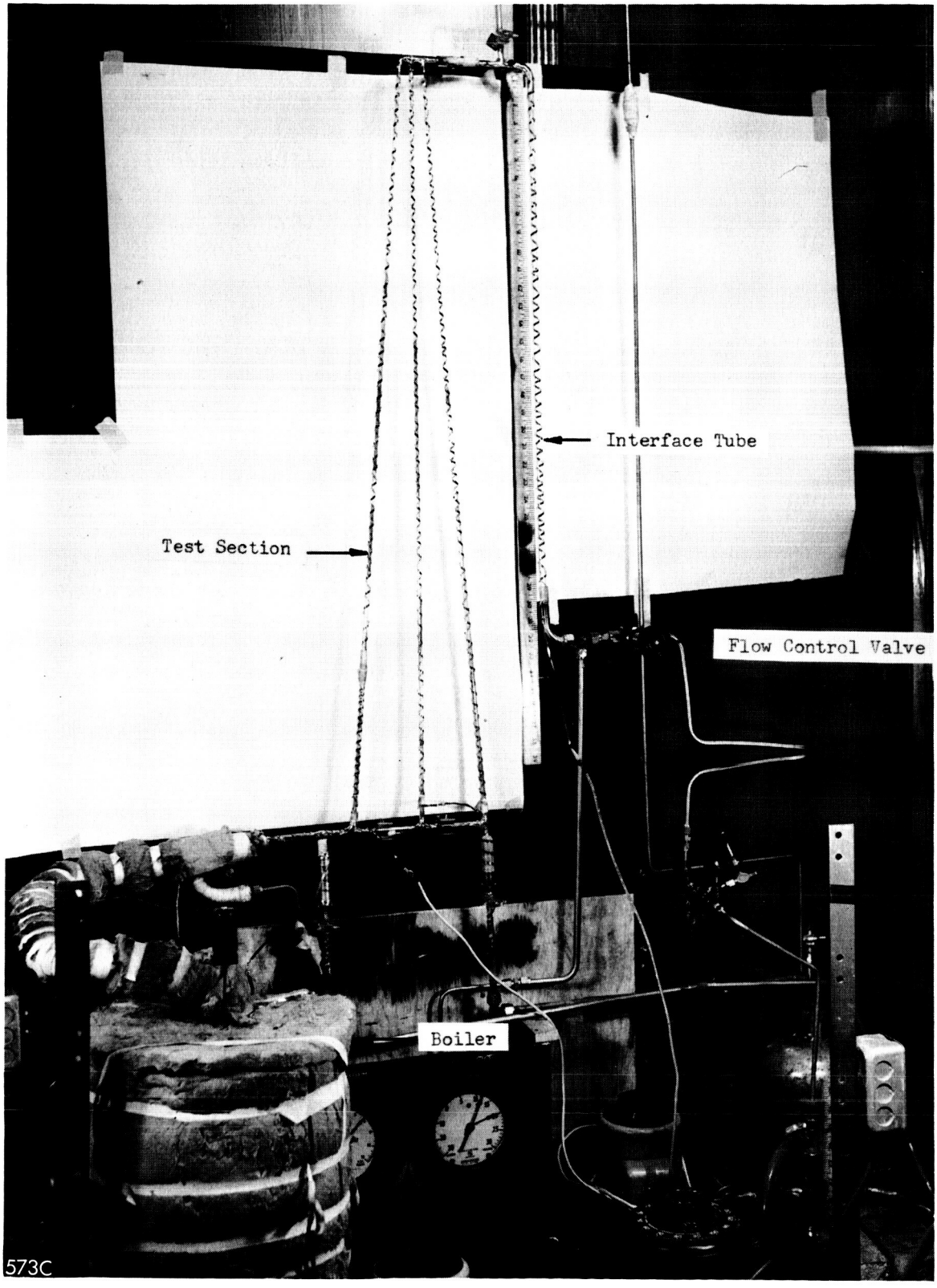

FIGURE 4-7

flow measurements by time rate of filling of the graduated cylinder.

Stability tests were performed by permitting the parallel tube exit velocity and quality to steadily decrease until slugging and unstable flow occurred. Interface location at this event then indicated the stability limit. Six of these runs were performed with an interface tube diameter of 6 mm. This tube was then replaced with a 10 mm tube and the tests repeated four times. Comparison of the results of these tests yields a check on the heat transfer calculations employed to arrive at the quality and velocity conclusions. Results of the tests are tabulated in Table 4-1. The repeatability of stability data is noted.

TABLE 4-1

MULTIPLE TUBE BREADBOARD TEST RESULTS
(CONDITIONS AT INCIPIENT INSTABILITY)

	6 mm Interface Tube						10 mm Tube			
Run Number	1.	2.	3.	4.	5.	6.	1.	2.	3.	4.
Boiler temperature, °F	670	670	670	670	670	670	660	660	660	660
Flow rate, lb/min	0.40	0.40	0.40	0.40	0.40	0.40	0.52	0.52	0.52	0.52
Location of interface at incipient instability, in.	30.0	29.5	30.8	30.5	30.0	29.5	15.0	16.0	15.5	16.0
Average exit quality, %	19.7	19.4	20.0	19.9	19.7	19.4	17.4	18.2	17.8	18.2
Average inlet velocity, fps	28.2	28.2	28.2	28.2	28.2	28.2	35.4	35.4	35.4	35.4
Average exit velocity, fps	12.6	12.7	12.4	12.4	12.6	12.7	14.5	13.9	14.2	13.9

As previously analyzed, the minimum design velocity necessary for antigravity parallel tube operation is a function of tube unbalance. Although the unbalance between tubes was not quantitatively established in this rig, it was felt that these unbalances were higher than those expected in the CSC I-1A unit. This is due to the difficulty of fabricating glass hardware with geometric accuracy.

Table 4-1 indicates that the parameters designed into CSC I-1A with regard to parallel tube stability were sufficiently conservative to insure stability in the CSC I-1A unit. Specifically, the glass rig operated with an average outlet velocity very near the curve of Figure 3-18 while CSC I-1A will operate with an average outlet velocity double that indicated in the figure.

4.3.2 Fin Test

The purpose of the Sunflower condenser fin test was to obtain design curves for sizing the fins for the CSC I-1A environment. It is possible that this fin sizing could have been accomplished analytically according to the general heat transfer relationships for convective and radiant heat transfer. However, it was considered more accurate to obtain data from a test apparatus, thus eliminating the necessity of estimating a natural convective heat transfer coefficient.

The sensitivity of condenser operation to vapor velocity (Section 3.1.1) shows the importance of accurate determination of these fin sizes. Off design of the heat rejection can cause the vapor velocity to vary appreciably. Under design of the heat rejection capability will cause a decrease in condenser stability margin due to a decreased vapor velocity and over design will cause a high pressure drop due to increased vapor velocity.

The test was conducted on 20-1/2 inch long 1100-0 aluminum fins with thicknesses of 0.40 inch, 0.050 inch, 0.090 inch and 0.125 inch and overall widths of 6 inches, 4-1/2 inches, and 2-1/2 inches. The fins were coated with a high emissivity paint, the same paint intended for the CSC I-1A fins. The condenser tube was simulated on these fin test sections by two electric tubular heaters which were rigidly attached to the aluminum fin. Heat transfer cement was used in the area between the heaters and fin to provide a low resistance heat transfer path. Temperatures were recorded from thermocouples located on the fin and on the heater sheaths by a temperature logger and pyrometer. Thermocouples located on the fin centerline were used to determine the fin root temperatures. Heat input was measured by a wattmeter which gave the electrical power input to the heaters. Laboratory ambient temperature was also measured.

The total heat input to the test section, or total heat rejection due to convection and radiation, was obtained for various fin widths, thicknesses, and fin root temperatures. In addition, a test was run on the heaters to determine its heat rejection as a function of surface temperature (Figure 4-8). Thus, by subtracting the heat rejection of the heaters from the overall heat rejection, the fin heat rejection was determined. This fin heat rejection was then plotted for design purposes and is shown in Figure 4-9.

CONDENSER TUBE HEAT REJECTION

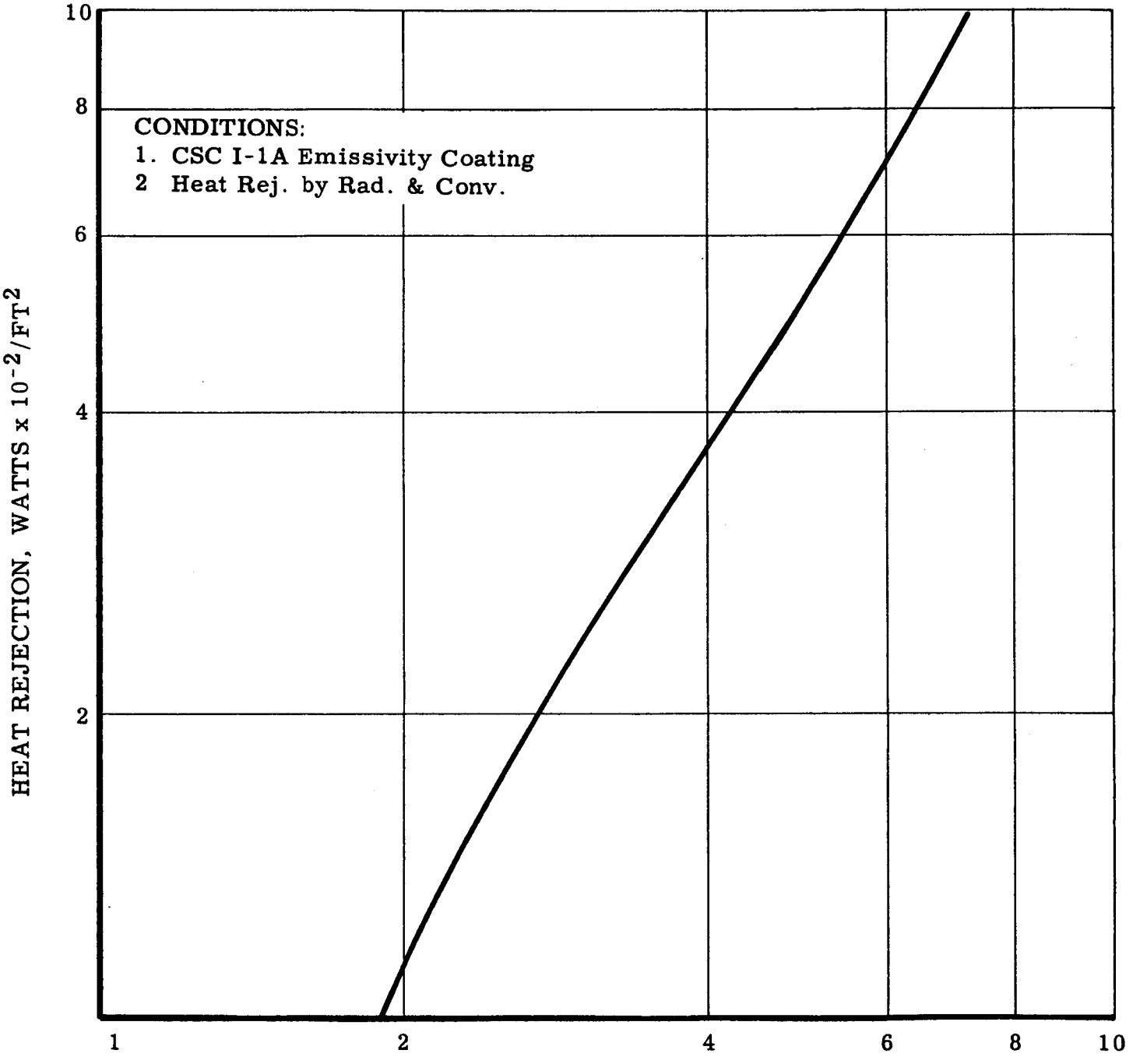

FIGURE 4-8

FIN HEAT REJECTION AS A FUNCTION OF WIDTH AND THICKNESS

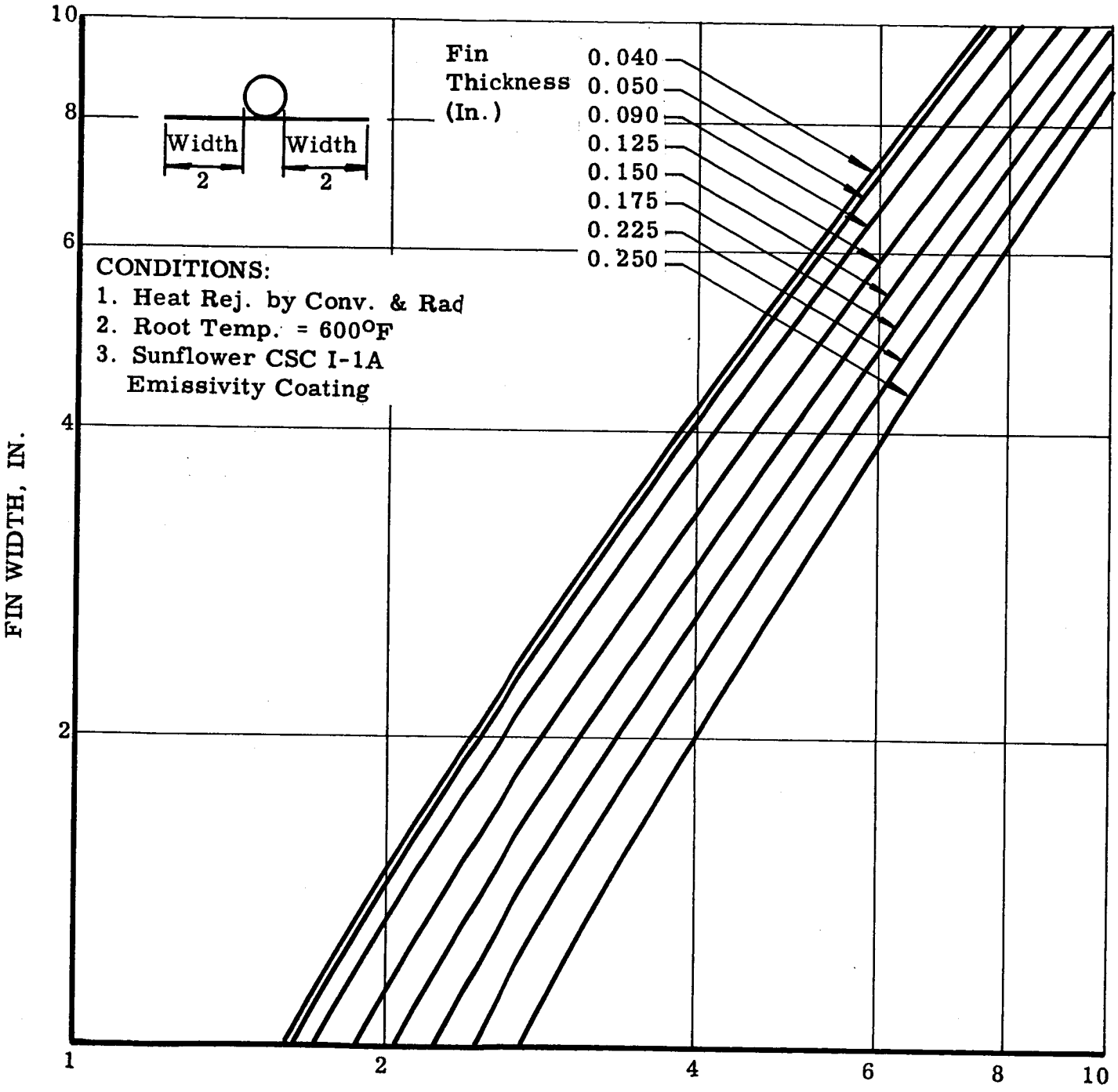

FIGURE 4-9

The fin widths are less than the overall widths previously recorded. This is the result of subtracting the heater width which yields the effective fin width.

Every effort was made to simulate the ambient conditions that were expected during the CSC I-1A component test. Difficulty of exact duplication is recognized as a limitation on the data.

4.3.3 Fin Test, Argon Versus Air Environment

Due to the necessity of operating the Sunflower I system in argon on the ground because of the lithium hydride danger, a test was conducted to compare the heat rejection rate of an aluminum fin in air and argon. Calculations indicated a ten per cent reduction in heat rejection in an argom atmosphere as opposed to air with a 600°F fin root temperature. However, a more accurate number was needed to predict condenser operating temperature and pressure levels in the Sunflower I system test.

The test was conducted in a sealed 4 foot x 4-1/2 foot x 7-1/2 foot test booth capable of being inerted with argon through two diffusers located on the floor. The oxygen concentration in the booth was measured with a magnetic oxygen analyzer. The test sample was an 1100-0 aluminum fin brazed to a 120 volt, 300 watt, incoloy-sheathed heater coated with a high emissivity enamel. Various fin and heater temperatures were recorded. A wattmeter, voltmeter, and ammeter were used to monitor and verify power input which was used as fin/tube heat rejection at the average fin root temperature. Both air and argon environment data were taken.

The test showed a 13 per cent reduction in heat rejection rate with an argon atmosphere at the Sunflower I condenser design temperature of 600°F (Figure 4-10). Exrapolation of this air/argon relationship to all the fins in the CSC I-1A design results in little error due to the high efficiency of even the larger end of the CSC I-1A fins.

4.4 CSC I-1A COMPONENT TEST

4.4.1 General Description

The CSC I-1A condenser test was divided into three phases to quantitatively establish the parameters affecting each portion of the condenser and to determine operating characteristics and possible problem areas. In all phases, the test was conducted with mass flow against gravity as a demonstration of condenser operation in the most adverse orientation of the $\pm$ 1g Sunflower I system operating requirement. An installation schematic for each phase of the condenser test is shown in Figures 4-11, 4-12, and 4-13. Figure 4-14 shows the Phase I and Figure 4-15 the Phase III installations.

Startup was accomplished by preheating the entire condenser to its operating temperature and evacuating before introducing vapor. The preheaters were shut off simultaneously with initiation of flow. For the first few seconds after flow started, the outer valves on the inlet header were kept open to drain off any liquid that may have been condensed on surfaces not adequately preheated. The valves were then

COMPARISON OF THE OPERATING TEMPERATURE
OF A FIN IN AIR AND ARGON

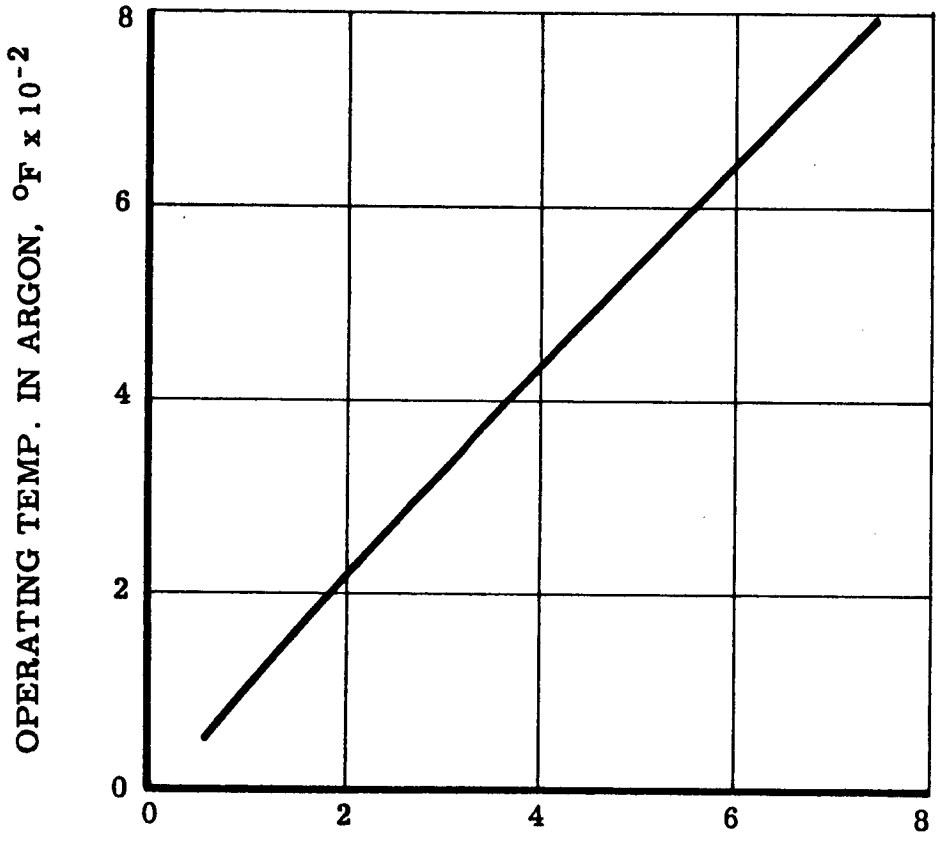

FIGURE 4-10

PHASE I CONDENSER TEST SCHEMATIC

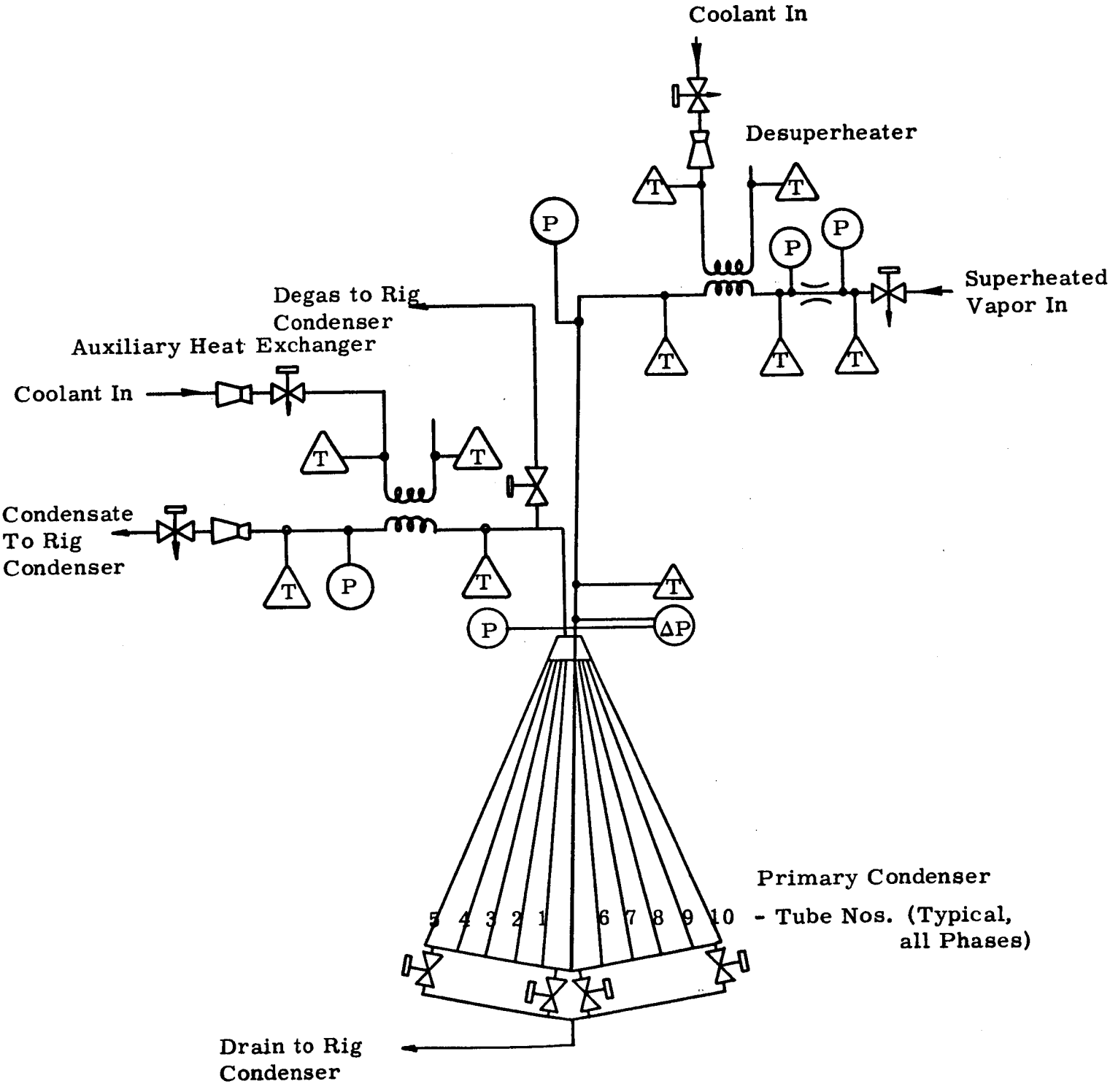

FIGURE 4-11

PHASE II CONDENSER TEST SCHEMATIC

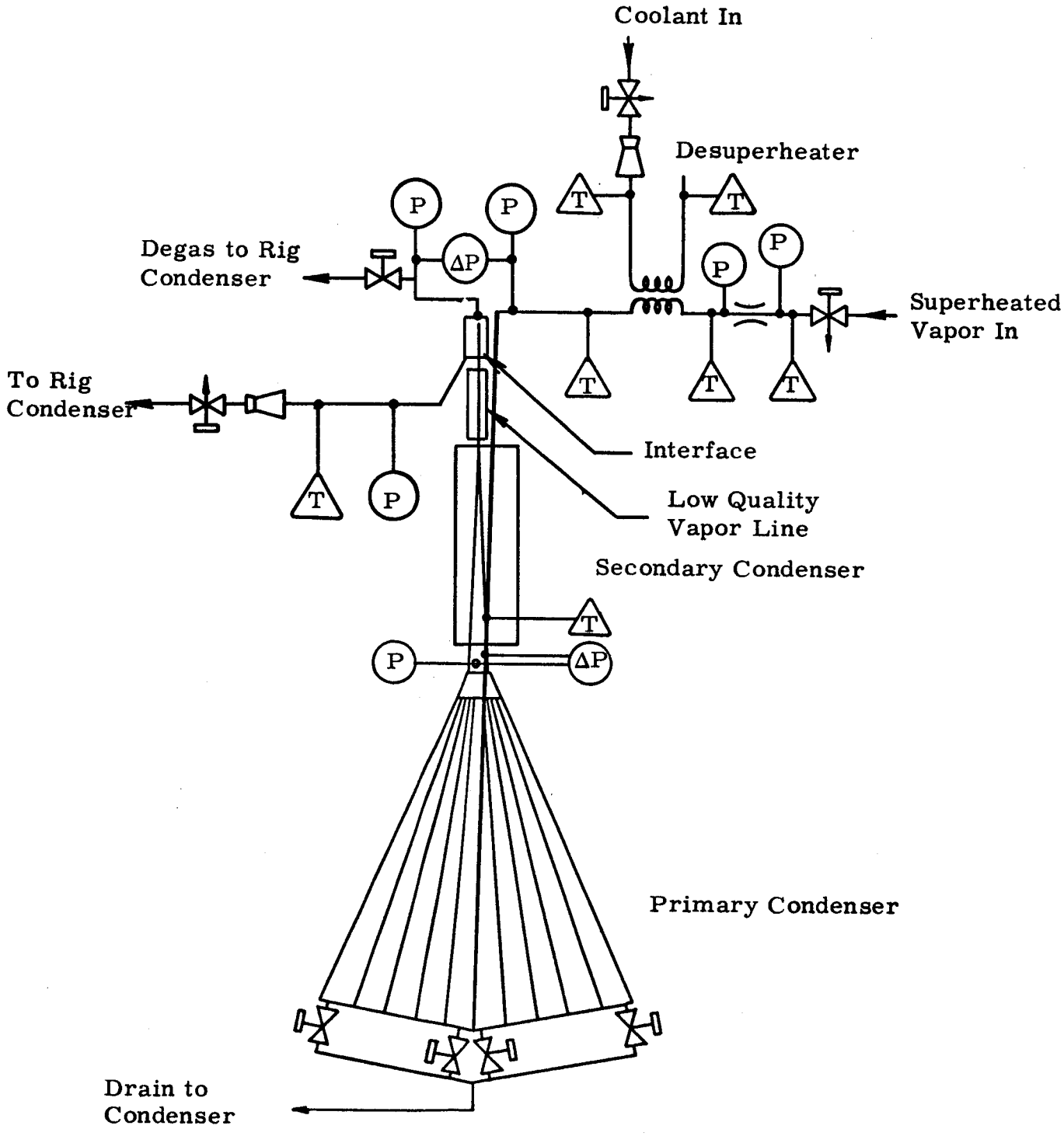

FIGURE 4-12

PHASE III CONDENSER-SUBCOOLER TEST SCHEMATIC

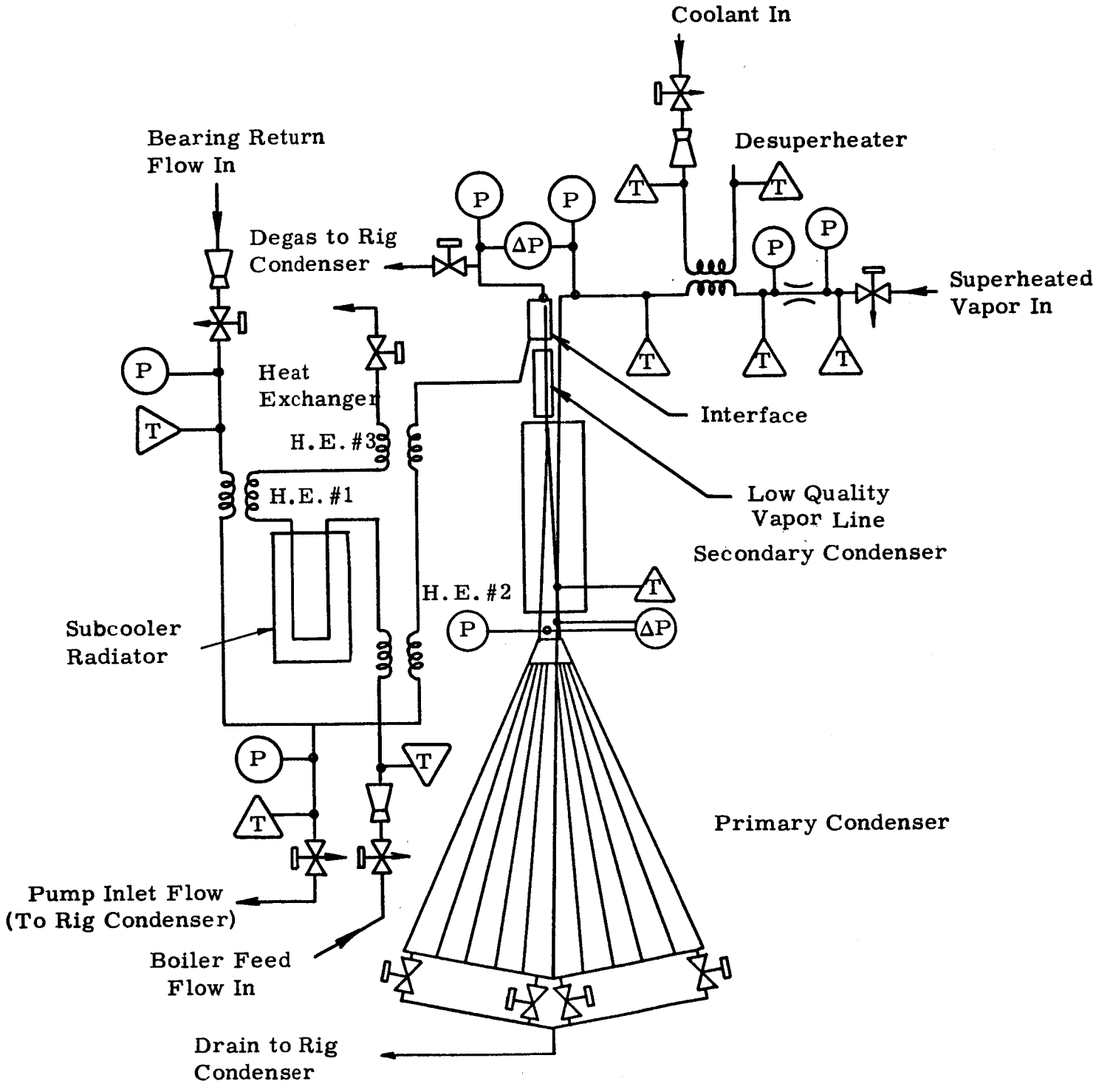

FIGURE 4-13

PHASE I INSTALLATION

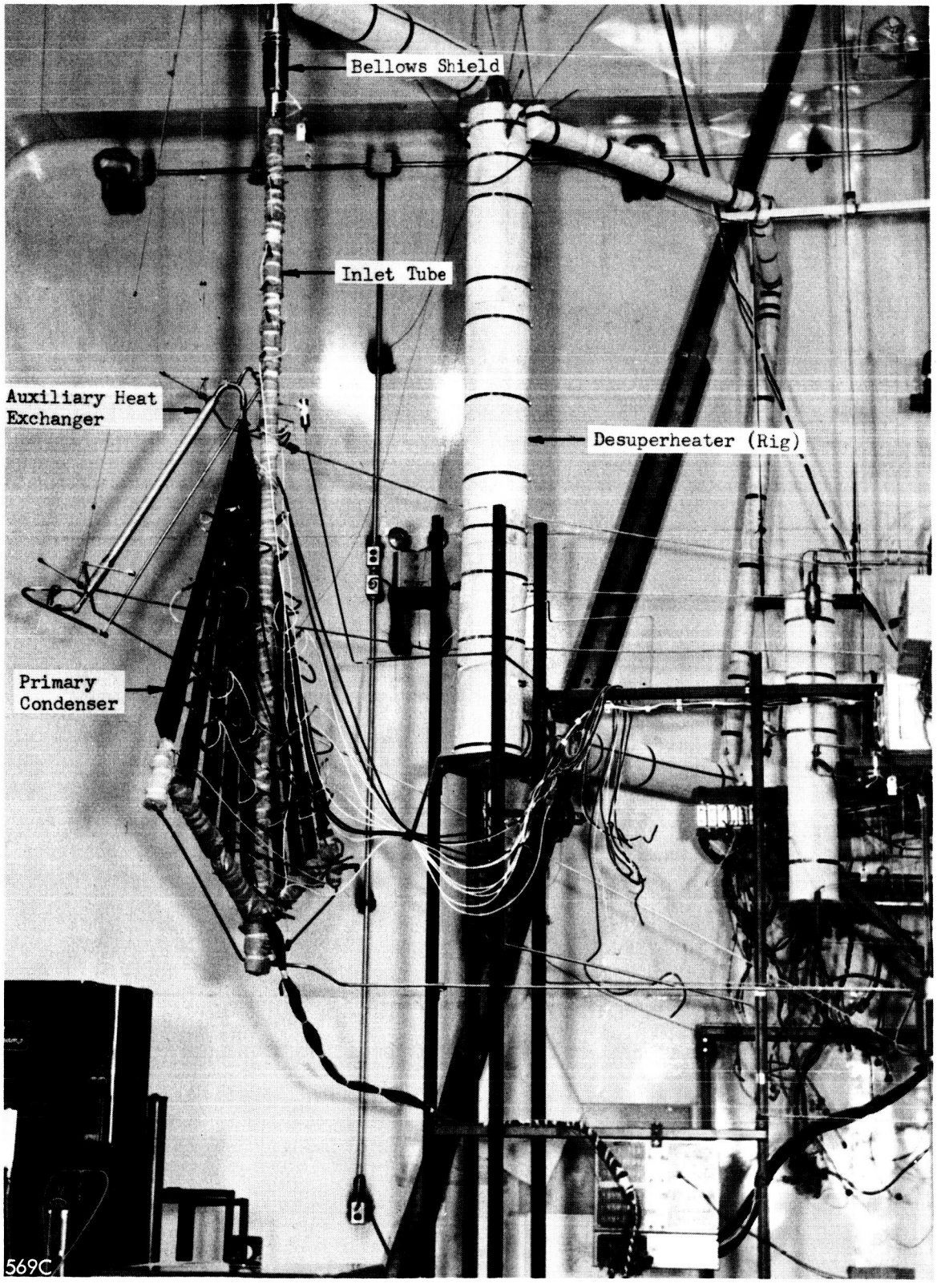

FIGURE 4-14

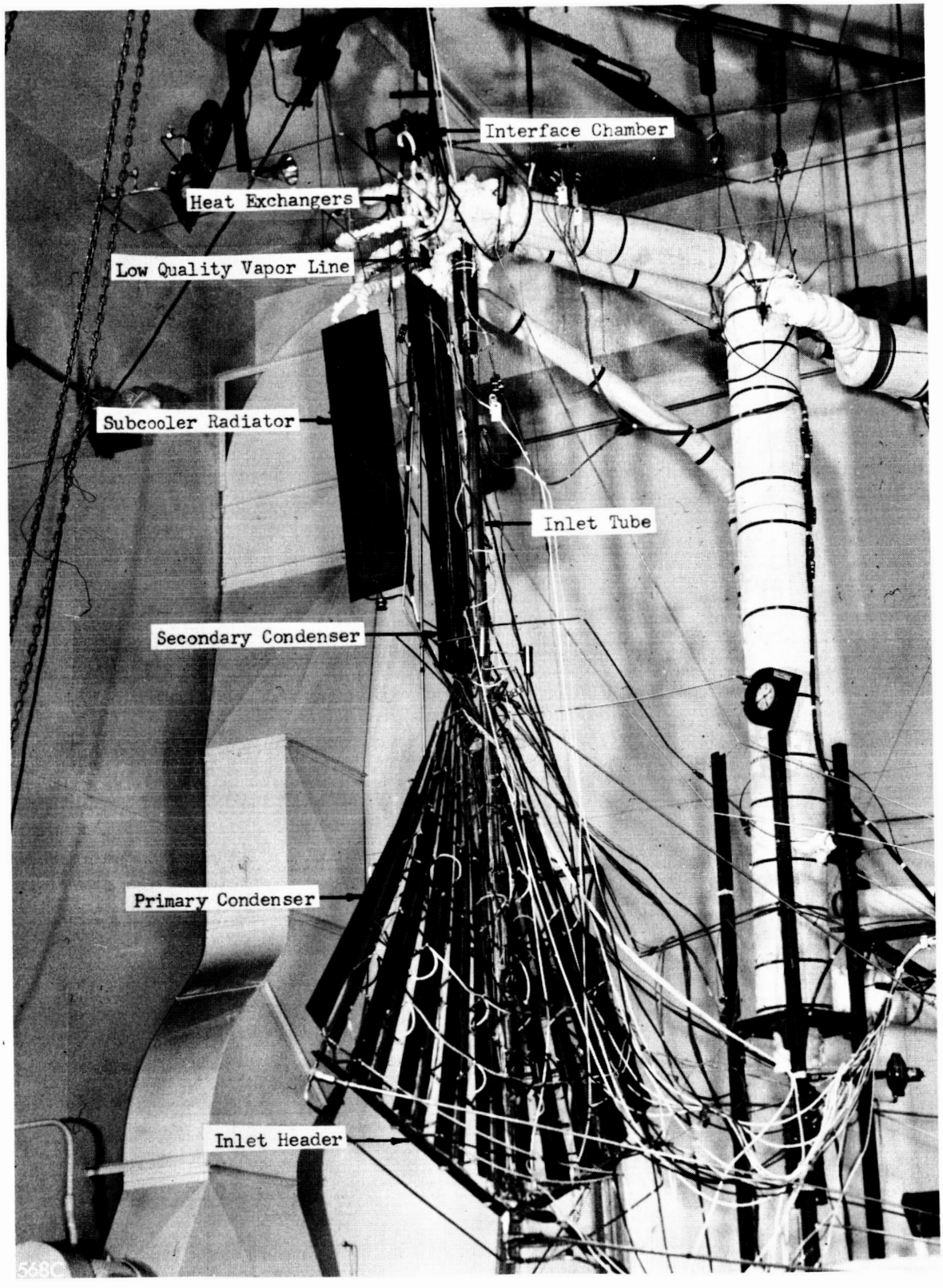

PHASE III INSTALLATION

FIGURE 4-15

closed and operation established. The inner valves on the inlet header were used only for draining the condenser after shutdown.

Prior to entering the condenser, the incoming vapor was passed through a liquid mercury-cooled desuperheater. By writing a heat balance, the quality of the vapor entering the condenser could be determined.

Numerous steady state data points were taken at various combinations of the independent parameters to define condenser off-design as well as design performance. Transient data were also taken to determine condenser response to step inputs.

Instrumentation included bourdon tube pressure gages, mercury-water pressure drop manometers, nozzles, venturis and orifices with associated pressure measurements for flow determination, two 24 point temperature loggers, and one 48 point millivolt meter for temperature read-out.

Phase I

Phase I was a test of the primary condenser only and was intended to verify the design integrity and determine its off-design and transient performance. Figure 4-11 shows a schematic of the installation and Figure 4-14 a photograph.

An auxiliary heat exchanger was installed downstream of the primary condenser. This liquid mercury-cooled exchanger was used to vary and measure the outlet quality from the primary condenser. By maintaining the liquid-vapor interface in this exchanger, a heat balance yields the vapor weight flow condensed downstream of the primary condenser. Using this and the total mass flow, the outlet quality may be calculated.

Varying the inlet vapor flow, inlet quality, and outlet vapor flow, an operating map of the primary condenser could be generated in this phase.

The vapor velocity levels required for stability were also examined. Generally, at each inlet condition the outlet vapor flow was decreased stepwise (data were taken at each step) until the condenser became unstable because of insufficient vapor velocity. The condenser was then shut down, drained, restarted at a different inlet condition, and the process repeated. Stabilization time between data points was a minimum of 30 minutes. Transient response to inlet and outlet vapor flow variations were also measured. The instrumentation utilized in this phase included

1. A bourdon tube pressure gage at the condenser inlet.
2. A bourdon tube pressure gage at the condenser outlet.
3. An immersion thermocouple at the condenser inlet.
4. An immersion thermocouple in the inlet tube.

5. A ΔP manometer from the middle of the inlet tube to the outlet header.

6. Numerous surface temperatures along the inlet tube, inlet header, condenser tubes and fins, and outlet header.

Phase II, Part a

Having determined the primary condenser operating characteristics in Phase I, the auxiliary heat exchanger was removed and the secondary condenser and interface chamber were added. The low quality vapor line was omitted in order to define secondary condenser operation without the effects of this line. A schematic of the installation is shown in Figure 4-12.

In this phase, inlet conditions could be varied, but the variation of primary condenser outlet quality was somewhat limited, being accomplished by adding heat to the secondary condenser. Operation of the unit was checked at various combinations of the independent parameters.

The instrumentation used in Phase I, a pressure drop manometer between the condenser inlet and interface, and a bourdon tube pressure gage at the interface were used in this phase.

Phase II, Part b

In part b the low quality vapor line was added, duplicating intended system configuration for the condensing portion of the condenser-subcooler. This part of Phase II dealt with evaluating the pressure drop of the low quality vapor line and its effect on overall condenser operation. Data taken and instrumentation were basically the same as in Phase II a.

Phase III

In this phase the subcooling portion of the condenser-subcooler (heat exchangers and subcooler radiator) was added to exactly duplicate the system hardware. An installation schematic is shown in Figure 4-13 and a photograph in Figure 4-15. Auxiliary liquid mercury flows were supplied to simulate the bearing return and boiler feed flows.

This phase was intended to evaluate the subcooler heat exchangers and radiator as well as the performance of the complete component. The flow rates and temperatures of the auxiliary liquid flows and the independent parameters available in Phase II were varied.

Instrumentation to evaluate the subcooler performance was added for this phase. New data taken included flow measurement, inlet pressure, and inlet and outlet temperatures of the flows in each heat exchanger.

4.4.2 Results and Analysis

Successful operation of each portion and of the complete condenser-subcooler was achieved during the test. (All test phases were run with flow against lg.) Operation was sustained over a wide range in weight flow and inlet quality as well as during various transients. In all cases the incoming mixture was delivered to the interface as condensate and liquid hold-up did not accumulate. Before a general discussion of the test results can be started, it is necessary to discuss the two problem areas of the test. A more comprehensive summary of the CSC I-1A test results can be found in Reference 16.

The higher-than-design pressure level was traced to several factors. Errors in extrapolating the fin test data of Section 4.3.2, a larger than expected vapor saturation to fin root temperature drop, and the decrease in effective fin area are due to the large flat heater used for preheating. The result was that a design pressure of 7.0 psia occurred at 10.0 lb/min flow rather than the design value of 13.72 lb/min. Due to the magnification of saturation pressure with temperature, design flow was obtained at 15.4 psia. Another result of this off-design condition was the reduction of the vapor velocity (due to the dependency of density on saturation pressure) in the condenser to 50 ft/sec at design weight flow as opposed to the design value of 94 ft/sec; the result was a decreased stability margin. Despite these anomolies, operation over a wide range of flows was experienced.

Unfortunately, an incorrect condenser flow indication during Phases I and II indicated that the condenser heat rejection was very near design. This is the reason for lack of design flow data during these phases. At the start of Phase III the error and discrepancy in heat rejection were discovered. An attempt was made to lower the operating pressure in Phase III by removing insulation from the inlet tube and inlet header and allowing condensation to take place in these areas. Although this helped (see Phase III test results) design pressure level at design flow was never reached. This discrepancy in heat rejection capability makes comparison of design and experimental dependent parameters difficult, but comparisons are made wherever possible.

The second difficulty encountered was the deterioration in condenser performance as a function of time. The sympton was an inability to operate the primary condenser without experiencing slugging during Phase I at values of inlet and outlet vapor weight flows which had not previously incited slugging. Based on general TRW experience in the mercury condensing field, this phenomena is probably due to some form of wetting between the mercury and tube walls.

Confirmation of the existence of wetting was substantiated by an X-ray taken of one of the condenser tubes after completion of testing. This X-ray showed numerous drops clinging to the tube walls with a contact angle of approximately 90°. Further, tests at TRW have shown that mercury, given time as a function of temperature, will wet stainless steel (Reference 17).

Those variables affecting non-wetting condenser stability in an antigravity field can best be expressed by the drop Froude number which can be defined

$$N_{FR} = \frac{\text{drag forces on drop exerted by vapor}}{\text{gravity forces on drop}}$$

$$N_{FR_{drop}} = \frac{C_D \, \rho_V \, \frac{V_V^2}{2g} \, \frac{\pi D_D^2}{4}}{\frac{\pi}{6} \, D_D^3 \, \rho_l} \approx K_1 \, \frac{\rho_V \, V_V^2}{D_D}$$

where

C_D = coefficient of drap, vapor on drop

K_1 = constant for a given condenser operating point

ρ_V = density of vapor

V_V = velocity of vapor

D_D = drop diameter

g = gravitational constant

ρ_l = density of liquid

Should complete wetting occur, a Froude number of the resulting film can be derived as

$$N_{FR_{film}} = \frac{t_i \, \pi \, D_t \, dL}{\pi \, D_t \, dL \, \delta \rho_l} = \frac{t_i}{\delta \rho_l}$$

where

t_i = vapor condensate interfacial shear

D_t = tube diameter

δ = film thickness

dL = incremental length

but $\frac{dP \, \pi \, D_t^2}{4} = t_i \, \pi \, D_t \, dL$

and

$$dP = \frac{f_i \, dL}{D_t} \frac{\rho_V V_V^2}{2g}$$

where

f_i = interfacial friction factor

Therefore

$$t_i = \frac{f_i}{8} \rho_V V_V^2$$

and

$$N_{FR} = \frac{f_i \rho_V V_V^2}{8 \delta \rho_l} \approx K_2 \frac{\rho_V V_V^2}{\delta}$$

In either case it can be seen that the Froude number is a strong function of vapor velocity and a weaker function of drop or film size and vapor density. Moreover, as the vapor velocity decreases, both the drop diameter (see Figure 3-3) and film thickness increase which makes the Froude number an even stronger function of vapor velocity.

Based on this, the minimum experimentally determined value of this vapor velocity necessary for non-slugging operation as a function of operating time was plotted and is shown in Figure 4-16. Since the velocity in the condenser varies with length depending on outlet quality, a particular point in the condenser had to be chosen. Since the experienced slugging first occurred in the upper end of the condenser and since this portion has a greater mass population of liquid, the velocity here was plotted. Other variables which affect this number are vapor density and drop or film history (momentum) but their effect is small in comparison to vapor velocity and their values did not vary to a great extent during these tests. The figure shows a drastic increase in the minimum velocity required for non-slugging operation with increased operating time.

Using the analysis of Section 3.1.1, the effect of the contact angle on condenser stability can be investigated. Allowing β_m to vary in equation (6) (σ is kept constant since Reynolds, in Reference 1, postulates that surface tension is fairly constant even under changing contact angles), the curves of Figure 4-17 are generated for Case I operation. As can be seen, the minimum velocity required to experience Case I operation and avoid Case II operation increases with decreasing contact angle (tendency toward wetting). (Figure 4-18 shows the effect of contact angle on initial drop acceleration.) Further analysis of the drop velocity as a function of length of travel and contact angle for constant vapor velocity results in Figure 4-19. (The analysis of Section 3.1.1 was

PRIMARY CONDENSER MINIMUM EXIT VAPOR VELOCITY NECESSARY TO AVOID SLUGGING AS A FUNCTION OF OPERATING TIME

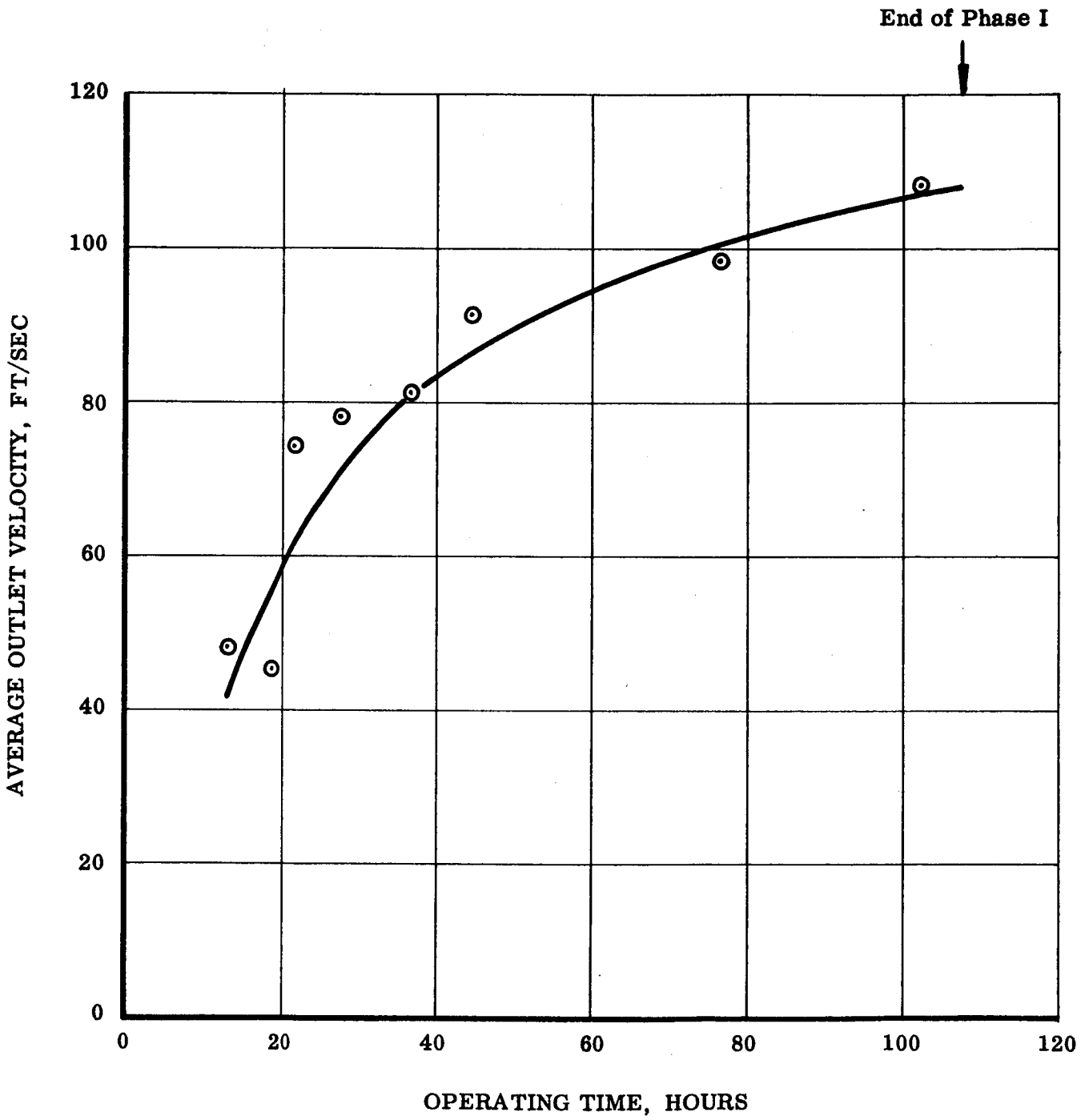

FIGURE 4-16

EFFECT OF CONTACT ANGLE ON MAXIMUM DROP SIZE

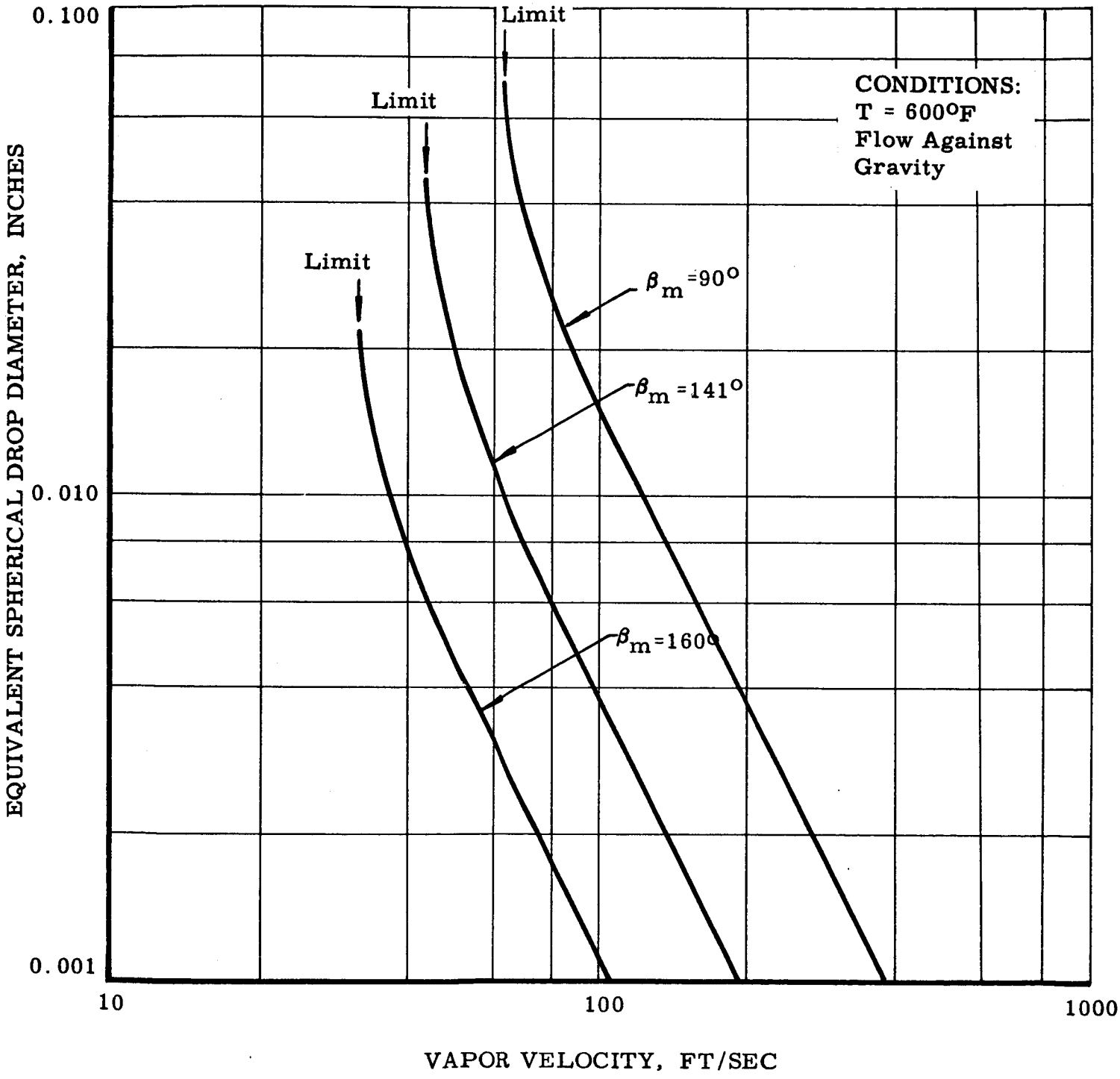

FIGURE 4-17

EFFECT OF CONTACT ANGLE ON INITIAL DROP ACCELERATION

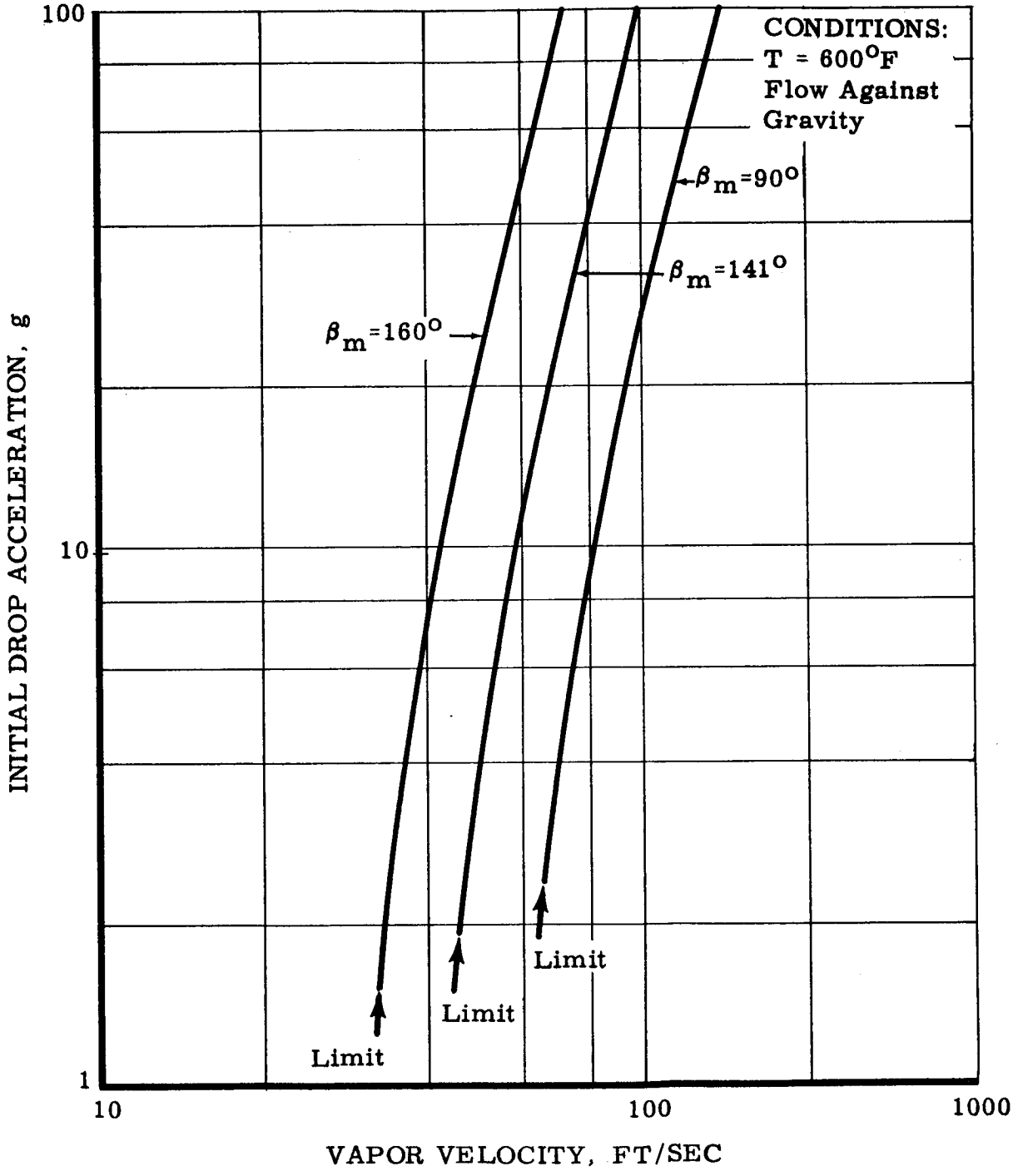

FIGURE 4-18

DROP VELOCITY AS A FUNCTION OF LENGTH OF TRAVEL AND CONTACT ANGLE

CONDITIONS: VAPOR VELOCITY = 94 FT/SEC
T = 600°F

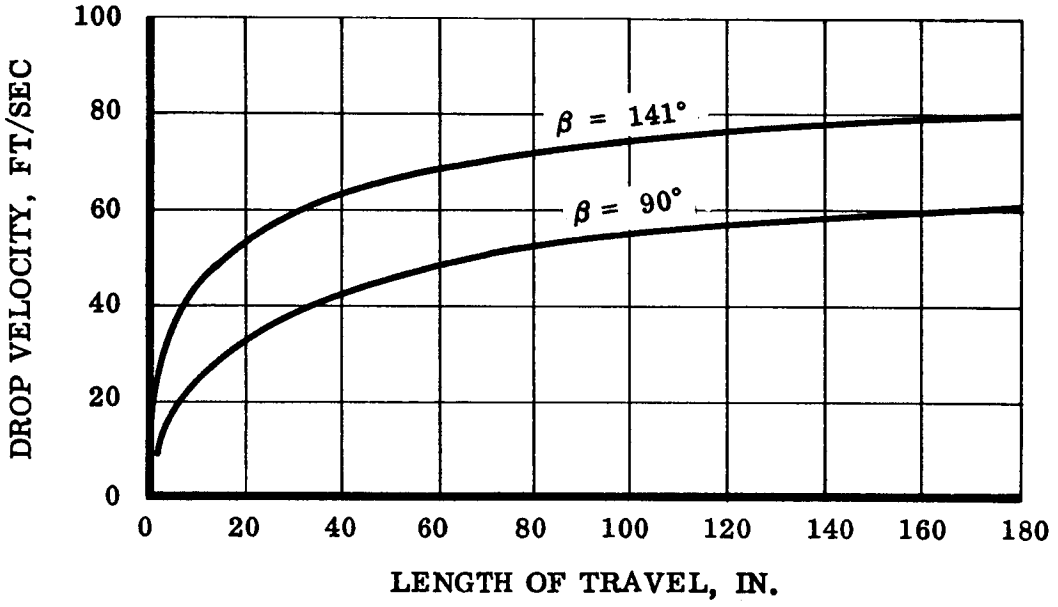

FIGURE 4-19

used here). The adverse effect of decreasing contact angle on condenser stability is evident from these three figures.

Although it is not known whether the tendency toward wetting would progress to a degree where film condensation would occur, this situation can be investigated to determine the limiting stability condition, that condition being the minimum vapor velocity necessary to transport a liquid film without runback in opposition to lg. The first step is to analyze the conditions at the incipient runback point to differentiate between negligible and predominant factors. Reference 18 gives the following film velocity profiles for conditions of a stable film, incipient runback, and runback.

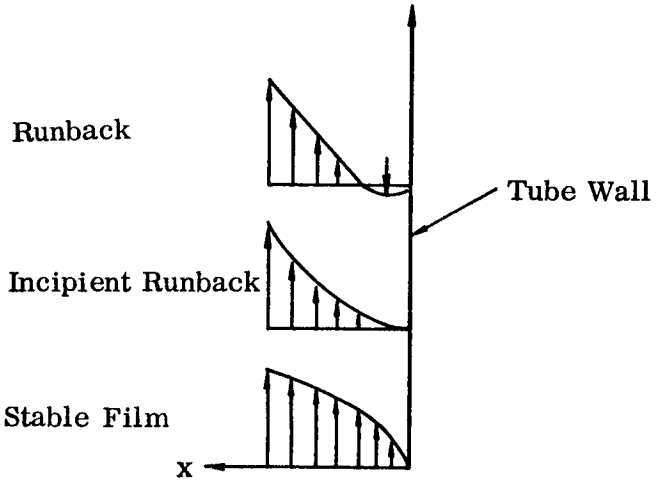

At the incipient runback point the velocity gradient at the wall is zero and the wall shear stress is therefore zero. We will assume that there is no velocity in the X-direction and that the change in velocity in the Y-direction is negligible. This latter assumption is pessimistic since it neglects the effect of the liquid momentum gain due to the effect of decreasing liquid velocity as the incipient runback point is reached. The last assumption is that the vapor pressure gradient is negligible, which is also pessimistic since the pressure gradient would tend to support the film. Consider an incremental area within the liquid film.

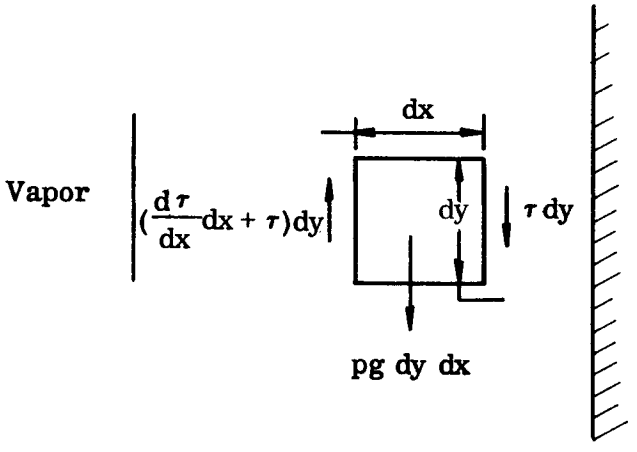

Balancing the forces yields

$$\left(\frac{d\tau}{dX}\ dX + \tau\right) dy = n\rho\ dy\ dX + \tau dy \qquad (30)$$

but

$$\tau = \frac{\mu}{g_c}\ \frac{d\,Vy}{dX}$$

and

$$\frac{d\tau}{dX} = \frac{\mu}{g_c}\ \frac{d^2\,Vy}{dX^2}$$

which on substitution into equation (30) yields

$$\frac{d^2 Vy}{dX^2} = \frac{n\rho g_c}{\mu}$$

Integrating

$$\frac{d\,Vg}{dX} = \frac{n\rho g_c X}{\mu} + C_1$$

But since the limit for stability is $\frac{d\,V_g}{dX} = 0$ at $X = 0$ and $C_1 = 0$,

therefore

$$Vy = \frac{n X^2 \rho g_c}{2\mu} + C_2$$

but

$$C_2 = 0 \quad \text{at } x = 0,\ Vy = 0$$

Finally

$$Vy = \frac{n X^2 \rho g_c}{2\mu}$$

and at $x = \delta$, $Vy = V_1$

$$\frac{n \rho g_c}{\mu} \frac{\delta^2}{z} = Vi \tag{31}$$

δ = film thickness

Since the velocity profile is parabolic, the average velocity is 1/3 of the interfacial velocity (Vi) and from continuity

$$\frac{Vi}{3} \rho \delta \pi d = \dot{m}_l \tag{32}$$

Substituting equation (31) into equation (32) yields

$$\frac{n \rho_l^2 g_c \delta^3 \pi d}{6\mu} = \dot{m}_l$$

but

$$\tau_i = n \delta \rho_l$$

Finally

$$\tau_i = \left(\frac{6\mu \dot{m}_l \rho_l n^2}{\pi d g_c}\right)^{1/3} \tag{33}$$

which gives the expression for the interfacial shear at the runback point. However, the net interfacial shear is made up of two components: the frictional shear τ_f and the momentum shear τ_m, where

$$\tau_i = \tau_f + \tau_m$$

$$\tau_f = \frac{f}{4} \rho_V \frac{V_V^2}{2g} \tag{34}$$

$$\tau_m = \frac{\Delta \dot{m}_V V_V}{\pi d \Delta L g_c} \tag{35}$$

where $\Delta \dot{m}_V$ = vapor condensed.

Equating equations (33), (34), and (35) yields

$$\left(\frac{6\mu \dot{m}_l \rho_l n^2}{\pi d g_c}\right)^{1/3} = \frac{f}{4} \rho_V \frac{V_V^2}{2g_c} + \frac{\Delta \dot{m}_V V_V}{\pi d \Delta L g_c} \qquad (36)$$

Since the slugging first occurred in the small diameter section of the Sunflower I condenser, equation (36) will be evaluated at this point.

$$N_{Re_D} = \frac{Vd\rho}{\mu} = 5950$$

$$f = \frac{0.316}{N_{R_e}^{1/4}} = 0.036 \qquad (37)$$

Based on the CSC I-1A design conditions, equation (36) and (37) yield

$$n^{2/3} (0.650) = 1.68 \times 10^{-5} V_V^2 + 1.092 \times 10^{-3} V_V$$

Solving for V_V yields a minimum vapor velocity of 165 ft/sec for film condensation. This minimum vapor velocity could be lower, not only for the reasons previously mentioned, but also because the friction factor is based on a smooth surface between the vapor and liquid. With a turbulent vapor core this may not be the case; however, the effect of the boundary would have to be investigated experimentally to accurately determine the vapor-liquid friction factor. Comparing this velocity with that necessary for non-slugging operation at the end of Phase I (Figure 4-16) indicates that the wetting was not severe enough to cause film condensation.

Phase I

With the ability to vary the inlet and outlet conditions of the primary condenser in Phase I, a detailed investigation into the interaction of the various parameters was possible. (For purposes of investigation, only non-slugging runs will be considered). Neglecting the slight increase in two-phase pressure drop that would result from variation in liquid flow, the dependent parameters become simple functions of inlet and exit vapor flow. A primary condenser operating map showing the dependency of inlet pressure, pressure drop, and condensing tube inlet and exit vapor velocities on the independent parameters, inlet and exit weight flow, is shown on Figure 4-20. The exhibited heavy dependency of exit vapor velocity on exit vapor flow is not only the result of flow rate changes, but also of changes in vapor specific volume due to the pressure drop and pressure level variations shown on the map. The effect of any of the dependent parameters by a change in another can easily be determined from this map.

Figure 4-21 shows the primary condenser transient response to step inputs in flow. Inlet and outlet quality and superheat conditions could not be controlled since they are

PRIMARY CONDENSER EXPERIMENTAL OPERATING MAP
(PHASE I, NON-SLUGGING)

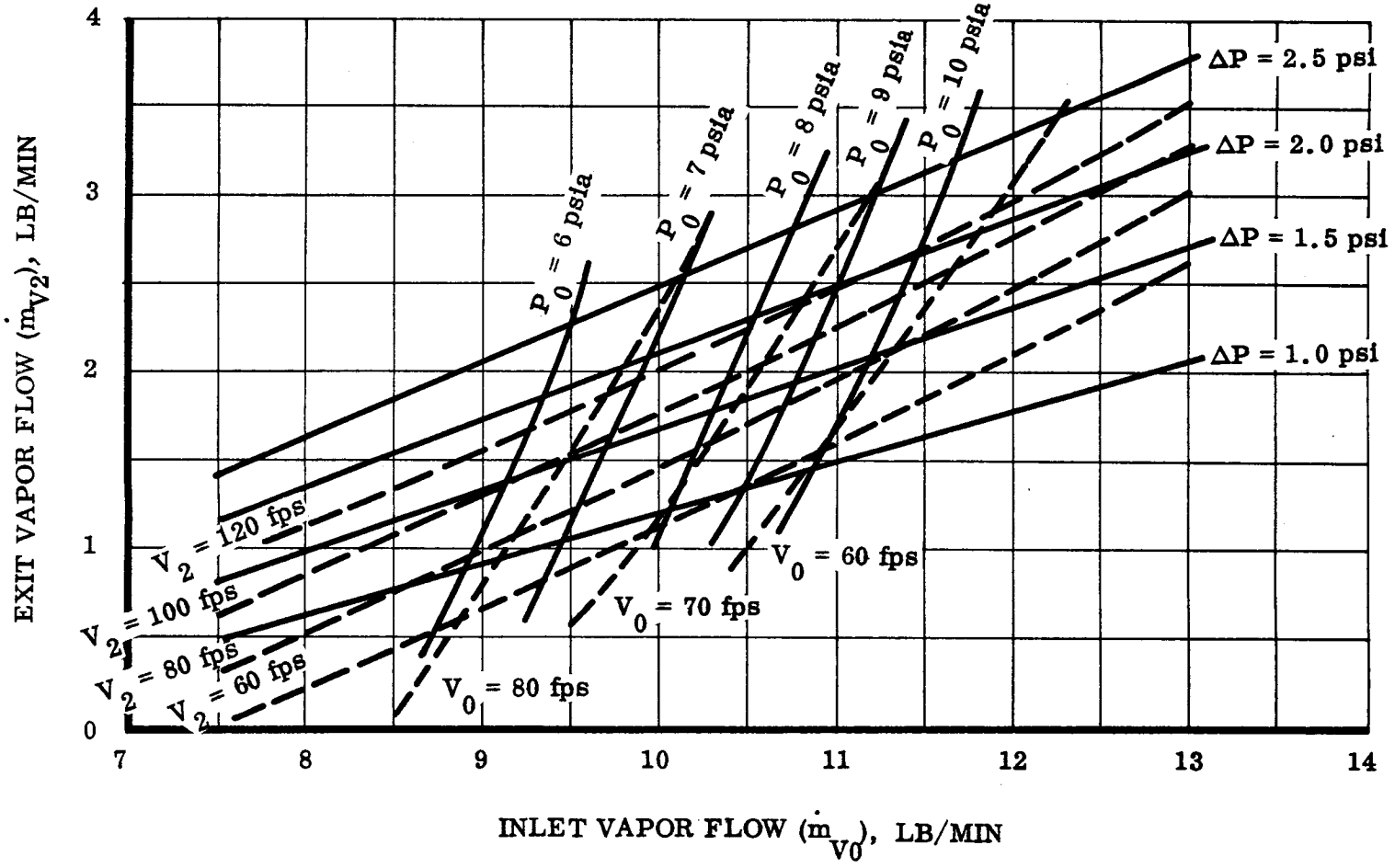

FIGURE 4-20

PRIMARY CONDENSER TRANSIENT RESPONSE TO
STEP CHANGES IN INLET VAPOR FLOW

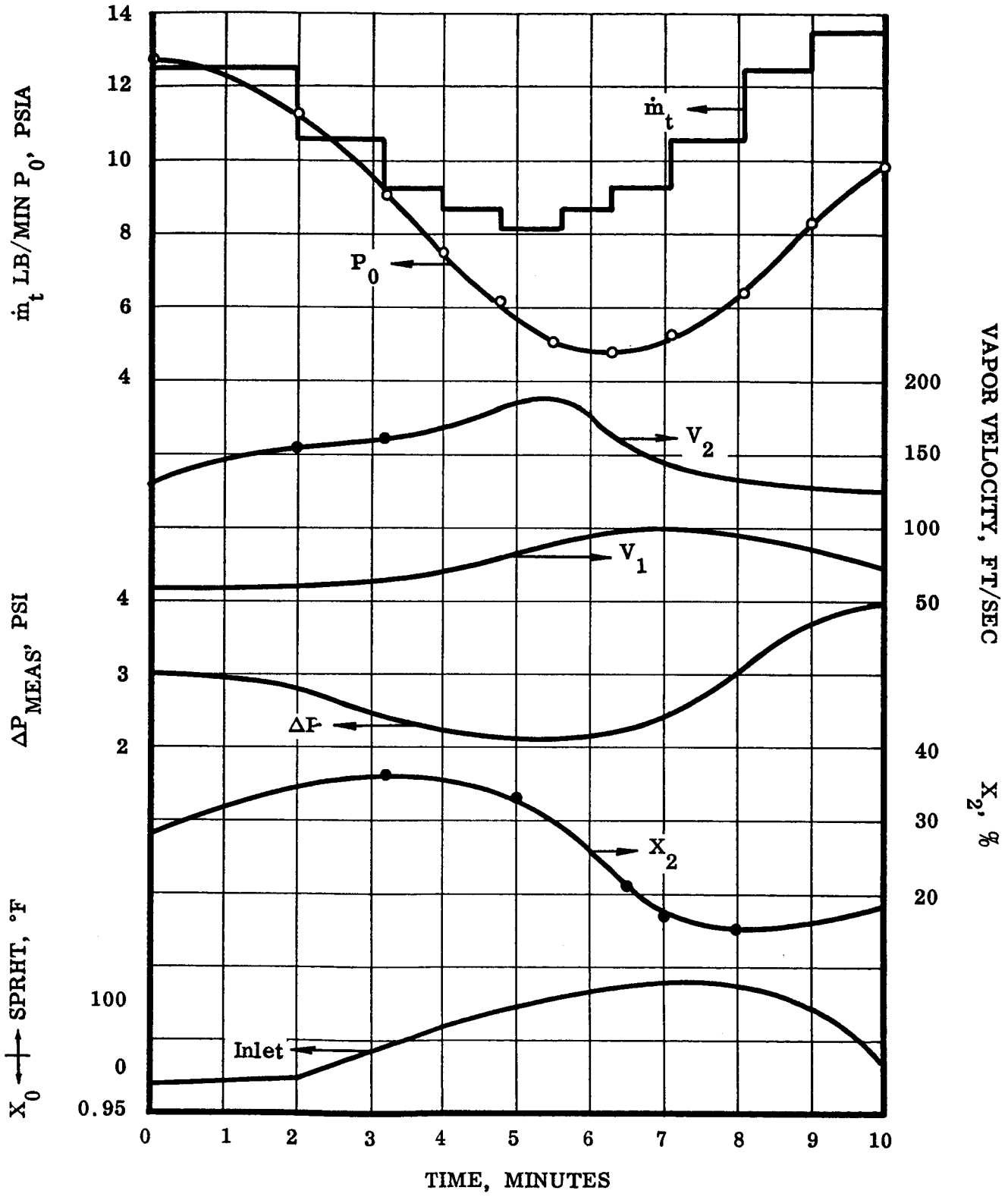

FIGURE 4-21

functions of the flow. As the flow rate is lowered, the primary condenser pressure drop decreases because of the lag in pressure response due to thermal capacity of the condenser; i. e., less flow at the same pressure is being experienced. As the pressure begins to catch up with the flow and the flow is increased, the pressure drop rises for the opposite reason: more flow at the same pressure is being experienced.

Variations in condensing tube vapor velocities follow the trends expected; i. e., velocity increase with flow rate decrease and vice versa, but at slower rates than shown by the operating map of Figure 4-20 due to the thermal lag.

Unfortunately, no response times can be obtained from this curve (their value is minimal at any rate due to the incomplete nature of the condenser) because stability was not achieved between step inputs.

Figure 4-22 depicts the primary condenser transient response to a steady decrease in exit quality or outlet vapor flow. As this flow is decreased, it is accompanied by increasing inlet pressure level and decreasing pressure drop and condensing tube inlet and exit velocities as expected from the operating map (Figure 4-20). When the outlet velocity reaches the value which will incite slugging (approximately 70 ft/sec at this point in time), the pressure drop rises due to increasing slugging. Raising the outlet vapor velocity would not clear the condenser, so the test was terminated.

Phases II and III

The results and discussion of condenser performance for Phases II and III will be presented together due to the similarity in hardware. The only difference is the omission of the low quality vapor line in Phase IIa.

Due to the progressive wetting experienced in Phase I and inability in Phases II and III to raise the outlet vapor velocity sufficiently high, the data taken in these last two phases were during slight slugging operation of the condenser.

Having fixed the overall condenser configuration, all of the dependent variables, except the small differences in pressure drop with greater inlet liquid weight flow, become a function of the inlet vapor weight flow only. The slight slugging which occurred in Phases II and III had very little effect on the inlet pressure when compared to identical conditions in Phase I when no slugging was present.

Figure 4-23 shows the variation of condenser inlet pressure with inlet vapor flow. This curve is important since it will affect the turbine output during system operation. At the beginning of Phase III the indicated weight flows in Phases I and II were discovered to be incorrect and the pressure level at design flow was well above nominal. Due to the dependency of cycle efficiency on the condenser pressure level, an attempt was made toward the end of Phase III to lower this pressure by removing the insulation from the inlet tube and inlet header and allowing these portions of the condenser to act as condensing surfaces. Data taken (three points) during this attempt are shown in Figure 4-23. Several other schemes were tried in an attempt to lower the inlet pressure further.

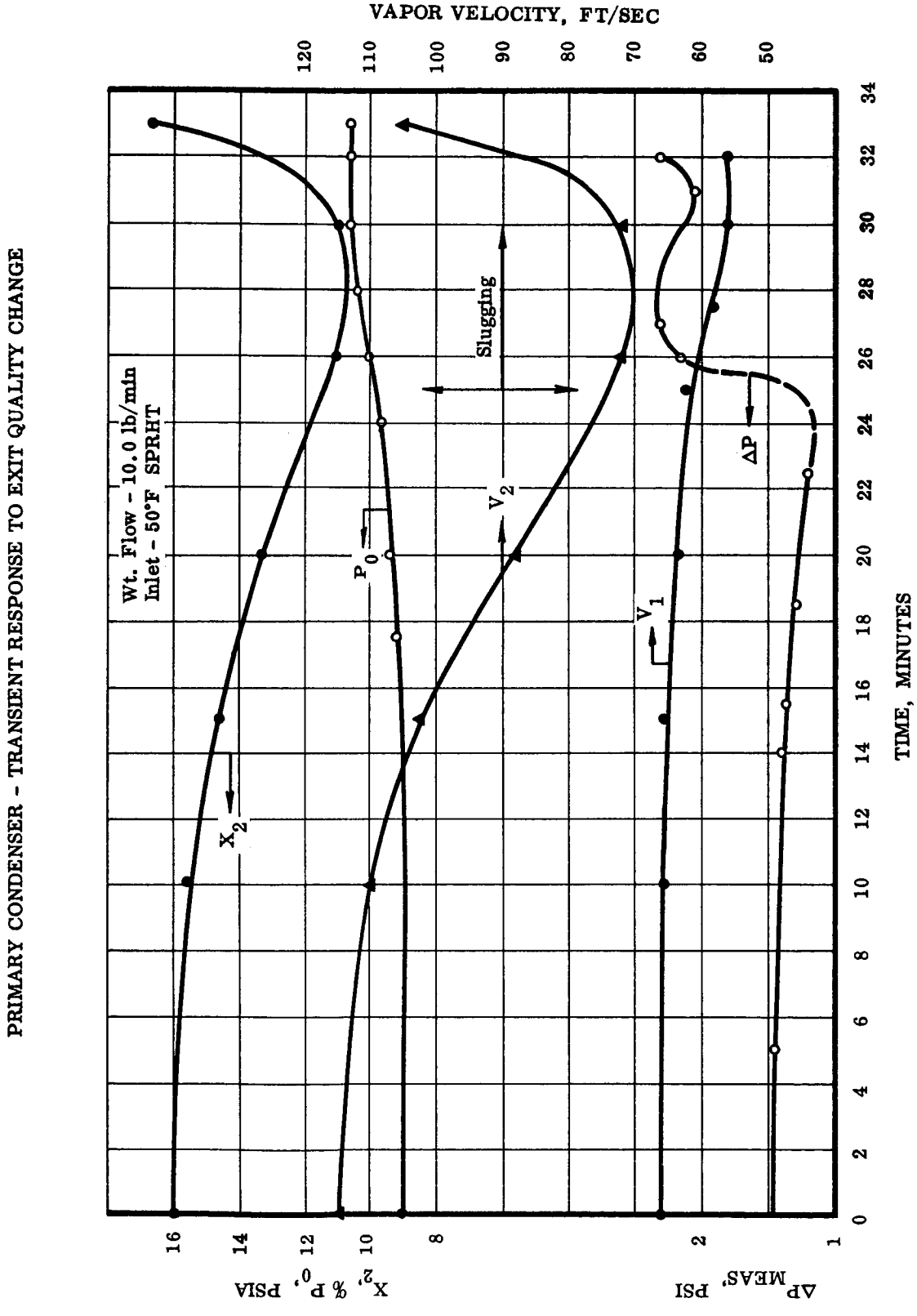
PRIMARY CONDENSER - TRANSIENT RESPONSE TO EXIT QUALITY CHANGE
VAPOR VELOCITY, FT/SEC
120
110
100
90
80
70
60
50
Wt. Flow - 10.0 lb/min
Inlet - 50°F SPRHT
Slugging
P_0
V_2
V_1
X_2
ΔP
X_2, % P_0, PSIA
16
14
12
10
8
ΔP_{MEAS}, PSI
2
1
TIME, MINUTES
0
2
4
6
8
10
12
14
16
18
20
22
24
26
28
30
32
34

FIGURE 4-22

COMPLETE CONDENSER, INLET PRESSURE VS INLET VAPOR FLOW

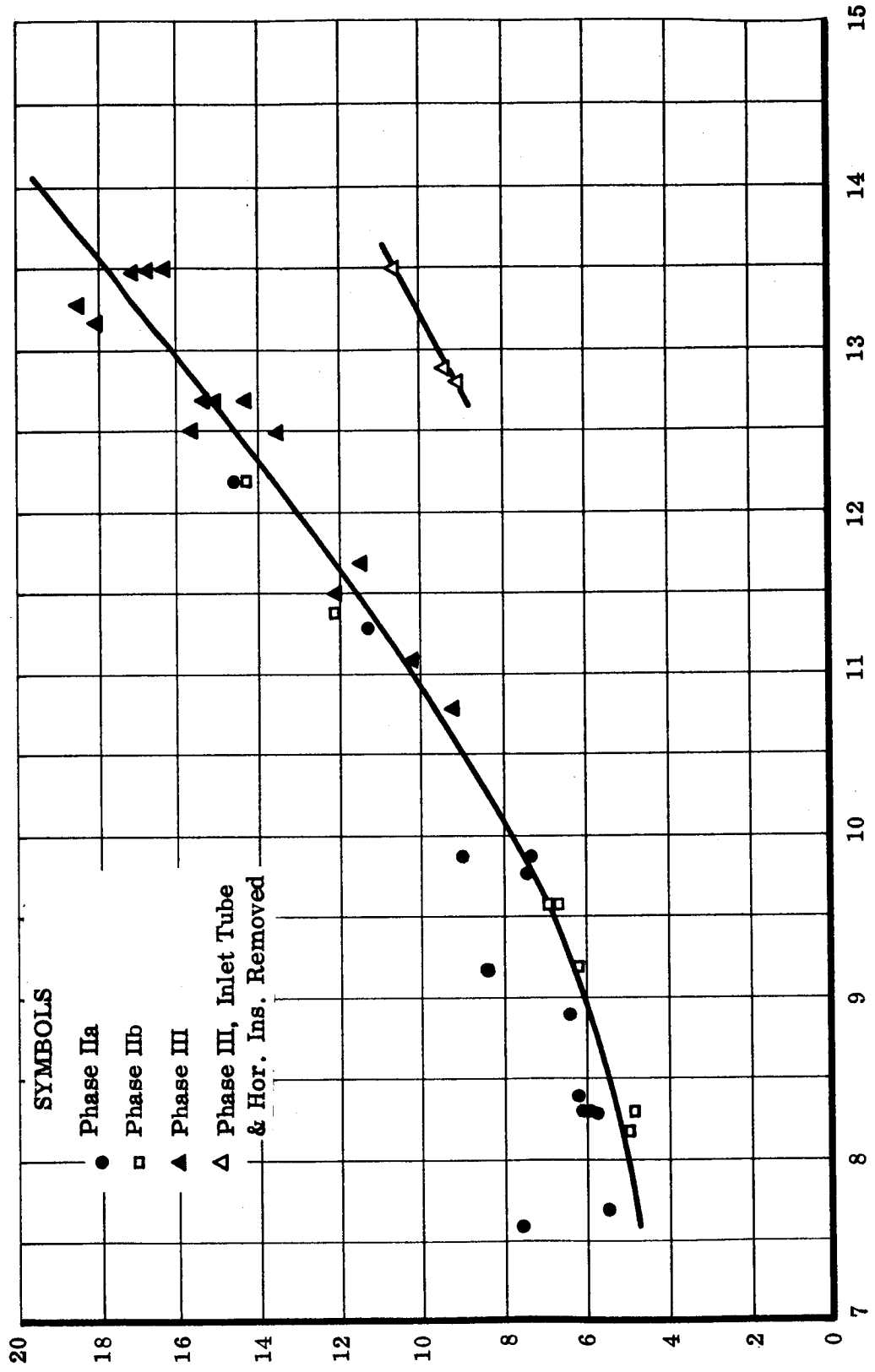

FIGURE 4-23

These included the use of fans blowing directly on the condenser and the use of an air conditioner (previously installed in the test booth) to lower the ambient temperature. Both of these methods lowered the condenser operating pressures somewhat, but the former incited severe slugging by causing tube-to-tube thermodynamic inequalities and the latter was never completely successful due to a malfunction in the air conditioning system. For these reasons, data are not presented for these runs.

The resultant error in heat rejection (when compared to design), using the inlet tube and header as condensing surfaces, was 17 per cent. With proper operation of the air conditioning system, this error could probably have been brought down to 5 to 10 per cent. An example of the sensitivity of pressure level to accuracy in heat rejection is given by Figure 4-24. This curve was derived using the vapor pressure versus temperature relationship for mercury and the heat rejection versus temperature characteristic of fins operating in atmosphere (Section 4.3.2).

Figure 4-25 presents the variation in primary condenser exit vapor flow rate with inlet vapor flow in Phases II and III. Also plotted is the same variation with 1.4 kw heat input into the secondary condenser. This heat input has the effect of decreasing the heat rejection of the secondary condenser and as a result reduces the outlet vapor flow rate from the primary condenser for any given inlet vapor flow rate.

The effect of increased slugging is shown as the Phase III exit vapor flow is lower than the Phase II exit vapor flow for the same inlet vapor flow. This is due to the increased primary condenser pressure drop in Phase III which result in a lower secondary condenser operating temperature, and hence a lesser capacity to condense vapor.

Primary condenser vapor velocity variation in Phases II and III can be seen in Figure 4-26. As expected, the velocity level, both inlet and outlet, decreased with increasing vapor flow rate because the specific volume decrease overcomes the weight flow increase. The outlet velocity with 1.4 kw heat input to the secondary condenser is also plotted from Phases II and III. Here the velocity levels in Phases II and III were well below the velocities necessary to obtain non-slugging operation of the primary condenser toward the end of Phase I. As a result, Phases II and III data were taken with slight slugging occurring in the condenser.

By superimposing the Phase II, $Q = 0$ curve of Figure 4-25 on Figure 4-20, a prediction of vapor velocity with a complete non-slugging condenser can be obtained. These curves of condensing tube inlet and exit velocities that would have been experienced with a complete non-slugging condenser are shown in Figure 4-26 (curves "A" and "B"). The lower value of exit vapor velocity here is a result of the lower condenser pressure drop that would be experienced without slugging, resulting in a higher exit pressure and lower vapor velocity. The outlet vapor velocity level in the secondary condenser cannot be accurately calculated due to the uncertainty in interface heat rejection. The same is true of the low quality vapor line velocity. The inlet tube vapor velocity is approximately 140 per cent of the condensing tube inlet velocity (V_1), and the inlet header velocities vary between 120 and 40 per cent of this same velocity. The latter variation results from the use of CSC I-1 header (designed for a total of 18 tubes).

EFFECT OF ERROR IN CONDENSER HEAT REJECTION
ON CONDENSER PRESSURE LEVEL

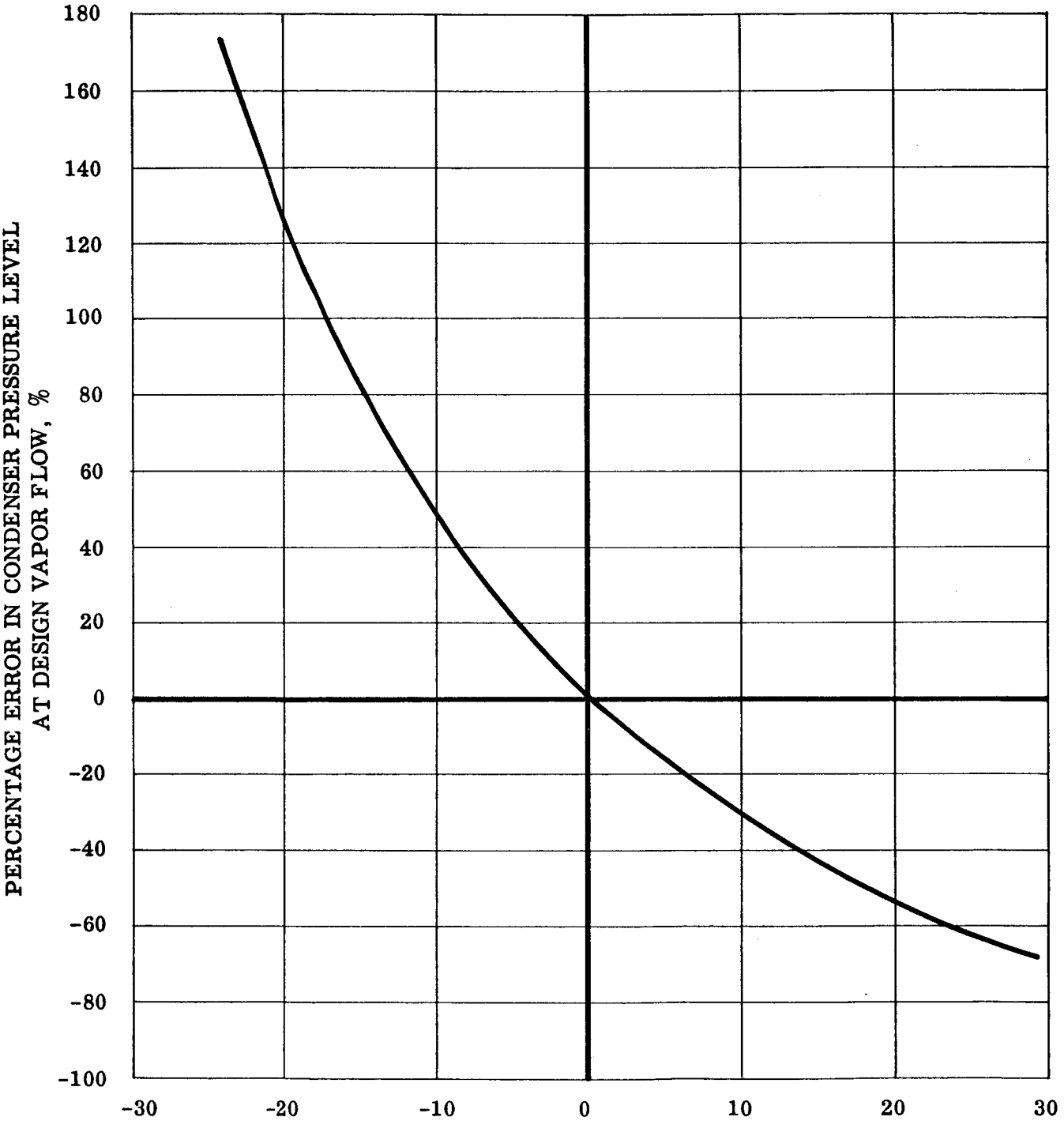

FIGURE 4-24

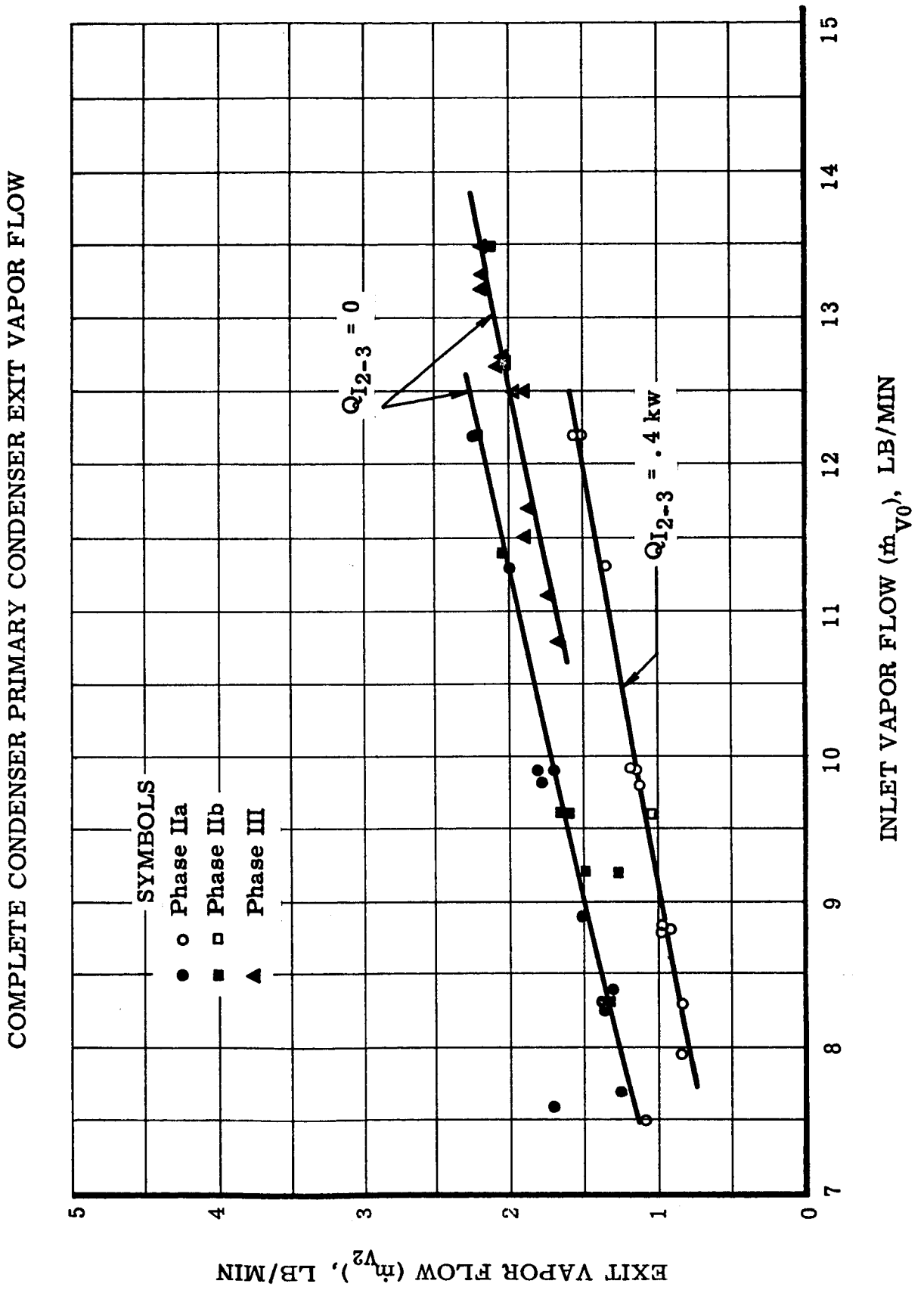
COMPLETE CONDENSER PRIMARY CONDENSER EXIT VAPOR FLOW
SYMBOLS
Phase IIa
Phase IIb
Phase III
$Q_{I2-3} = 0$
$Q_{I2-3} = .4$ kw
EXIT VAPOR FLOW ($\dot{m}_{V2}$), LB/MIN
INLET VAPOR FLOW ($\dot{m}_{V0}$), LB/MIN
0
1
2
3
4
5
7
8
9
10
11
12
13
14
15

FIGURE 4-25

COMPLETE CONDENSER PRIMARY CONDENSER VAPOR VELOCITY

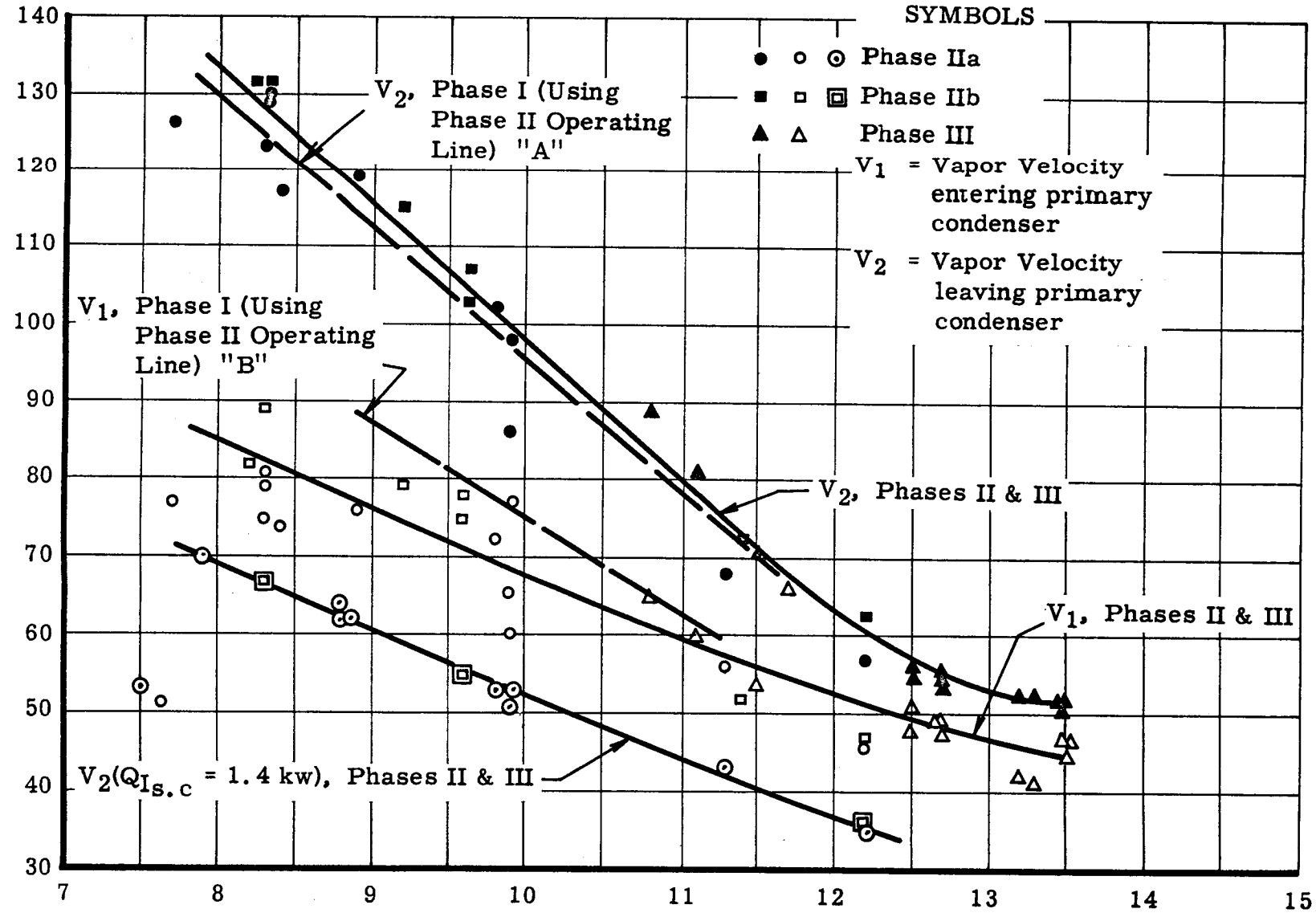

FIGURE 4-26

In analyzing the pressure drop data from Phases II and III, it was found important to separate the total condenser pressure drop (beginning of inlet tube to interface) into three parts: primary condenser pressure drop and beginning of inlet tube to outlet header, secondary condenser, and low quality vapor line.

Figure 4-27 shows the primary condenser pressure drop in Phases II and III as a function of inlet vapor weight flow. This curve shows the pressure drop to be higher than would be expected from the Phase I non-slugging data. In fact, this curve would indicate a steady decrease in primary condenser pressure drop as flow is increased, as is shown in the figure. This higher pressure drop in Phases II and III is the result of slugging which increases as the flow rate is increased due to the lowering of the vapor velocity (see Figure 4-26).

The data points of Phase III denoted with a Δ show much higher primary condenser pressure drops than the others. These runs were taken at the very end of the testing and are the result of an advanced degree of wetting and slugging.

Next, the secondary condenser pressure drop was plotted versus inlet vapor weight flow (Figure 4-28). This pressure drop was obtained from the difference in saturation pressure corresponding to the temperatures at the beginning and end of this portion of the condenser. These temperatures were obtained from skin thermocouples and corrected for a calculated 2°F temperature drop to account for the ΔT through the condensing "film" and tube wall. The slight difference in the II-a hardware should have little effect on this pressure drop. Again, the expected trend of decreasing pressure drop with increasing vapor flow rate was not experienced due to the increase in wetting-incited slugging at the higher flow rates.

During Phases II and III, three different levels of interface heat rejection capability were employed. In Phase II, an uninsulated chamber with larger than required fins was used to insure adequate heat rejection capacity to maintain sufficient velocity in the low quality region of the condenser. In the first part of Phase III the design interface chamber was used (a capability of condensing 0.6 per cent at 13.72 lb/min); however, when the slugging became worse during the Phase III testing, it was thought that increasing the vapor velocity in the upper portion of the condenser by increasing the interface heat rejection capability would help alleviate the situation. The insulation was removed and the remainder of the Phase III data taken with this inteface configuration.

The actual heat rejection capability of either of the two off-design chambers is difficult to calculate due to the odd shape, but little importance was placed on this matter since pressure drop was of secondary importance in this component test.

The effect of this heat rejection variation can be seen in the plot of the low quality vapor line pressure drop versus inlet vapor flow (Figure 4-29). The magnitude of the pressure drop increases as the interface heat rejection increases. Analysis of the absolute value of these pressure drops, however, is difficult because of the uncertainty in vapor flow

PRIMARY CONDENSER MEASURED PRESSURE DROP VS INLET VAPOR FLOW

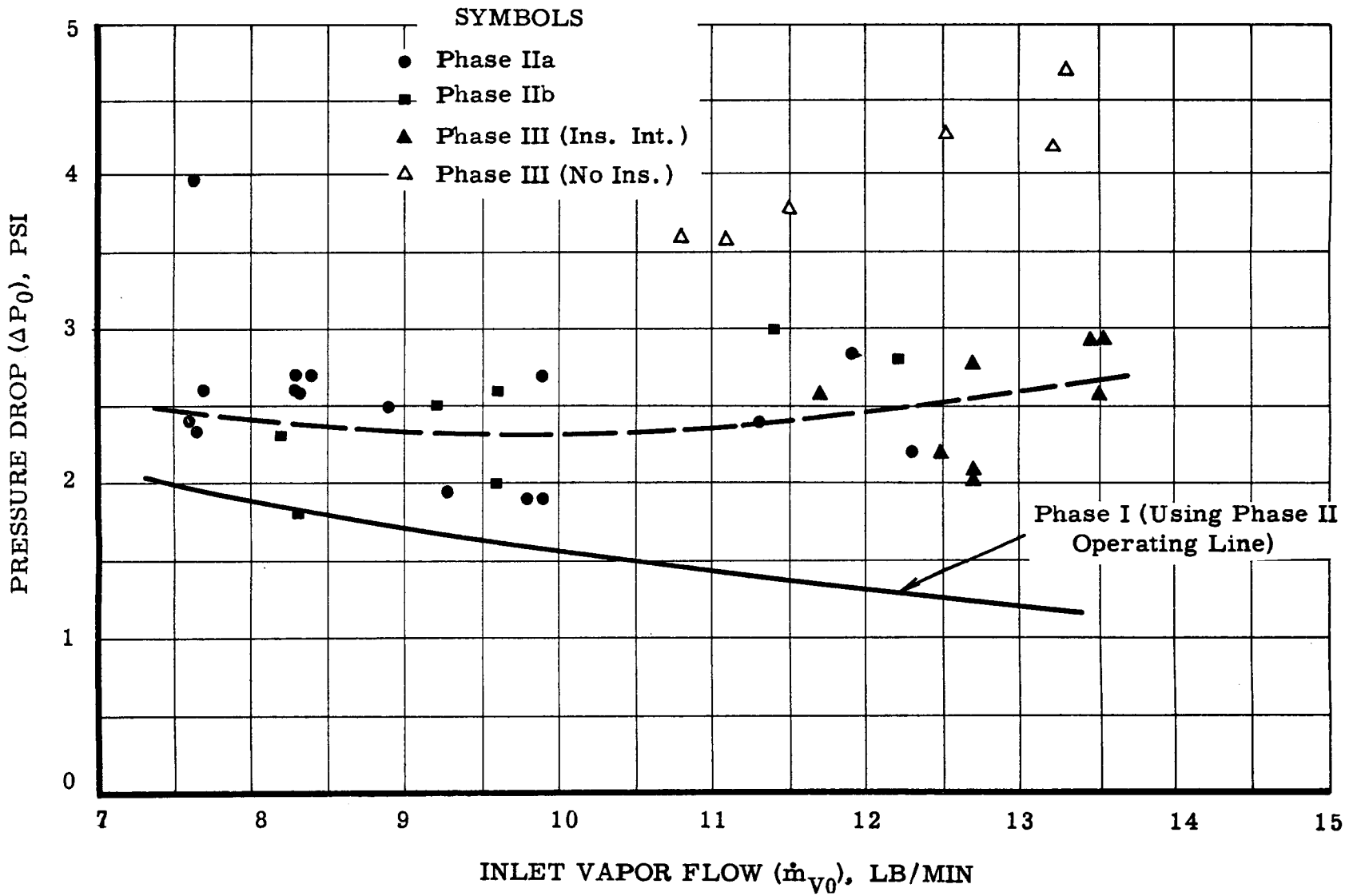

FIGURE 4-27

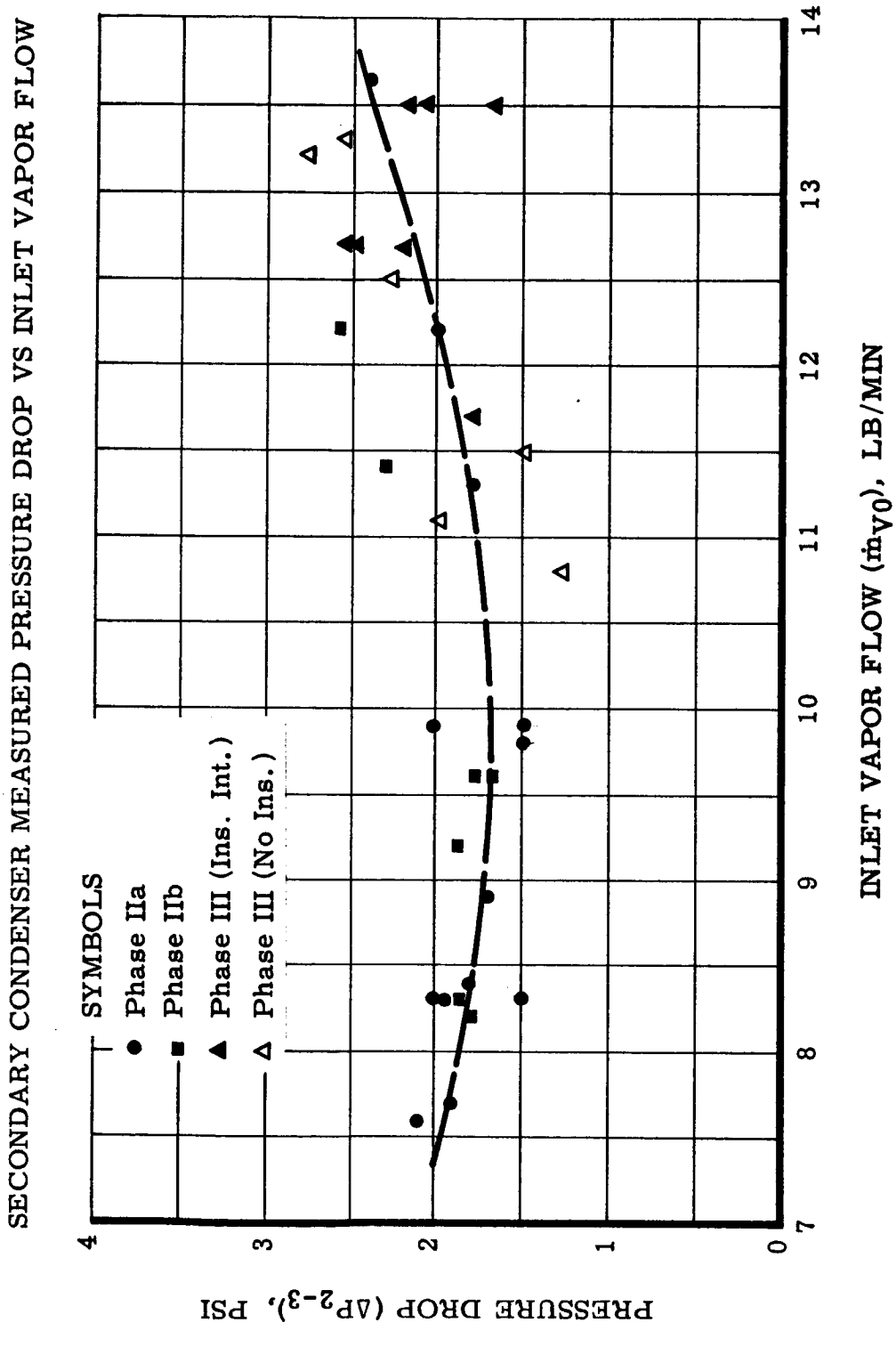
SECONDARY CONDENSER MEASURED PRESSURE DROP VS INLET VAPOR FLOW
SYMBOLS
Phase IIa
Phase IIb
Phase III (Ins. Int.)
Phase III (No Ins.)
PRESSURE DROP (ΔP_{2-3}), PSI
INLET VAPOR FLOW ($\dot{m}_{V0}$), LB/MIN
0
1
2
3
4
7
8
9
10
11
12
13
14

FIGURE 4-28

LOW QUALITY VAPOR LINE MEASURED PRESSURE DROP VS INLET VAPOR FLOW

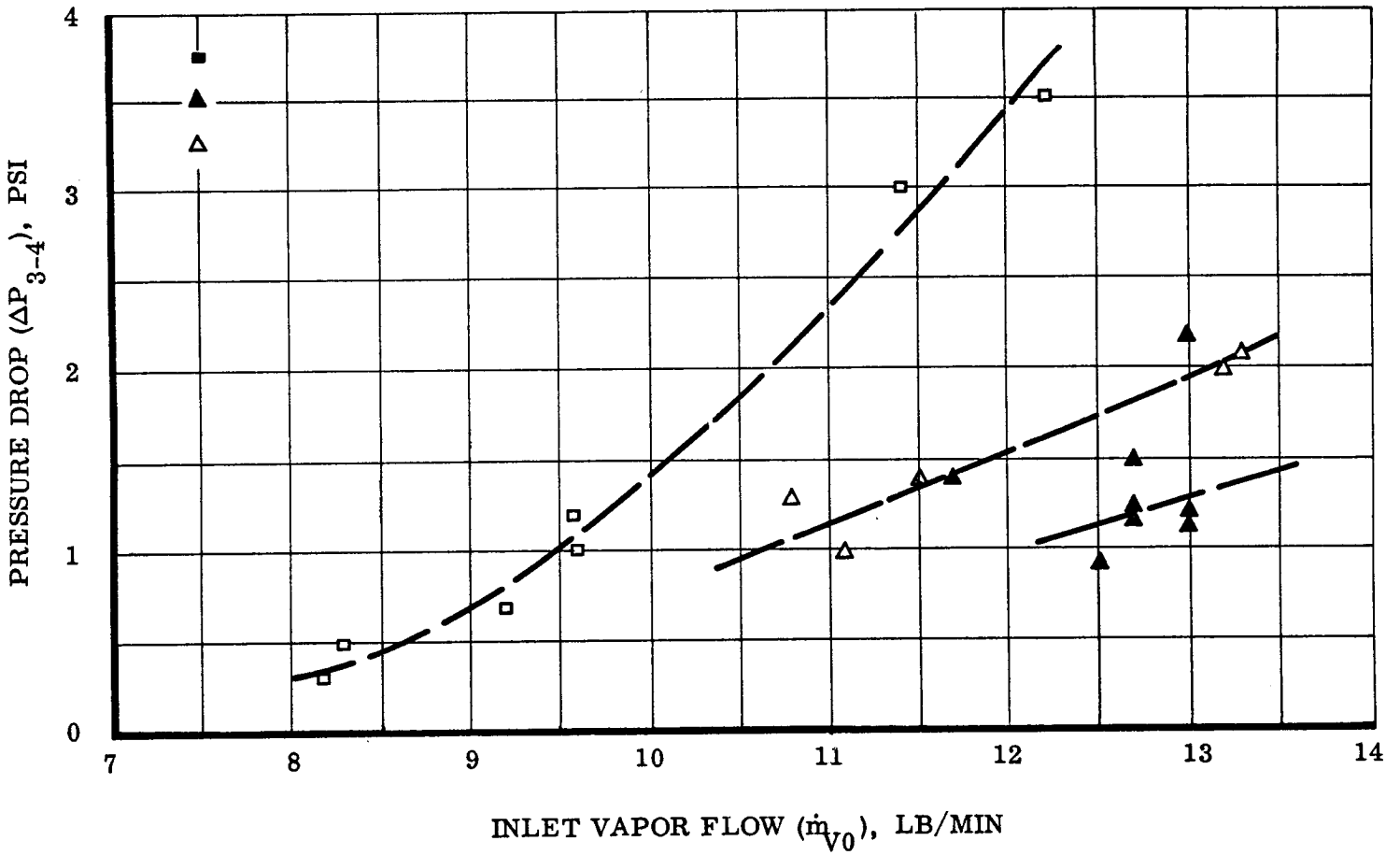

FIGURE 4-29

rate. The overall condenser pressure drop is shown in Figure 4-30. As expected, this overall drop is a strong function of the interface configuration because of its effect on the low quality vapor line pressure drop. Phase II-a, which had no low quality vapor line, shows the minimum overall pressure drop. Again, analysis or comparison to design is difficult because of high overall condenser pressure, progressive wetting, and higher than design interface heat rejection in most cases.

Figure 4-31 shows a complete condenser start-up transient. In this start, the procedure of Section 3.1 was used with condenser preheat between 500 and 600°F. The full preheat temperature was not attainable at the interface since it is not needed and therefore was not designed into the heater capability. Stabilization of the complete condenser took approximately 20 minutes with the interface temperature taking the longest to level out, due to the dependency of its pressure on the operation of the remainder of the condenser and on its high mass.

Figures 4-32 and 4-23 show the response of the complete condenser to step inputs in flow rate. In each case the time constant is between 2.5 and 3.0 minutes.

Figure 4-34 presents a complete condenser pressure profile based on the saturation pressure corresponding to skin (corrected) and immersion thermocouples and actual pressure measurements. The pressure profile of the primary condenser tubes (in this case, it is tube No. 9) can be seen with the higher gradient at the downstream end of the tube. (This would occur even at constant vapor velocity due to the L/D effect.) This is also true of the secondary condenser tube. The high pressure drop in the low quality line can be seen. This run utilized the interface chamber with the maximum heat rejection capability and consequently the highest low quality vapor line pressure drop. Good agreement was obtained with the various methods of determining local pressure; i.e., corrected skin thermocouple, immersion thermocouple, pressure gages, and pressure drop manometers.

Subcooler

The subcooler radiator was designed for a liquid mercury weight flow of 13.72 lb/min at an inlet temperature of 490°F and a temperature drop of 164°F. Comparison of performance with design is shown in Figure 4-35.

Lower values of overall heat transfer coefficient were obtained from heat exchanger No. 3. It is thought that this is due to its short length since the values of the overall heat transfer coefficient obtained in this heat exchanger are more subject to entrance effects and accurate determination of heat transfer area. The longer heat exchangers (No. 1 and No. 2) exhibited overall heat transfer coefficients closer to the expected value of 600 Btu per hour feet^2 °F than did heat exchanger No. 3. Although the short length of the heat exchangers was taken into account in the design, the deviation of the U values from predicted was probably the result of the uncertain nature of heat exchanger entrance regions.

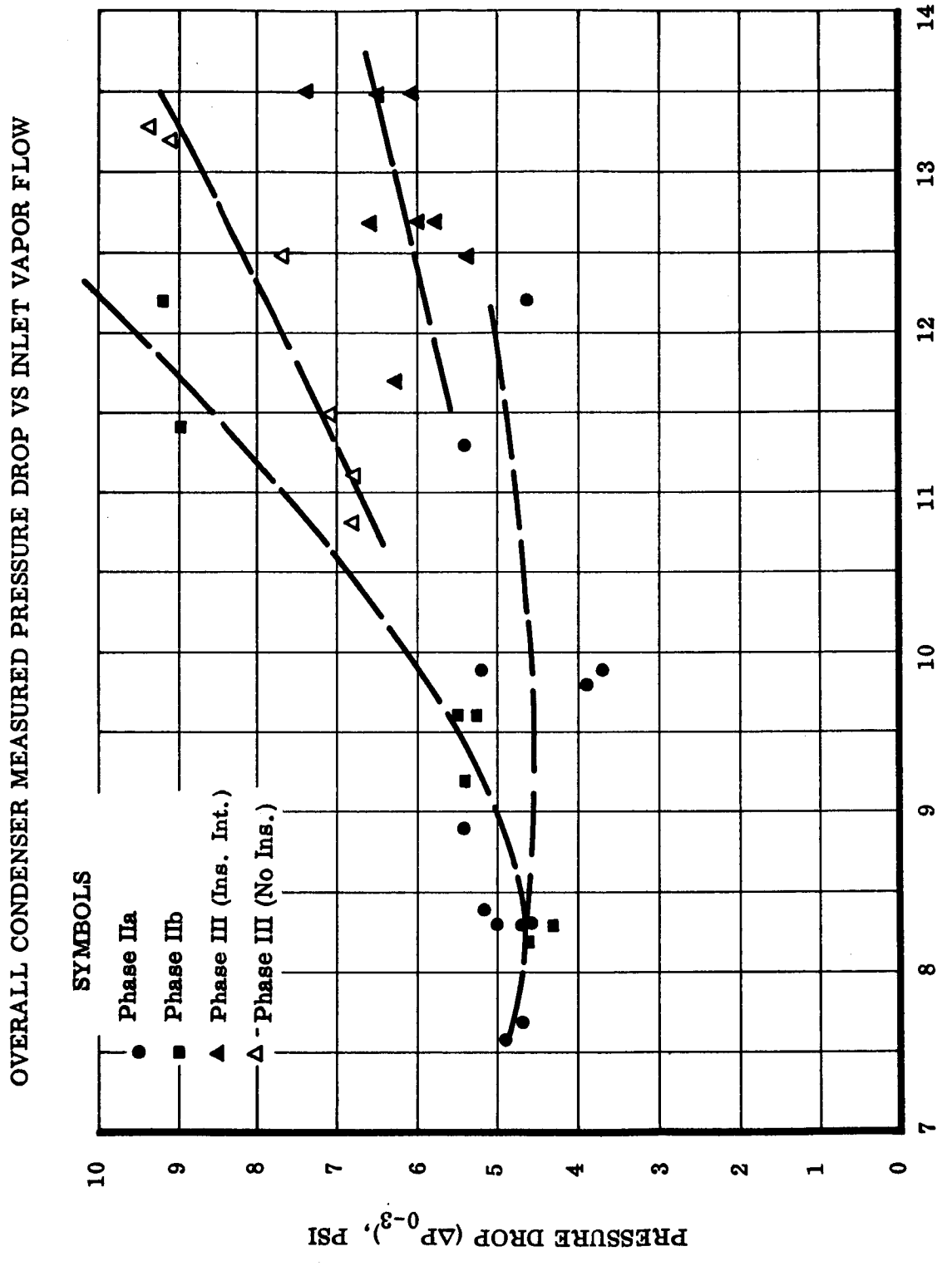
OVERALL CONDENSER MEASURED PRESSURE DROP VS INLET VAPOR FLOW
SYMBOLS
Phase IIa
Phase IIb
Phase III (Ins. Int.)
Phase III (No Ins.)
PRESSURE DROP (ΔP_{0-3}), PSI
INLET VAPOR FLOW ($\dot{m}_{V0}$), LB/MIN
0
1
2
3
4
5
6
7
8
9
10
11
12
13
14

FIGURE 4-30

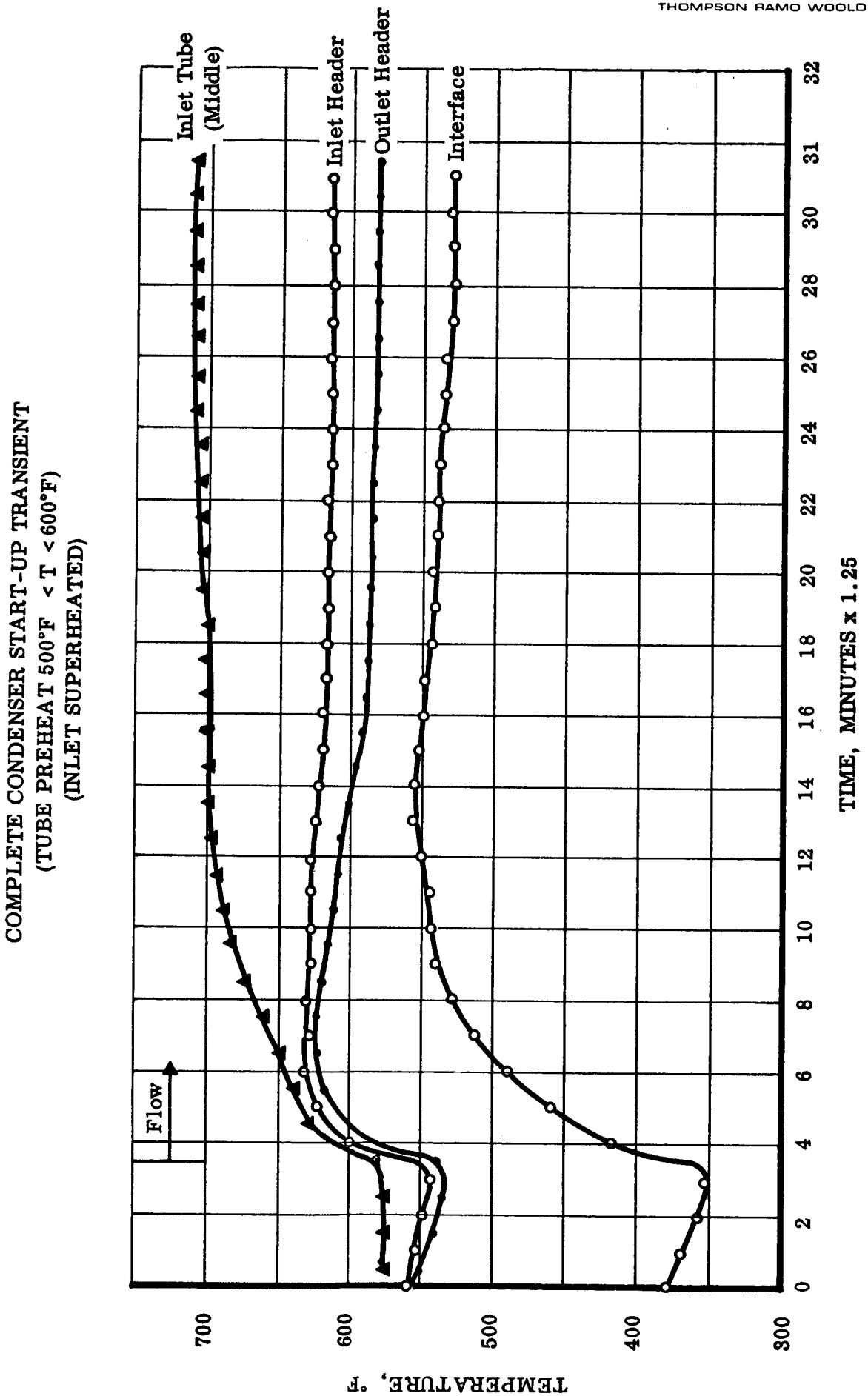
COMPLETE CONDENSER START-UP TRANSIENT
(TUBE PREHEAT 500°F < T < 600°F)
(INLET SUPERHEATED)
Inlet Tube (Middle)
Inlet Header
Outlet Header
Interface
Flow
TEMPERATURE, °F
700
600
500
400
300
0
2
4
6
8
10
12
14
16
18
20
22
24
26
28
30
31
32
TIME, MINUTES x 1.25

FIGURE 4-31

COMPLETE CONDENSER TRANSIENT RESPONSE TO
STEP INCREASE IN INLET VAPOR FLOW
(11.4 LB/MIN TO 11.9 LB/MIN)

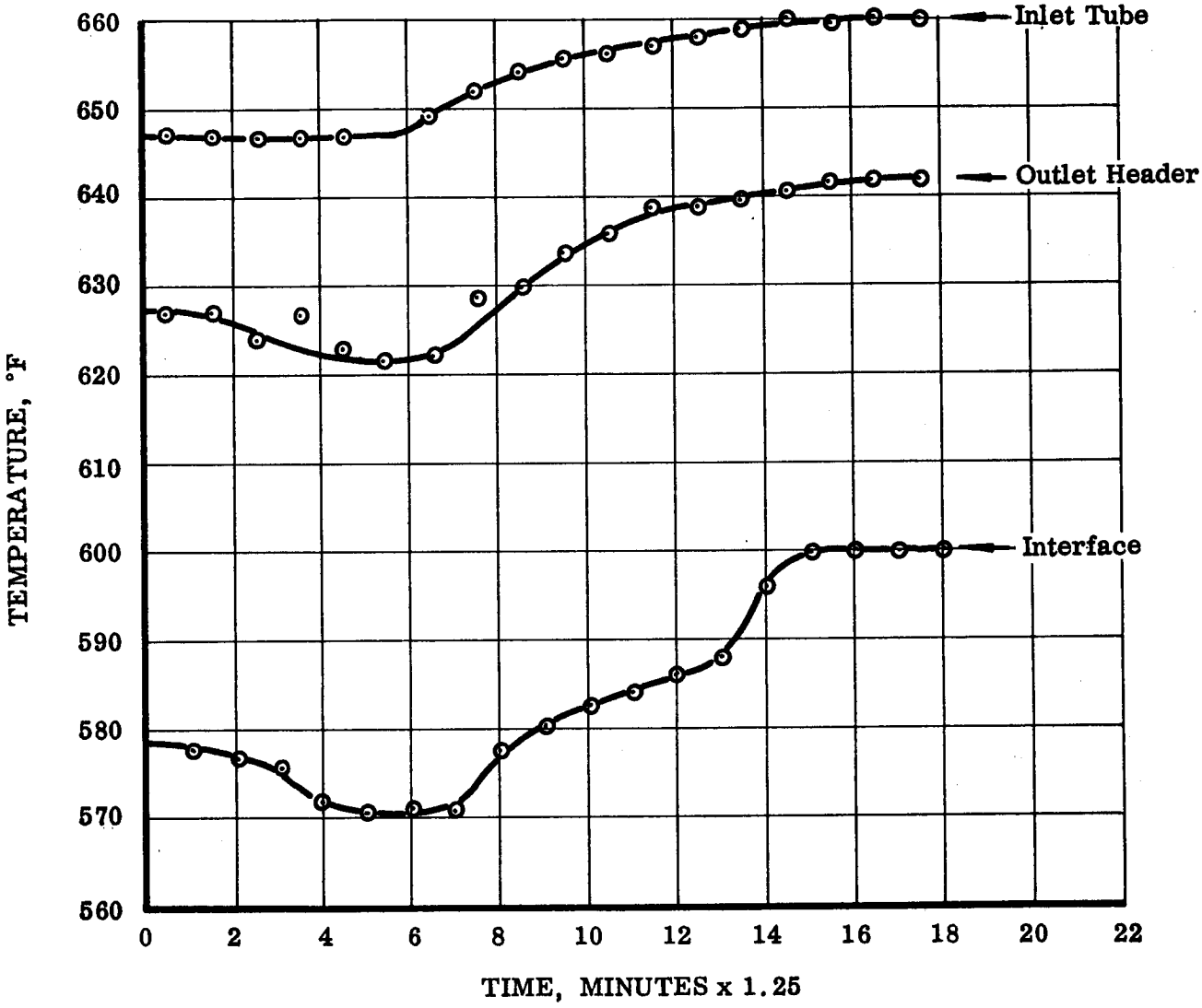

FIGURE 4-32

COMPLETE CONDENSER TRANSIENT RESPONSE TO DECREASING INLET VAPOR FLOW (13.1 LB/MIN TO 125 LB/MIN)

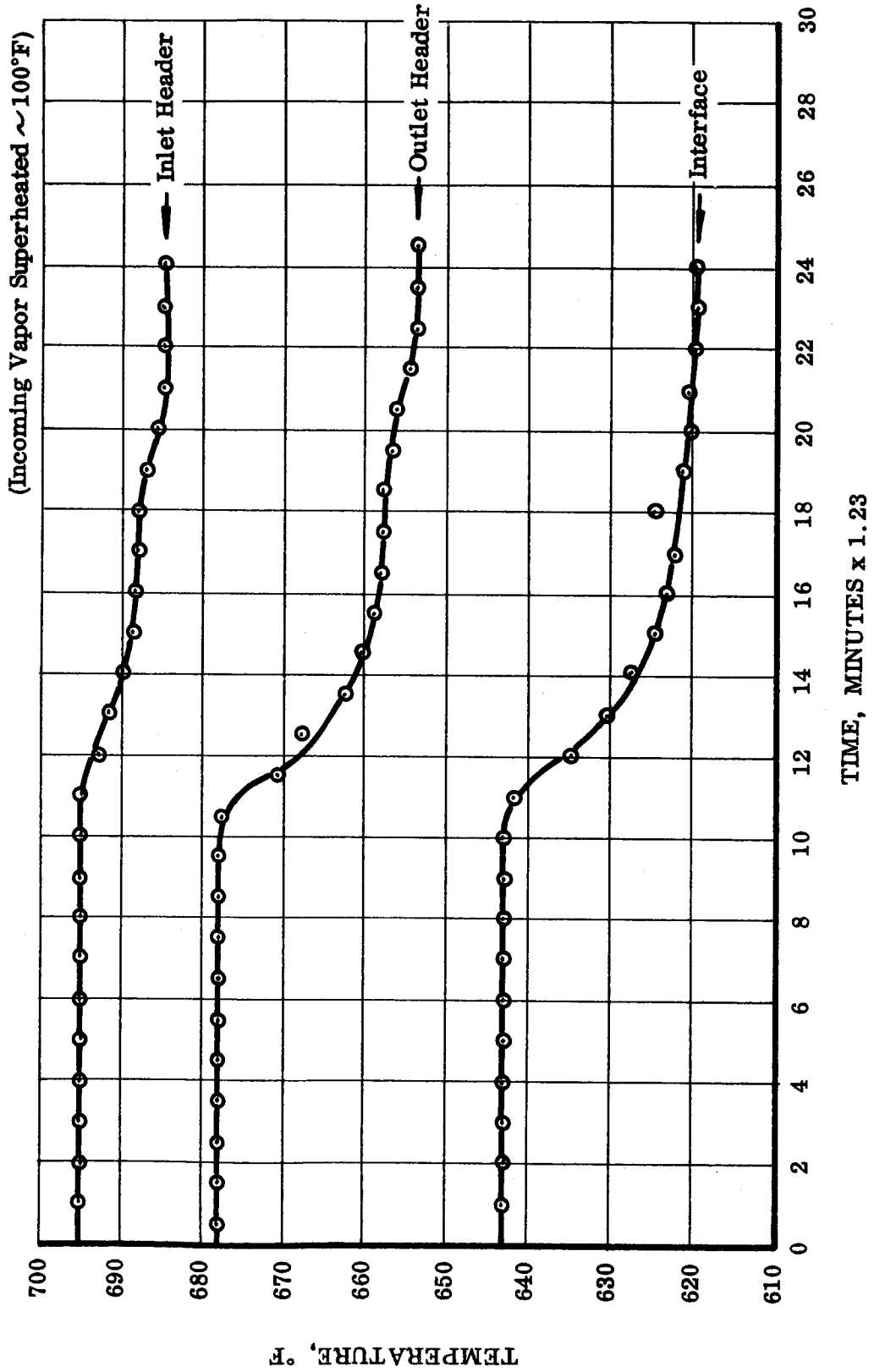

FIGURE 4-33

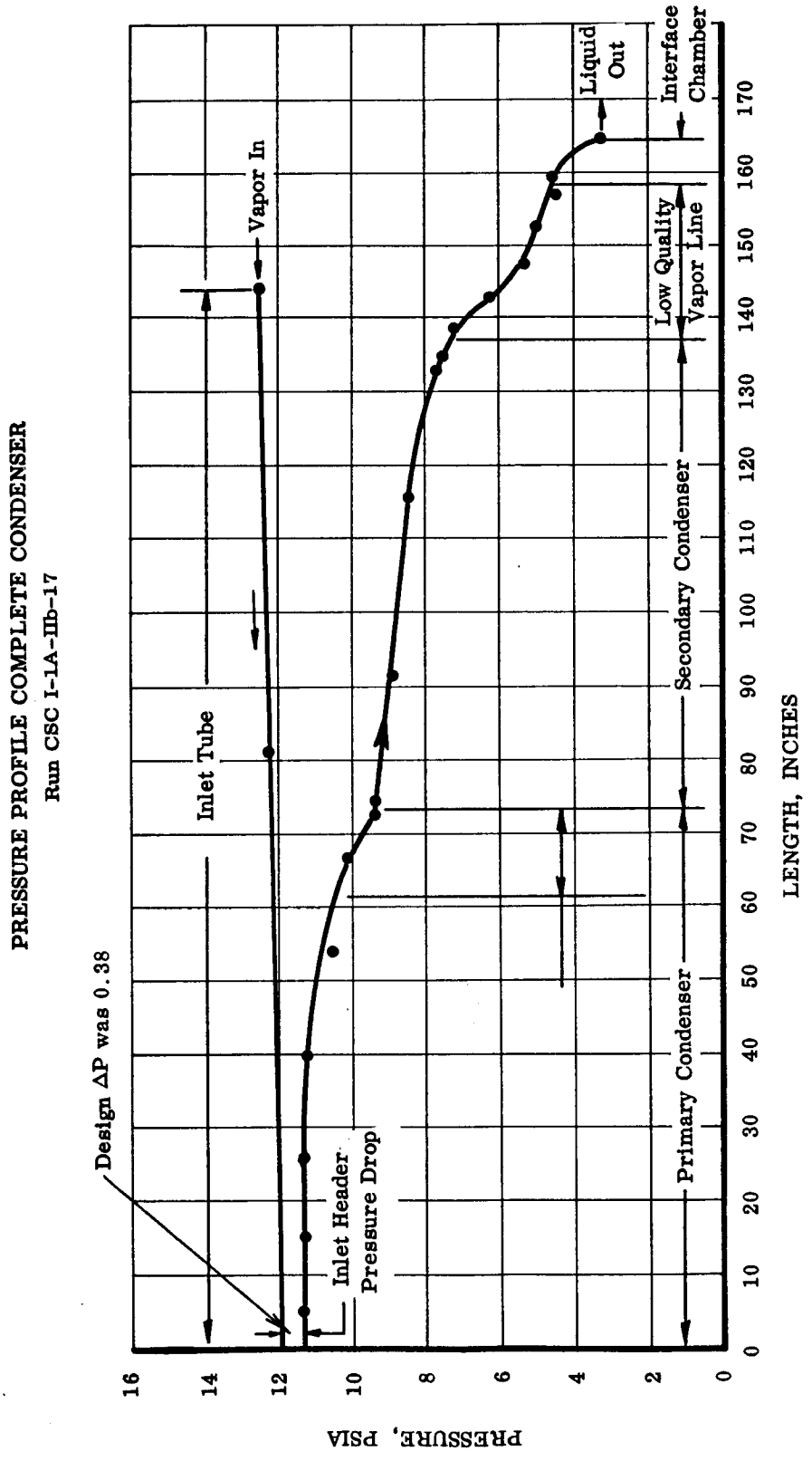
PRESSURE PROFILE COMPLETE CONDENSER
Run CSC I-1A-IIb-17
Design ΔP was 0.38
Inlet Tube
Vapor In
Liquid Out
Interface Chamber
Low Quality Vapor Line
Secondary Condenser
Primary Condenser
Inlet Header Pressure Drop
PRESSURE, PSIA
LENGTH, INCHES
16
14
12
10
8
6
4
2
0
0
10
20
30
40
50
60
70
80
90
100
110
120
130
140
150
160
170

FIGURE 4-34

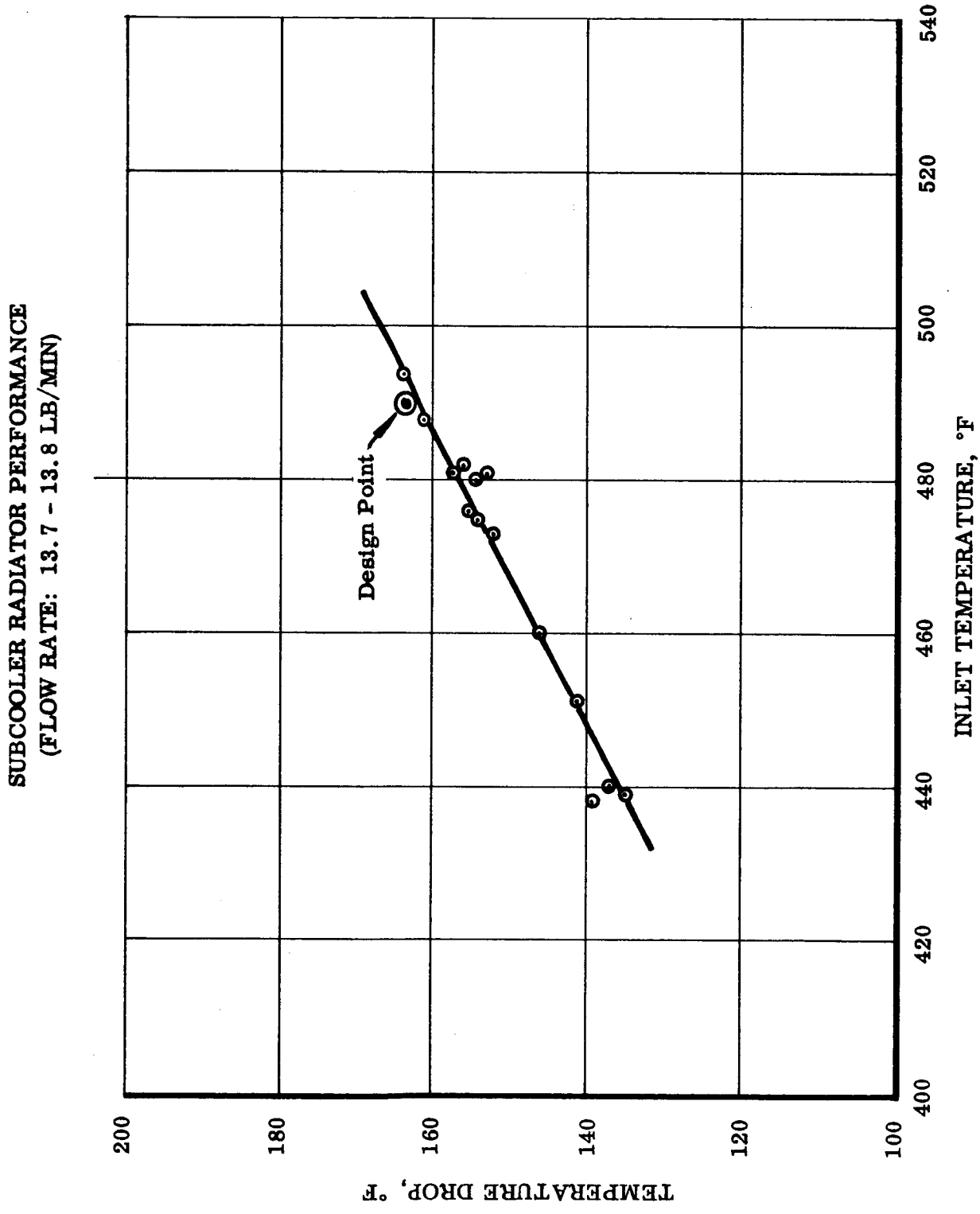
SUBCOOLER RADIATOR PERFORMANCE
(FLOW RATE: 13.7 - 13.8 LB/MIN)
Design Point
TEMPERATURE DROP, °F
200
180
160
140
120
100
INLET TEMPERATURE, °F
400
420
440
460
480
500
520
540

FIGURE 4-35

Section 5.0
CONCLUSIONS

1. The Sunflower I system acceleration requirement (up to 1g in any direction) resulted in design compromises in the condenser subcooler component. These compromises resulted in a higher weight and pressure drop then an equivalent condenser designed for zero g.

2. The redesign of CSC I-1A accurately solved the parallel tube stability problems of the I-1 unit. Startup, steady-state, and transient operation was demonstrated with vapor flow against gravity.

3. The basic problem preventing proper operation of the CSC I-1 unit was its low tolerance to tube-to-tube geometric and thermal unbalances. This resulted in low transport velocities in the upper (small diameter) ends of one or more of the condenser tubes. The problem was aggravated by the adverse gravity vector which required a relatively high transport velocity for proper operation. The less than critical diameter of the condenser tubes at the smaller end permitted the larger drops travelling at low velocities to bridge the tube and form a plug which could not be removed since a pressure drop across the slug equal to or greater than the liquid density times the length of the slug could not be produced.

   The number of bends required in the low quality region (outlet header and outlet tube) could have aggravated the problem. These bends may have contributed to the separation and agglomeration of the liquid which caused maloperation of the condenser.

4. Parallel tube stability with two-phase mercury condensing flow in opposition to gravity is possible without using the normal pressure drop producing methods of stabilization. This stability can be achieved by maintaining a high vapor velocity throughout the condensing section. The magnitude of this velocity is a function of tube geometric and thermal unbalances, header frictional pressure drop, vapor density, and drop contact angle.

   Maintenance of this velocity requires the use of tapered condensing tubes. In addition, since a multiple tube array with flow against gravity is statically and dynamically unstable if multiple interfaces are held in the tubes (unless a high frictional pressure drop is experienced), this configuration is eliminated. Maintenance of an interface in a single position downstream of the multiple tubes is one possible approach. In this configuration the outlet quality of the parallel tubes is finite and a single tube condenser is used to reject the remaining latent heat.

5. The deterioration in performance noted during the CSC I-1A component test (higher vapor velocity required for non-slugging operation as a function of

operating time) has been attributed to some form of wetting of the tube walls by the mercury. In this case a pseudo-wetting of mercury to mercuric oxide to tube material oxide probably occurred rather than an intimate mercury-stainless steel wetting. This problem appears to be of consequence in condensers flowing against gravity, since the greater the degree of wetting, the greater the design compromise to insure stability. The effect is problematical to a much lesser degree in condensers designed to operate in only zero or micro-gravity.

6. The heat rejection capability of the CSC I-1A unit was under-designed, resulting in above design pressure level at design flow. The discrepancy has been traced to excessive extrapolation of the experimental data from which the fins were sized and the shielding effect of the preheaters.

7. Success of start-up with flow against gravity is a function of inlet quality. The minimum quality under which start-up was achieved was not calculable during the CSC I-1A test due to the transient effects of the desuperheater. Steady-state operation, however, was experienced with inlet qualities down to 0.755.

8. The design of headers for multiple tube condensers appears to be less critical than anticipated. The CSC I-1A inlet header designed for 18 tubes, 7.0 psia, and 13.72 lb/min mass flow rate operated acceptably with 10 tubes at pressures from 4 to 15 psia, flows from 7 to 14 lb/min, and from superheat to 75.5 per cent quality. The qualitative limits of stable operation for the header were indeterminant in the CSC I-1A unit since tube unbalances could not be experimentally separated from header maloperation.

9. In the design of a mercury condenser flowing against gravity, it is wise to avoid any flow passage diameter less than the critical diameter (see the footnote in Section 3.3.1) and imperative that they be avoided in any parallel path portion of the condenser.

10. Care should be taken in the design of the heat rejection capability of the interface chamber (in a Sunflower-type condenser design) since overall condenser pressure drop is a function of this heat rejection.

Section 6.0
RECOMMENDATIONS

1. Verify the necessity of the Sunflower I system acceleration requirement. A unidirectional acceleration of zero to magnitudes greater than one can be tolerated by the condenser-subcooler without significant design compromise. With this latter requirement, the system could be modified so ground checkout could be effected with condenser flow in the direction of gravity.

2. Determine experimentally the effect of tendency toward wetting on mercury condenser performance. If serious design compromises are indicated, investigate methods of promoting or maintaining non-wetting operation. If non-wetting cannot be insured for mission times, determine analytically and experimentally the requirements for wetting film stability.

3. Evaluate the feasibility of the two interface maintaining devices described in this report (or any others that appear promising) and experimentally develop them on the ground and in zero g. In addition to the interface maintenance and inventory absorbing capabilities of the two reported schemes, they may be modified to detect and bleed off noncondensables which may accumulate in the system (such as hydrogen diffused through the boiler tube walls). This consideration is important for long missions.

4. Develop a lightweight scheme for orbital preheat, such as pyrotechnic heaters. Most dynamic space systems require this preheat, so the application would be general.

5. Experiment to determine the optimum emmissive coating for the Sunflower condenser. Data needed include: effect of thermal cycling and endurance in atmosphere, effect of vibration on mechanical bond, integrity of mechanical bond using both aluminum and stainless steel substrates, and endurance in the 500 to 800°F temperature range in space vacuums. (The latter requirement may take some coatings which deteriorated at high temperatures attractive for the Sunflower application.) Although the Sunflower condenser operates in a temperature range where solar absorbtivity of the condenser should be considered, the systems orientation in space makes this quality unimportant.

6. Design of a flight Sunflower I condenser-subcooler based on the knowledge gained from the two condenser components tested in this report. The resulting component should be tested in a space environment and subjected to physical loadings as specified.

7. Consider maintaining a single interface downstream of the parallel tube array, as in the Sunflower I condenser, in space condensers where parallel tube stability is a problem due to shifting interface positions, low frictional pressure drops, and/or system internal (flow) and external (vibration) dis-

turbances. The advantages over a conventional multiple interface-in-condenser tube approach are: less sensitivity to system acceleration or vibration, less liquid hold-up, less sensitivity to inventory shifts due to possible boiler oscillations, capability of predicting the location of and bleeding off of non-condensables, and capability of operating with flow against gravity with reasonable pressure drop.

Section 7.0
REFERENCES

1. Reynolds, W. C. Hydrodynamic Considerations for the Design of Systems for Very Low Gravity Environments. Technical Report number LG-1, Department of Mechanical Engineering, Stanford University, September, 1961.

2. Bickerman, J.J. Surface Chemistry. Academic Press, Second Edition, 1958.

3. Koestel, A., Reinmann, J.J. "Mercury Condenser Research and Development." TRW ER-4410, April, 1961, or "Government-Industry Conference on Mercury Condensing," NASA TN D-1188, February, 1962.

4. Baer, E., McLaughlin, T. F. "The Determination of Surface Properties of Polymers from Liquid Drop Stability on an Inclined Plane, "Journal of Applied Polymer Science, Vol. V, Issue No. 14, 1961.

5. Kiraly, R.J., Koestel, A. "The SNAP II Power Conversion System Topical Report No. 8, Condenser Development and Design Study." TRW ER-4104, June, 1960.

6. Bjork, R. L. "Meteroids Versus Space Vehicles." American Rocket Society Paper No. 1200-60, May, 1960.

7. Summers, J. L. and Charters, A.C. "High Speed Impact of Metal Projectiles in Targets of Various Materials." Proceedings of the Third Symposium on Hypervelocity Impact, Armour Research Foundation, Chicago, Illinois, 1959.

8. Lieblein, S. "Analysis of Temperature Distribution and Radiant Heat Transfer Along a Rectangular Fin ofConstant Thickness." NASA TN D-196, November, 1959.

9. Kutateladze, S.S., Borishanskii, V.M., Novikov, I.I., Fedynskii, O.S. "Liquid Metal Heat Transfer Media," translation of Supplement No. 2 of the Soviet Journal of Atomic Energy by Consultants Bureau, Inc., New York.

10. Lyon, R.N., Editor. Liquid Metals Handbook. Second Edition, Washington, Atomic Energy Commission, Department of the Navy, 1952.

11. Griffith, P., Kulinski, E.S. "Water Condensing Tests." TRW ER-4200, October, 1960.

12. Quandt, E.R. "Analysis and Measurement of Flow Oscillations," Chemical Engineering Progress Symposium Series, Volume 57, Number 32, 1961.

13. Petrash, D.A., Zappa, R.F. "Experimental Study of the Effects of Weightlessness on the Configuration of Mercury and Alcohol in Sperical Tanks." NASA TN D-1197, April 1962.

14. Vild, T. J., Sill, D. E., Huber, D. D. "Test Results-Sunflower I Condenser-Subcooler CSC I-1." TRW ER-5023, September, 1962.

15. Gido, R. G., Koestel, A. "SNAP 2 Power Conversion System Topical Report No. 17-Mercury Boiling Research." TRW ER-4833, October, 1962.

16. Vild, T. J., Sill, D. E. "Test Results-Sunflower I Condenser-Subcooler CSC I-1A." TRW ER 9032, October, 1962.

17. Koestel, A., Gido, R. G. "Progress Report No. 3, Mercury Wetting and Non-Wetting Condensing Research." TRW ER-5214, January, 1963.

18. Dennington, R. J., Koestel, A., Saule, A. V., Shure, L. I., Stevens, G. T., Taylor, R. B. "Space Radiator Study." TRW ER-4544, October, 1963.

19. Loeffler, I. J., Lieblein, S., Clough, N. "Meteoroid Protection for Space Radiators." American Rocket Society Paper 2543-62 (with Addendums), September, 1962.

20. Koestel A., Smith, C. M. "Radiator Design Limitations for Dynamic Converters." Presented Before the Sixth AGARD Combustion and Propulsion Colloquium, Cannes, France, March, 1964.

Section 8.0
NOMENCLATURE

A	Area
C_D	Drag coefficient
D	Diameter
F	Force
G	Weight flow per unit area
L	Length
LMTD	Log mean temperature difference
N_{Re}	Reynolds number
N_{FR}	Froude number
P	Pressure
ΔP	Pressure drop
$P_{(o)}$	Probability of no meteroid penetration
Q	Heat transferred per unit time
R	Radius
T	Temperature
U	Overall heat transfer coefficient
V	Velocity
W_T	Weight
X	Flowing quality
ΔX	Quality change
f_v	Vapor friction factor

g_c	Gravitational constant, $\frac{\text{lbm - ft}}{\text{lbf - sec2}}$
h_{fg}	Heat of vaporization
l	Length
$\dot{m}$	Mass flow rate
g_r	Local gravity, ft/sec^2
n	g_l/g_c, lbf/lbm
q	Heat rejected per unit length and time
r	Radius
t_p	Protection thickness
v	Specific volume
x	Distance
y	Distance
α	Angle or deviation from design quality
β	Contact angle
δ	Drop diameter or film thickness
ϵ	V_D/V_V
ϵq	Deviation from design heat rejection
ϵD	Deviation from design diameter
Θ	Angle
σ	Surface tension, liquid-gas
τ	Interfacial shear, exposure time
ρ	density
μ	Absolute viscosity

Φ_r	$\Delta P_{TF}/\Delta P_V$
Φ_V	dP_{TF}/dP_V
η	Fin efficiency

Subscripts

0	Initial or inlet (inlet of inlet tube for CSC I-1A results)
1	Inlet, inlet of primary condensing section - CSC I-1A results
2	Primary condenser exit or secondary condenser inlet - CSC I-1A results
3	Secondary condenser exit or low quality vapor line inlet - CSC I-1A results
4	Low quality vapor line exit - CSC I-1A results
5	Interface - CSC I-1A results
a	Aluminum
b	Bearing
c	Condensing, condensate
D	Design, drop, drag
f	Frictional
e	Exit
Int.	Integrated
I	Input
l	Liquid, local
m	Momentum, mean, meteoroid
p	Boiler, Projected
s	Static, local, steel

TF	Two phase
T	Total or tube
V	Vapor
NON-ISO	Non-isothermal

APPENDIX A

STATE OF THE ART OF METEOROID PROTECTION

Advancements in technology have superceded some of the earlier work done on the Sunflower program. One area which suffers from this malady is the approach used in determining the necessary protection from meteoroids.

As stated in the body of the report, the meteoroid protection requirement for the Sunflower system was formulated from the work done in References 6 and 7. Since this time (Fall, 1960) a more universally accepted approach has been generated. It is quite possible, however, that the new model may suffer the same fate as more data are accumulated; none the less, updating of the protection is in order.

In Reference 19, the following conclusive formula is given as the meteoroid protection requirements for the armor method.

$$t = \frac{a}{2.54}\,\gamma\left(\frac{6}{\pi}\right)^{1/3}\rho_P^{-1/3}\left(\frac{62.4}{\rho_t}\right)^{\Phi}\left(\frac{\bar{V}}{C}\right)^{\Theta}\left(\frac{\alpha A \tau}{-\ln P(o)}\right)^{\frac{1}{3\beta}}\left(\frac{2}{3n\Theta\beta+2}\right)^{\frac{1}{3\beta}}$$

where

t = thickness of protection material, inches

a = 1.75 (correction for finite target)

γ = 2, constant

ρ_P = meteoroid density, now "agreed" to be $0.44\,\frac{gm}{cm^3}$

ρ_t = density of protection material, lb/ft^3

Φ = 1/2, constant

$\bar{V}$ = 98,400 ft/sec, average meteoroid velocity

$C = 12\sqrt{Etg/\rho_t}$

E_t = Modulus of elasticity of protection material, $lb/in.^2$

g = 32.2 ft/sec^2

θ = 2/3, flux constant

α = 5.3×10^{-11}, flux constant

β = 1.34, flux constant

A = outer tube area, ft^2

τ = mission time, days

$P_{(o)}$ = prob. of no penetration

η = 1, oblique penetration constant based on normal velocity component

Entering the values, except those for the properties of the armor material, results in

$$t = 3.31 \left(\frac{A \tau}{-\ln P_{(o)}} \right)^{1/4} (\rho_t E_t)^{-1/6}$$

The resulting curve for 316 stainless steel is plotted in Figure A-1. For comparison the methods of Section 3.1.2 and Reference 6 are plotted on this curve.

If the mission time, vulnerable area, and probability of no penetration as specified for the Sunflower system are entered in this equation (1 year, 51.41 ft^2, and 0.99, respectively) the thickness of stainless steel required is 0.150 inch. This is between the 0.304 inch required by Reference 6 and the 0.069 required by the method used in this report. (It should be noted that inner tube area is used here, rather than outer tube area as required in Reference 19, to eliminate iteration).

If the contemporary model of Reference 19 is accepted, the conclusion in this report that aluminum protection offers no weight advantage over stainless steel is no longer valid. Figure A-2 compares the relative weight for different materials. The weight of 316 SS @ 600°F is normalized to 1.0 (M_t = weight parameter = $K E_t^{-1/3} P_t^{5/6}$) and the armor weights of other materials are compared. The thicknesses of other materials can be found from Figures A-1 and A-2 coupled with the relationship

$$t_x = M t_x \frac{0.288}{\rho_x} t_{st}$$

STEEL METEOROID PROTECTION REQUIREMENTS

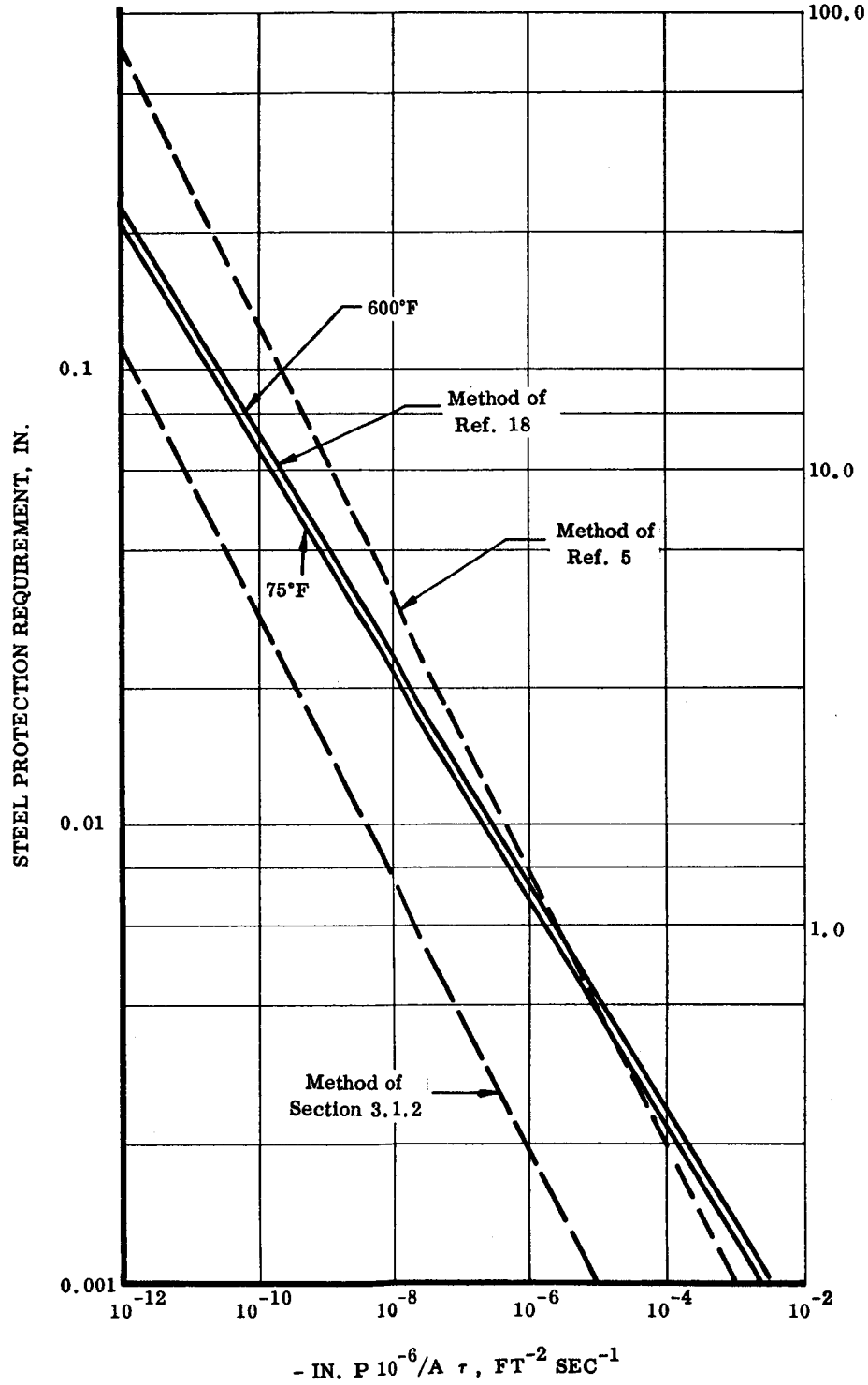

FIGURE A-1

RELATIVE WEIGHT FOR METEOROID PROTECTION
(PROBABILITY, EXPOSURE TIME AND EXPOSURE AREA CONSTANT)

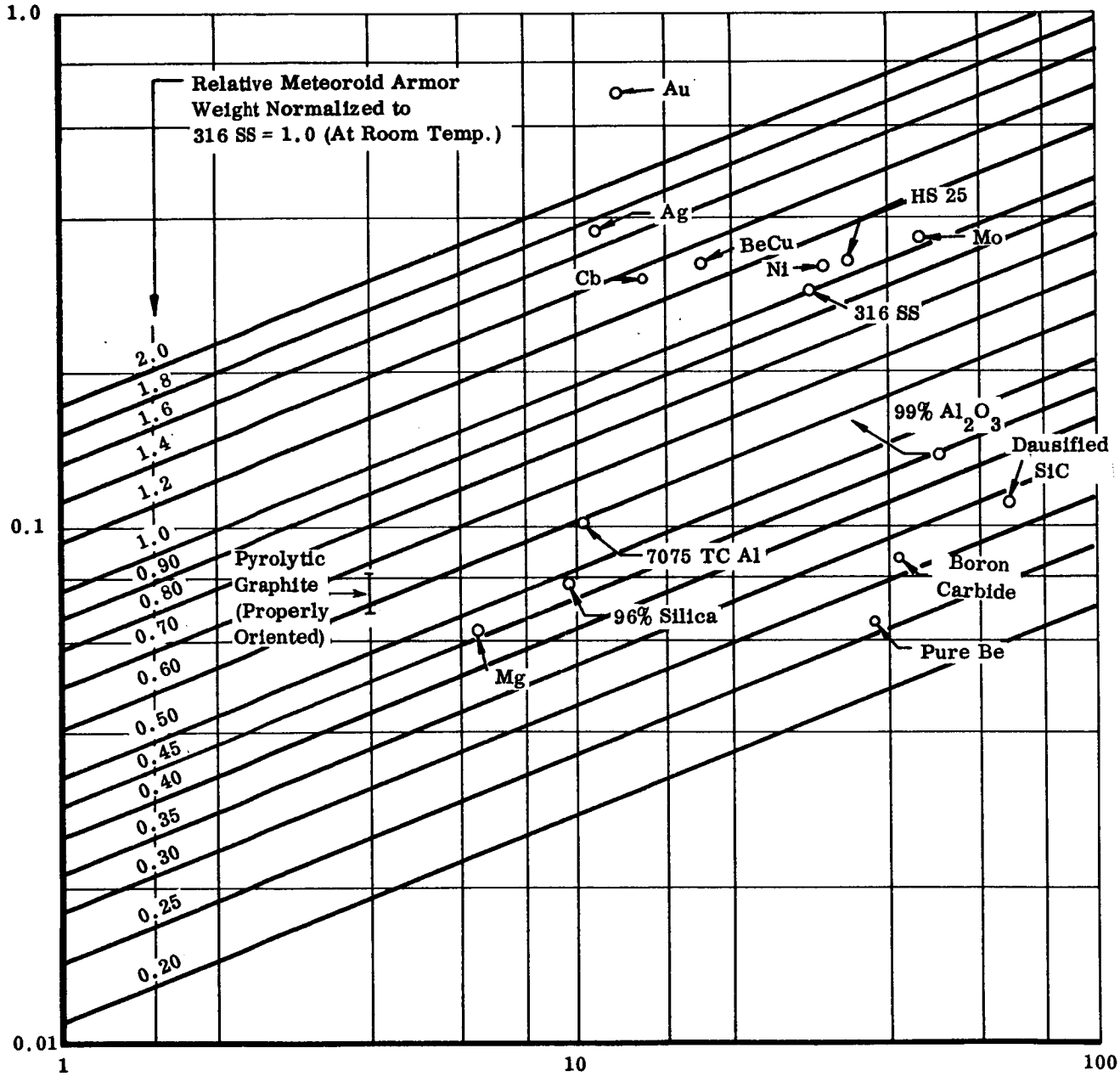

FIGURE A-2

where

t_x = thickness of any armor material, inches

Mt_x = weight parameter for the material from Figure A-2

ρ_x = armor density, $lb/in.^3$

t_x = 316 SS thickness from Figure A-1

The weight advantages of a number of materials (i.e., aluminum, beryllium) become obvious, but other considerations such as operating temperature level and compatibility with the working fluid must again be considered.

APPENDIX B

IMPROVED TWO PHASE MERCURY PRESSURE DROP

A rather comprehensive contribution to the field of two phase flow of mercury is made in Reference 20. A new theoretical correlation is developed here which matches the data of various experimenters over the following ranges:

Tube diameters	0.75 to 0.397 inch, both constant and tapered
Condensing length	0.625 to 8.0 ft
Local N_{RE}	324 to 50,000
Pressure level	1.5 to 35 psia
Qualities	0.02 to 1.0
Acceleration environment	1g (horizontal) and 0g

Reference 20 gives the details of the derivation, but Figure B-1 does show the theoretical correlation which is on a local basis. Using this figure, the two-phase pressure drop that would be expected in the CSC I-1A primary condenser tubes (including the adiabatic section) was recalculated and found to be 2.28 psid rather than the 1.86 psid indicated by Section 4.2.5. The correlation of Reference 20 does not include any gravity effect, but it is felt that the velocities and Reynolds numbers attained in the Sunflower condenser make it insensitive to the direction of a 1g body force (see Section 3.3.1). The pressure drop calculations from Reference 20 are shown in Table B-1.

It is difficult to ascertain which of the methods is more accurate from the CSC I-1A test data, since it was not instrumented as a research condenser. Based on the wider agreement of Reference 20 with independent data, it is believed that this correlation is more valid.

LOCAL MERCURY TWO PHASE PRESSURE DROP CORRELATION FROM REF 20

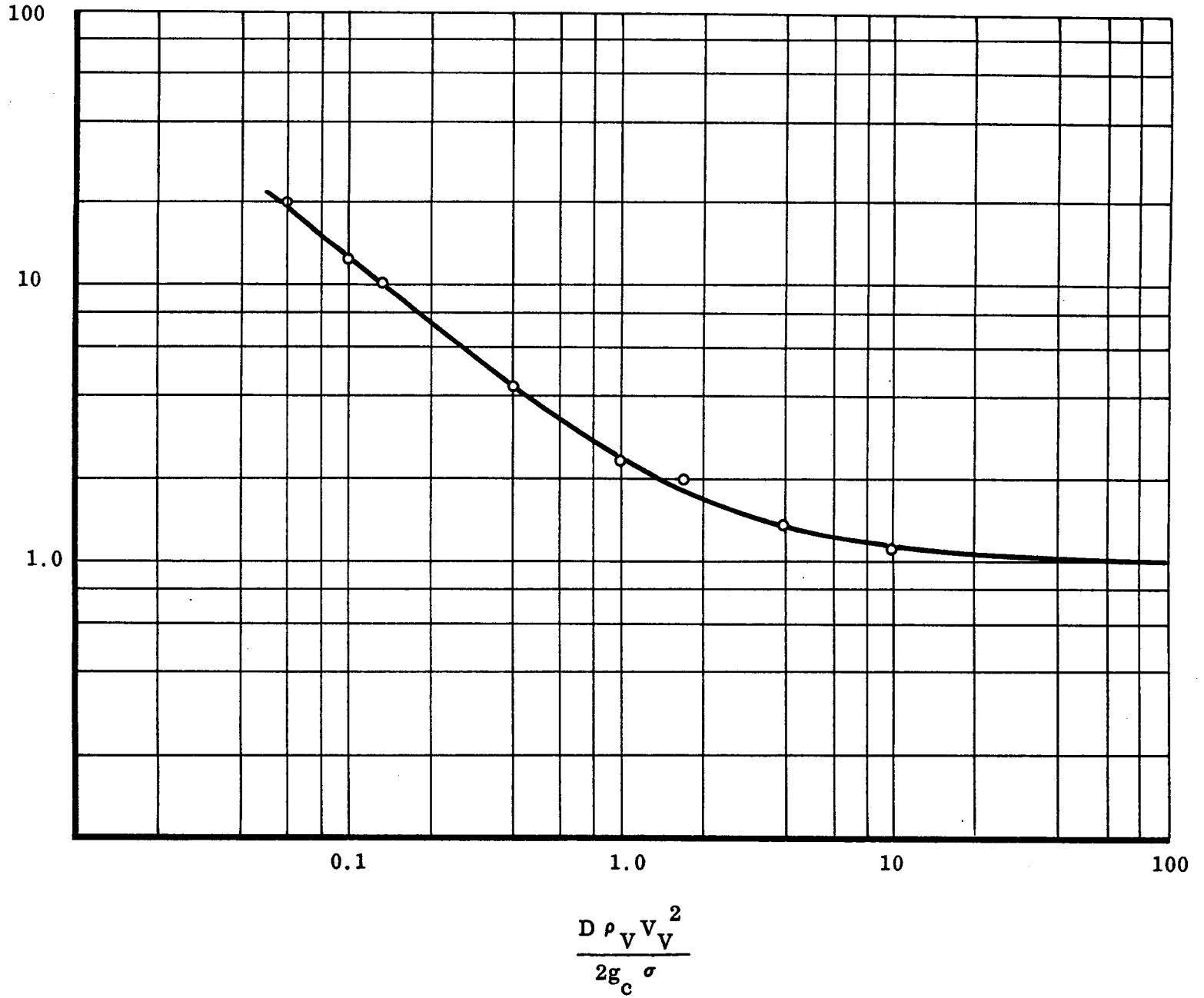

FIGURE B-1

TABLE B-1

PREDICTED CSC I-1A PRIMARY CONDENSER ΔP_{TF} BY THE METHOD OF REFERENCE 20

Section No.		L inches	D_{ave} inches	X_{ave}	$\dot{m}_{V\,ave}$ (lb/min.)	$N_{RE\,ave}$	f	ΔP_g psi	N_{wl}	$\Phi_V^2 X^{3/4}$	Φ_V^2	ΔP_{TF} (psi)
Cond. Section	1	6.156	0.580	0.892	1.12	13,680	0.0280	0.0308	26.2	1.10	1.20	0.0370
	2		0.543	0.784	0.985	12,800	0.0285	0.0335	24.5	1.11	1.34	0.0447
	3		0.506	0.684	0.855	11,950	0.0290	0.0365	22.9	1.12	1.49	0.0544
	4		0.470	0.586	0.735	11,100	0.0300	0.0407	21.2	1.13	1.69	0.0688
	5		0.433	0.500	0.678	10,200	0.0305	0.0450	19.6	1.14	1.92	0.0862
	6		0.396	0.420	0.527	9,350	0.0310	0.0498	17.9	1.15	2.21	0.1100
	7		0.359	0.345	0.434	8,470	0.0320	0.0567	16.2	1.16	2.58	0.1460
	8		0.323	0.279	0.348	7,620	0.0330	0.0650	14.6	1.17	3.05	0.1980
	9		0.286	0.224	0.280	6,750	0.0340	0.0755	12.9	1.19	3.64	0.2750
	10		0.249	0.172	0.207	5,880	0.0350	0.0895	11.3	1.2	4.50	0.4030
Adiabatic Section		11.0	0.0231	0.126	0,149	4,560	0.0350	0.1445	8.75	1.25	5.95	0.8550
						TOTAL	ΔP_{TF}					2,278

APPENDIX C

ALTERNATE CONDENSER CONCEPTS

As pointed out in Section 4.4.2 there are two basic unresolved problems with the CSC I-1A unit. These are: under-design of fin area for ground operation by a factor of approximately 17%, and a marginal operating characteristic in terms of stable condensate transport after wetting occurs. The heat rejection capacity must be corrected to permit system design point operation, and this may be straightforwardly accomplished. However, the action to be taken with regard to the wetting problem requires more detailed thought.

The degree of wetting which would occur over a one year operating period with the chosen materials would have to be determined before a meaningful condenser design could be accomplished. However, a more conservative approach would be to assume a complete wetting condition and base the condenser design on this criteria. The effects upon system operation in the event full wetting does not occur during early operation would merely reduce the condenser ΔP and increase the NPSH to the centrifugal pump.

The minimum vapor velocity for stability with film condensation (worst case) is 165 ft/sec as calculated in Section 4.4.2.

In addition to this individual tube velocity requirement, a factor must be applied to compensate for tube-to-tube stabilities, differential heat rejection, and tube diametral errors as explained in Section 4.1. Assuming a tolerance on heat rejection of 2% and a 1% error in tube diameter, the required velocity for the Sunflower primary parallel tube condenser becomes 225 ft/sec for an outlet quality of 12.6%.

The effect of this single requirement raises the condenser pressure drop above the limitations allowable by the other system components. To incorporate the direct radiator concept into the Sunflower system, the cycle would have to be modified with performance penalties, or the environmental specification of 1g operation in any direction would need to be relaxed in the "uphill" direction.

A similar calculation performed for the direct radiating condenser indicates that operation against 0.1g (possible system acceleration requirement) would require a parallel tube vapor velocity of 80 ft/sec and a pressure drop of approximately 2.0 psid. Therefore, the condenser would be very nearly identical to the present Sunflower condenser and would be operable within the system specifications. Some idea of the effect of wetting can be obtained from Figure C-1. Here the vapor velocity necessary for successful operation against 1 and 0.1g is expressed as a function of the drop contact angle. Here C_D is allowed to vary to a value that would be expected from the drop shape rather than held constant at 1.0 as done in the body of this report.

EFFECT OF CONTACT ANGLE ON VAPOR VELOCITY REQUIREMENT
(OPERATION AGAINST GRAVITY)

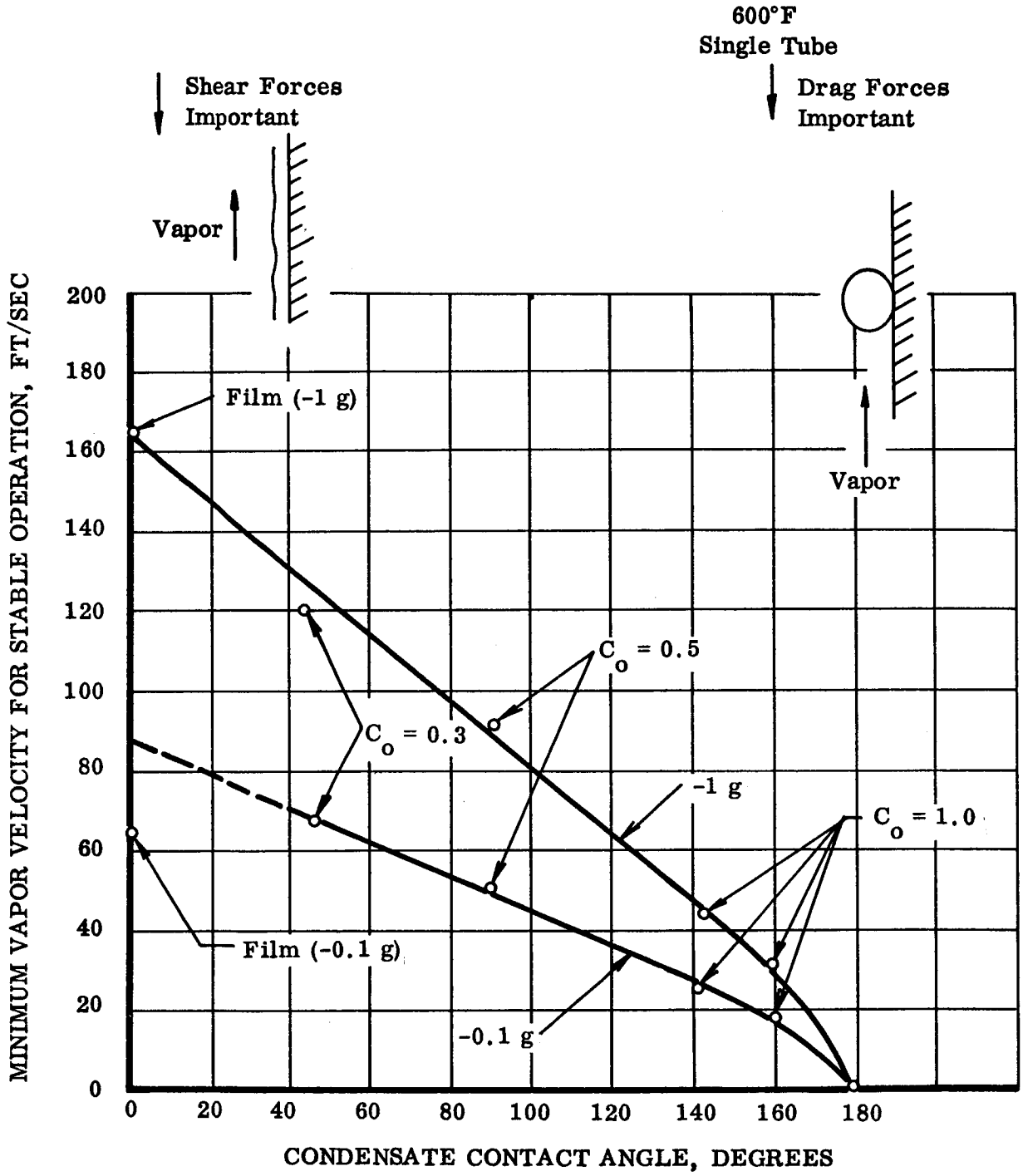

FIGURE C-1

A problem which would be encountered, however, is the difficulty in ground testing a condenser in the 0.1g requirement. Another area requiring considerable effort would be the repackaging of other system components to allow the 0.1g condenser operation and the system auxiliary booth and instrumentation changes required to support such a test.

A solution which results in some increase in system weight would be to adopt an indirect condenser concept which could be made reliably compatible to -1g operation under wetting conditions. The design concept employs a single, compact, tapered condensing tube from which heat is rejected by high pressure mercury supplied by the package pump in exactly the same manner as heat rejection is accomplished from the subcooling heat exchangers of the current design. The preliminary calculations which have been performed on this concept have employed the following approach.

Turbine exhaust is directed down an insulated tube to the entry of a single tapered tube condensing section. This transport is accomplished in an insulated tube to minimize liquid content in the fluid at the 180° turning-entry into the condenser. Condensation then occurs in the single, vertically upward, tapered tube. Heat is rejected from this tube to high pressure fluid from the pump. All of the pump outlet flow is employed to transport heat from the condenser to radiating fins. This includes jet pump flow, boiler flow, and bearing flow. Using this flow a total coolant ΔT of 885°F is required (e.g., 8 passes at 110.6°F per pass).

Optimization of this design approach requires some attention to pump design and pump power consumption details. However, it is apparent that pump output pressure may be relatively independently increased so that the heat transportation passes may be made in series without the total pressure drop being an unattractive burden. Without attempting to present an optimized design, the general features may be indicated by a preliminary design trial summarized as follows.

The present Sunflower pump is capable of 57 ppm. Using this flow rate and an allowable pressure drop in the coolant of 150 psi,the following indirect condenser will satisfy the system acceleration requirement.

1. Coolant temperature rise (with 95.2% inlet quality and 1% outlet quality)

$$\Delta T = \frac{13.72 \text{ lb/min } (0.952-0.01)\ 127 \text{ btu/lb}}{57 \frac{\text{lb}}{\text{min}} \times 0.0326 \frac{\text{Btu}}{\text{lb}\,^\circ\text{F}}} = 885^\circ\text{F}$$

Assuming a condenser two phase ΔP of 1 psid, the exit pressure = 6 psia and T_{SAT} = 591°F.

Assume maximum coolant temperature = 550°F to keep $\eta_{\text{NON-ISO}}$ high.

Using 8 passes:

All the properties for the vapors (both mercury and cesium) were taken from Report No. WADD TR 61-96.

For cesium equation (C-1) can be written as

$$\dot{m}_{Cs} = \frac{1.23\ PC_D A}{\sqrt{T}} \qquad (C\text{-}2)$$

and for mercury

$$\dot{m}_{Hg} = \frac{1.49\ PC_D A}{\sqrt{T}} \qquad (C\text{-}3)$$

Assume the average temperature across the orifice is 900°F (or 1360°R) and $C_D \approx 0.84$[1].

Equations (C-2) and (C-3) can be rewritten as:

$$\dot{m}_{Cs} = 0.192\ PD^2 \qquad (C\text{-}4)$$

and

$$\dot{m}_{Hg} = 0.233\ PD^2 \qquad (C\text{-}5)$$

where

$\dot{m}$ = flow rate, gm/sec.

P = upstream orifice pressure, torr

D = orifice diameter, in.

A plot of these equations for different orifice diameters is presented as Figure C-2. On the same curve the specified meter pressure lines are also drawn. By dividing the meter pressure by the required pressure ratio for a choked orifice $\left[2/k + 1\right]^{k/(k-1)}$, lines of minimum supply pressure can be drawn. In each case, the system operating pressures must exceed or be to the right of this minimum supply pressure line.

Because the minimum supply pressure for cesium are of greater magnitude than the minimum supply pressures for mercury, the orifice design for the cesium flow system is the controlling factor for the system orifice specifications.

[1] Shapiro, A. H., "The Dynamics and Thermodynamics of Compressible Fluid Flow", Ronald Press Company, p. 100, New York, New York, 1953.

8. Meteoroid protection

$$\text{Vulnerable Area} = A_v = \pi d_1 l$$

$$A_v = \frac{\pi\, 0.291 \times 183}{12} = 14.0\ \text{ft}^2$$

$$\text{Total Area} = \text{Radiator} + \text{Condenser} + \text{Boiler} + \text{Misc.} \approx 50\ \text{ft}^2$$

t_p = .068 in. steel (see Section 3.1.2)

9. Tube Weight

$$W_t = \pi\, dtl = \frac{\pi \times .291 \times .068}{144} \times 183 \times 485\ \frac{\text{lb}}{\text{ft}^2} = 38.3\ \text{lb}$$

10. Fin Weight

$$W_t = Atp = 53 \times .060 \times .096 \times 144 = 44\ \text{lb}$$

11. Total Weight

$$W_t = 68.5 + 38.3 + 44 = 150.8$$

Approx. Low pressure cond. = 10 lb + Misc. 15 lb = 25 lb

W_t 175 lb

Comparing with the present primary-secondary direct radiating design of 100 lb, an increment of 75 lb is indicated.

Due to the compatibility of the indirect condenser approach to either 1g or lower acceleration environment, and due to the inherent conservative aspects of a condenser employing such a design, it would appear valuable to pursue this approach.

TRW

THOMPSON RAMO WOOLDRIDGE INC.
23555 EUCLID AVENUE • CLEVELAND, OHIO 44117

December 4, 1964

Subject: Errata Sheet for Topical Report

Gentlemen:

Please correct the report entitled Sunflower I Condenser Subcooler Topical Report, TRW ER-5088 and/or NASA Report CR54013 by replacing page C-4 with the enclosed corrected page.

Very truly yours,

THOMPSON RAMO WOOLDRIDGE INC.

J.W. Picking, Jr.

Program Manager
Equipment Laboratories

JP:db

A problem which would be encountered, however, is the difficulty in ground testing a condenser in the 0.1g requirement. Another area requiring considerable effort would be the repackaging of other system components to allow the 0.1g condenser operation and the system auxiliary booth and instrumentation changes required to support such a test.

A solution which results in some increase in system weight would be to adopt an indirect condenser concept which could be made reliably compatible to -1g operation under wetting conditions. The design concept employs a single, compact, tapered condensing tube from which heat is rejected by high pressure mercury supplied by the package pump in exactly the same manner as heat rejection is accomplished from the subcooling heat exchangers of the current design. The preliminary calculations which have been performed on this concept have employed the following approach.

Turbine exhaust is directed down an insulated tube to the entry of a single tapered tube condensing section. This transport is accomplished in an insulated tube to minimize liquid content in the fluid at the 180° turning-entry into the condenser. Condensation then occurs in the single, vertically upward, tapered tube. Heat is rejected from this tube to high pressure fluid from the pump. All of the pump outlet flow is employed to transport heat from the condenser to radiating fins. This includes jet pump flow, boiler flow, and bearing flow. Using this flow a total coolant ΔT of 885°F is required (e.g., 8 passes at 110.6°F per pass).

Optimization of this design approach requires some attention to pump design and pump power consumption details. However, it is apparent that pump output pressure may be relatively independently increased so that the heat transportation passes may be made in series without the total pressure drop being an unattractive burden. Without attempting to present an optimized design, the general features may be indicated by a preliminary design trial summarized as follows.

The present Sunflower pump is capable of 57 ppm. Using this flow rate and an allowable pressure drop in the coolant of 150 psi,the following indirect condenser will satisfy the system acceleration requirement.

1. Coolant temperature rise (with 95.2% inlet quality and 1% outlet quality)

$$\Delta T = \frac{13.72 \text{ lb/min } (0.952-0.01) \text{ 127 btu/lb}}{57 \frac{\text{lb}}{\text{min}} \times 0.0326 \frac{\text{Btu}}{\text{lb °F}}} = 885°F$$

Assuming a condenser two phase ΔP of 1 psid, the exit pressure = 6 psia and T_{SAT} = 591°F.

Assume maximum coolant temperature = 550°F to keep $\eta_{NON-ISO}$ high.

Using 8 passes:

2. ΔT/Pass

$\Delta T = 885/8 = 110.6°F$ $\quad T_{IN} = 550°F$ and $T_{OUT} = 439.4°F$

$\eta_{\text{non iso.}} = 76.5\%$

Use a 4 inch wide, 0.060 thick fin.

$\eta_F = 92.6\%$

3. Heat rejection per radiator

$\emptyset = 57$ lb/min x 60 min/hr x 0.0326 Btu/lb-°F x 110.6°F = 42,300 Btu/hr

4. Heat rejection area

$$\emptyset = \delta \epsilon F (T_o^4 - T_A^4) A \eta_F \quad \eta_{\text{non iso.}}$$

$$A/\text{Pass} = \frac{12,300}{.171 \times .9 \times .9 (10.1^4 - 5.54^4) \times .765 \times .926} = 13.25 \text{ ft}^2$$

5. Total tube length

$$L = \frac{A \times N_{\text{passes}}}{N_{\text{sides rad.}} \times F_{\text{in. width}}} = \frac{13.25 \times 8}{2 \times 4} \times 12 = 159 \text{ ft.}$$

Adding 3 feet length per pass, the total becomes 159 + 3 x 8 = 183 feet.

6. ΔP high pressure (assume 20 psid in connection and bends)

$$P = F \frac{L \rho V^2}{Dg\ 2} \quad \text{(by transposition and substitution)}$$

$$1/d^5 = \frac{130\ (64.4)\ 812 \times \pi^2 \times 3600}{0.030 \times 183 \times 572 \times 16 \times 1728}$$

$$d^5 = 0.00208 \text{ in}^5$$

$$d = 0.291 \text{ in.}$$

7. Inventory

$$W_t = \frac{\pi d^2}{4} \quad le = \frac{\pi \times .291^2}{4 \times 144} \times 183 \times 812 = 68.5 \text{ lb}$$